NTNU

Norwegian University of
Science and Technology

Modulation Methods for Neutral-Point-Clamped Three-Level Inverter

Sveinung Floten
Tor Stian Haug

Master of Science in Energy and Environment
Submission date: June 2010
Supervisor: Lars Einar Norum, ELKRAFT
Co-supervisor: Roy Nilsen, Wärtsilä

Norwegian University of Science and Technology
Department of Electric Power Engineering

Problem Description

In the upcoming years there will be an increasing number of motor applications that will have line-to-line voltages in the range of 6.6 12 kV. Due to limited voltage ratings of IGBT s, multi-level converters and/or serial connections of devices are required to withstand these voltages. The industry standard today for medium voltage drives is the three level inverter topology; the Neutral Clamped Converter (NPC). Several modulation methods have been presented the recent years. Some of them were studied in the specialization project and Space Vector and Double-Signal will be studied further on in this master thesis.
In this master thesis the main focus should be:

- Further investigation of the DC-bus balance
- Derive current equations for both methods
- Study overmodulation including DC-bus balancing
- Compare Symmetrical modulation with Asymmetrical modulation
- Hardware implementation by using FPGA

Assignment given: 19. January 2010
Supervisor: Lars Einar Norum, ELKRAFT

Preface

This master thesis is the final part of our master degree program at Norwegian University of Science and Technology. The thesis is a continuation of the specialization project in the fall of 2009. The main supervisor has been Professor Lars Einar Norum and co-supervisor has been Roy Nilsen at Wärtsilä. We would like to thank both for helpful discussions and inputs during the year 2009/2010.

We would also like to pay gratitude to Ph.D. student at NTNU Sverre Gjerde and Kjell Ljøkelsøy at SINTEF Energy Research for guidance in the laboratory. Without their help we would not have made it through the laboratory.

At the end we would like to thank our fellow students here at NTNU for good times during our years at the university.

Tor Stian Haug and Sveinung Floten

June 2010

Abstract

Multilevel converters have seen an increasing popularity in the last years for medium- and high-voltage applications. The most popular has been the three-level neutral clamped converter and still research is going on to improve the control of it. This master thesis was a continuation of the specialization project fall 2009. The main topics of current thesis were to further investigate the DC-bus balancing issues, compare symmetrical (one sampling per triangular wave) and asymmetrical (sampling at the top and bottom of the triangular wave) modulation, derive current equations for Space Vector and Double-Signal, improve output voltage in overmodulation and be able to DC-bus balance, and to implement the methods in the laboratory.

Models of the three-level converter were made in the specialization project in both PSCAD and SIMULINK and further studies of the DC-bus balance were also made in this master thesis. None of the methods showed problems to regulate the DC-bus voltage when there was different capacitor values and unsymmetrical load. A PI controller was introduced for Space Vector but it did not show better performance than a regular P regulator.

Asymmetrical modulation showed a clearly better performance than symmetrical modulation when the switching frequency was low compared to the fundamental frequency, especially for Space Vector. The 1st harmonic line-to-line voltage was closer to the wanted value and the THD_i was significantly lower. Simulations also showed that the THD_i can vary significantly depending on at which angle the first sampling is done. This is most clear for asymmetrical Space Vector modulation, but also for the other cases this pattern occurs.

By implementing an overmodulation algorithm the amplitude of the 1st harmonic output voltage was closer to what was desired. Simulations showed how important it was to have three phase sampling symmetry in overmodulation. By having a wrong switching frequency the line-to-line output voltage dropped down to 2.06 when operating in six-step, when the wanted output value should be 2.205. Hence there is a quite large mismatch and the converter is sensitive to the switching frequency when it is operating in the higher modulation area. The balancing algorithm introduced for overmodulation is able to remove an initial offset without a notable change the 1st harmonic output.

Both Space Vector and Double-Signal were tested in the laboratory with two separated DC-sources. Asymmetrical and Symmetrical modulation were tested and so was also overmodulation. The laboratory results confirmed the simulated results, but since the switching was not synchronized in the laboratory, some errors occurred.

Table of Contents

1 Introduction 1

1.1 Converter Topology 1

2 Modulation Strategies 6

2.1 Pulse-Width Modulation 6

2.2 Space Vector PWM 8

2.2.1 Current Flow with Space Vector PWM 12

2.2.2 RMS Current Level 2 14

2.2.3 Average Current Level 2 21

2.2.4 Capacitor RMS Current 23

2.3 Double-Signal Modulation 24

2.3.1 Current Flow with Double-Signal 25

3 Overmodulation 29

3.1 Description of Overmodulation 29

3.2 Simulation Results 32

4 Symmetrical and Asymmetrical Modulation 34

4.1 Comparison of Symmetrical and Asymmetrical Modulation 34

5 DC-bus Balancing 42

5.1 DC-bus Balancing with Space Vector PWM 42

5.1.1 DC-bus Balancing with Proportional Controller 44

5.1.2 DC-bus Balancing with Prediction 45

5.1.3 Space Vector Balancing with PI Controller 47

5.2 DC-bus Balancing with Double-Signal 54

5.2.1 DC-bus Balancing with Proportional Regulation 54

5.2.2 Dc-bus Balancing with Prediction 56

5.3 Simulations Results 57

5.3.1 Simulations PI Controller for Space Vector 57

5.3.2 Simulation Results of 1^{st} Harmonic Output Voltage, THD_i and Maximum Voltage Unbalance at Stationary Operation 59

5.3.3 Simulation Results with Different Capacitor Values 59

5.4 Balancing in Overmodulation with Space Vector 64

5.4.1 Calculations of Neutral Point RMS Current 66

5.4.2 Implementation of Balancing Algorithm 68

5.5 Balancing in Overmodulation with Double-Signal 71

6 Laboratory Work and Comparison with Simulations 73
6.1 Implementation in the laboratory 74
6.2 Laboratory Results of Space Vector and Double-Signal PWM 76
6.2.1 Laboratory Results of Space Vector 76
6.2.2 Laboratory Results of Double-Signal 79
6.3 Laboratory Results of Symmetrical and Asymmetrical Modulation of Space Vector 82
6.4 Laboratory Results of Overmodulation 83
6.5 Laboratory Results of DC-bus balancing 84
7 Discussion 86
8 Conclusion 88
9 Scope of further work 89
10 References 90

Appendix A: Laboratory Results Space Vector 92
Appendix B: Laboratory Results Double-Signal 96
Appendix C: Laboratory Results of Symmetrical Modulation 100
Appendix D: Laboratory Results of Asymmetrical Modulation 104
Appendix E: List Lab Equipment 108

List of figures

Figure 1.1-1: Converter topology 2
Figure 1.1-2: Overview of space vectors 3
Figure 1.1-3: Bridge leg voltage 3
Figure 1.1-4: Line-to-line voltage 3
Figure 2.1-1: PWM with bipolar switching pattern 6
Figure 2.2-1: Space vector diagram for a three-level converter 8
Figure 2.2-2: Overview of hexagons 9
Figure 2.2-3: Duty cycle calculations for the six inner hexagons 10
Figure 2.2-4: Duty cycle calculations outside the six inner hexagons 10
Figure 2.2-5: Switching pattern for space vector modulation 11
Figure 2.2-6 Phase currents out of level 2 due to switch state 12
Figure 2.2-7 Phase current out of level 1 (neutral point) due to switch state 12
Figure 2.2-8 Phase current out of level 0 due to switch state 12
Figure 2.2-9 Space vector Duty Cycles 13
Figure 2.2-10 Variable of integral calculations 13
Figure 2.2-11: Separation of the vector space into modes 14
Figure 2.2-12: Reference vector mode 1 15
Figure 2.2-13: Reference vector in mode 2 16
Figure 2.2-14: Reference vector mode 3 18
Figure 2.2-15 I_2 RMS at f=1 20
Figure 2.2-16 I_2 RMS at f=0 20
Figure 2.2-17 Analytical calculations of I_2 RMS current, f=1/2 21
Figure 2.2-18 SIMULINK simulations of I_2 RMS current at 1050 Hz 21
Figure 2.2-19 I2 Analytical average current, f=0 22
Figure 2.2-20 Analytical average current, f=1 22
Figure 2.2-21 Analytical I_2 average current, f=½ 23
Figure 2.2-22 SIMULINK simulations of I_2 average current at 1050 Hz switching and 50 Hz fundamental, f=½ 23
Figure 2.2-23 Analytical calculations of I capacitor RMS current 24
Figure 2.2-24 SIMULINK simulations of capacitor RMS current at 1050 Hz switching and 50 Hz fundamental 24
Figure 2.3-1: Control signals for Double-Signal PWM 25
Figure 2.3-2: Upper control signals for Double-Signal 25
Figure 2.3-3: SIMULINK simulations of RMS current at 1050 Hz switching and 50 Hz fundamental 27
Figure 2.3-4: SIMULINK simulations of average current at 1050 Hz switching and 50 Hz fundamental 27
Figure 2.3-5: SIMULINK simulations of capacitor current at 1050 Hz switching and 50 Hz fundamental 28
Figure 3.1-1: Space vector diagram showing the overmodulation area 29
Figure 3.1-2: Six-step operation 30
Figure 3.1-3: Double signal switching states with a modulation index of 4/ π 30

Figure 3.1-4: Space vector switching states with a modulation index of 4/ π 30
Figure 3.1-5: Correction of reference vector in overmodulation 31
Figure 3.1-6: Flowchart of overmodulation algorithm 32
Figure 4.1-1: Sampling with symmetrical modulation 34
Figure 4.1-2: Sampling with asymmetrical modulation 34
Figure 4.1-3: THD_i of inductive load at different m_f with Double-Signal 35
Figure 4.1-4: THD_i of inductive load at different m_f with Space Vector 35
Figure 4.1-5: Harmonic spectra with m_f equal to 6 36
Figure 4.1-6: Switching vectors with symmetrical modulation during one fundamental period, m_f equal 6 36
Figure 4.1-7: Switching vectors with symmetrical modulation during one fundamental period, m_f equal 6 37
Figure 4.1-8 First harmonic deviation at m_f equal 6 37
Figure 4.1-9 First harmonic deviation at m_f equal 6 37
Figure 4.1-10 THDi at asymmetrical SV modulation m_a=1.1547 38
Figure 4.1-11 THDi at symmetrical SV modulation m_a=1.1547 38
Figure 4.1-12 THDi at asymmetrical DS modulation m_a=1.547 38
Figure 4.1-13 THDi at symmetrical DS modulation m_a=1.1547 38
Figure 4.1-14: Best case scenario with m_f equal 6 and m_a equal 1.1547 40
Figure 4.1-15: Worst case scenario with m_f equal 6 and m_a equal 1.1547 40
Figure 4.1-16: Harmonic spectra for best and worst case of asymmetrical modulation m_f equal 6 and m_a equal 1.1547 41
Figure 4.1-17: THD_i with m_f equal 6 41
Figure 4.1-18: THD_i with m_f equal 9 41
Figure 5.1-1: Small and medium vectors with their belonging phase currents 43
Figure 5.1-2: Flowchart for deciding the values of f_1 and f_2 with SV prediction 46
Figure 5.1-3: Average neutral point current with f equal to 0 51
Figure 5.1-4: Average neutral point current with f equal to 1 51
Figure 5.1-5: Block diagram for PI controller 52
Figure 5.2-1: Two possible situations that may occur by adding an offset signal. A) Normal switching situation. B) Too big offset signal is added 55
Figure 5.3-1: Response with positive k_i 58
Figure 5.3-2: Response with negative k_i 58
Figur 5.3-3: Space Vector PI controller with different capacitor values 60
Figur 5.3-4: Space Vector proportional balancing with different capacitor values 60
Figur 5.3-5 Space Vector prediction balancing with different capacitor values 61
Figur 5.3-6: Double-Signal prediction balancing with different capacitor values 61
Figur 5.3-7: Double-Signal proportional balancing with different capacitor values 61
Figure 5.3-8: Space Vector PI controller balancing with unsymmetrical load 62
Figure 5.3-9: Space Vector proportional balancing with unsymmetrical load 62
Figure 5.3-10: Space Vector prediction balancing with unsymmetrical load 63
Figure 5.3-11: Double-Signal proportional balancing with unsymmetrical load 63
Figur 5.3-12: Double-Signal prediction balancing with unsymmetrical load 63
Figure 5.4-1: Flowchart of balancing in overmodulation 65

Figure 5.4-2: Currents that can be used for balancing at inductive load 65
Figure 5.4-3: Analytical calculation of the neutral point RMS current in overmodulation 67
Figure 5.4-4: Voltage oscillations in overmodulation 68
Figure 5.4-5: Maximum balancing in overmodulation 69
Figure 5.4-6: THD_i in overmodulation with balancing algorithm and a switching frequency of 1050 Hz 69
Figure 5.4-7: Time to remove an unbalance of 4000 V (c=1.8mF, Î=1000A) in overmodulation for asymmetrical Space Vector 70
Figure 5.4-8: 1^{st} harmonic line-to-line voltage at different shifts and modulation indexes 71
Figure 5.5-1: Time to remove an unbalance of 4000 V (c=1.8mF, Î=1000A) in overmodulation for Double-Signal 72
Figure 5.5-1: FPGA card in the laboratory 73
Figure 5.5-2: The three-level converter in the laboratory 73
Figure 6.1-1: Implementation in FPGA 74
Figure 6.1-2: Hexagon coordinate system 75
Figure 6.1-3: Large division of hexagon 75
Figure 6.1-4: Subdivision of hexagon 75
Figure 6.1-5: Sub subdivision of hexagon 75
Figure 6.2-1: Line-to-line output voltage with Space Vector at a modulation of 0.2 76
Figure 6.2-2: Line-to-line output voltage with Space Vector at a modulation of 1.0 77
Figure 6.2-3: Harmonic spectra of the line-to-line voltage of Space Vector with a modulation index of 0.2 78
Figure 6.2-4: Harmonic spectra of the line-to-line voltage of Space Vector with a modulation index of 1.0 79
Figure 6.2-5: Line-to-line output voltage with Double-Signal at a modulation of 0.2 79
Figure 6.2-6: Line-to-line output voltage with Double-Signal at a modulation of 1.0 80
Figure 6.2-7: Harmonic spectra of the line-to-line voltage of Double-Signal with a modulation index of 0.2 81
Figure 6.2-8: Harmonic spectra of the line-to-line voltage of Double-Signal with a modulation index of 1.0 81
Figure 6.4-1: Line-to-line voltage with a m_a equal 1.334 83
Figure 6.4-2: Line-to-line voltage with a m_a equal 1.30 84
Figure 6.5-1: Simulations of the capacitor voltages equal the values in the laboratory 85

1 Introduction

Multilevel converters have the later years been looked upon as a good choice for medium- and high-voltage applications. It was first presented in [22]. Before the introduction of multilevel converters the traditional solution has been to connect semiconductors in series to withstand the high voltages. This requires fast switching to avoid unequal voltage sharing between the devices, which could lead to a breakdown. Multilevel converters have the advantage of clamping the voltages, which prevents the need of fast switching. MLC also have a smoother output voltage than traditional two-level converters. As wind turbines are increasing in power ratings, multilevel converters can be well suited in such applications.

The most popular multilevel converter and the one that will be studied in this report is the neutral point clamped three-level converter. One of the challenges with the NPC three-level converter is the increased complexity in the control of it. A lot of research have been done on this converter topology and a numerous of control methods have been presented in the literature. Still there is a focus of how to solve the voltage fluctuation between the two capacitors and most of the research today is to improve the DC-bus balance.

The focus in this master thesis will be to continue the work from the project in the fall of 2009, where DC-bus balancing, balancing in overmodulation, development of current equations and laboratory experiments are the most central topics. There will also be a comparison of asymmetrical and symmetrical modulation. DC-bus balancing was studied in detail in the previous project and in this master thesis a PI controller is included. The reason for studying the currents is to see if exist any difference which could increase the stresses on the capacitors and conductors.

One of the goals of the project was to verify that SIMULINK and PSCAD gave the same simulations results and it was concluded that this is the case. Hence in this project some of the simulations are done in SIMULINK while others are done in PSCAD. Further on will Space Vector and Double-Signal be implemented and tested in a laboratory setup. In this setup also symmetrical and asymmetrical modulation will be tested as well as overmodulation.

Some of the text written in [13] will be repeated in this master thesis.

1.1 Converter Topology

The converter studied in this project is a Neutral-Point-Clamped three-level converter with three bridge legs. “Three-level” means that each bridge leg, A, B and C can have three different voltage states. The converter topology can be seen in Figure 1.1-1. Switch 1 and 3 on each leg are complementary, which means that when switch 1 is on, switch 3 is off and vice versa. Switch 2 and 4 is the other complementary switching pair.

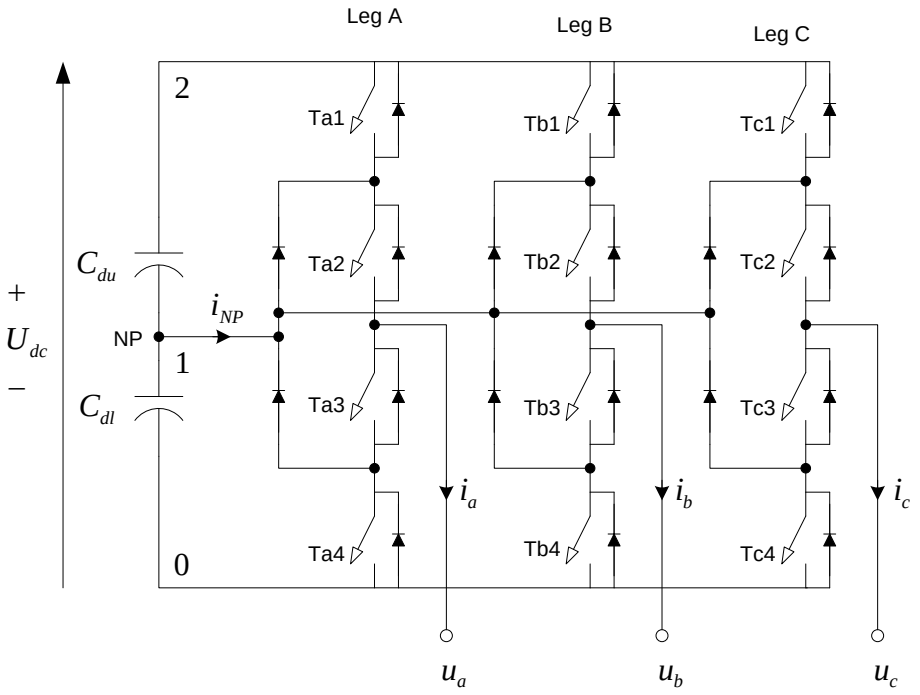

Figure 1.1-1: Converter topology

If each of the capacitors has a constant voltage of 0.5 U_{dc}, then having the two upper switches on will give an output voltage of U_{dc} compared to level 0, switch 2 and 3 on will give 0.5 U_{dc} and by having the two lower switches on, an output voltage of 0 will occur. In addition to these three states there is a forbidden state where the first switch is on while the second is off.

Table 1.1-1: Bridge leg voltages at different combinations of switch states

Leg State	U_{a0}	T_{a1}	T_{a2}	T_{a3}	T_{a4}
2	U_{dc}	ON	ON	OFF	OFF
1	0.5 U_{dc}	OFF	ON	ON	OFF
0	0	OFF	OFF	ON	ON

The combination of states for the bridge legs give the space vectors plotted in Figure 1.1-2. Space vector 210 means that bridge leg A is in state 2, leg B in state 1 and leg C in state 0. Some of the switching states give the same space vector as is seen for the inner vectors. All the modulation strategies discussed in the subsequent chapters use combinations of these switching states. The difference between the modulation strategies is the combinations of states and their respective extent.

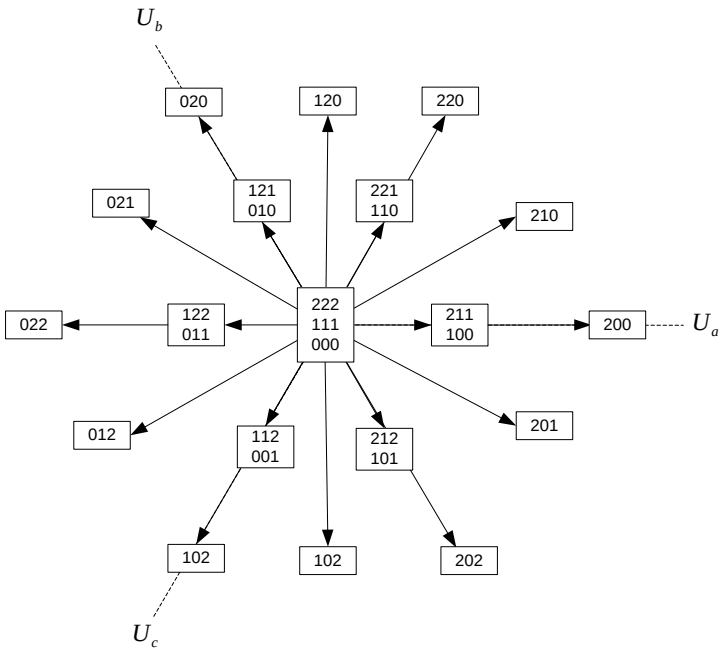

Figure 1.1-2: Overview of space vectors

In Figure 1.1-3 there is a smooth sinusoidal signal. The other signal is the output of a bridge leg trying to resemble this signal. By combining the different states a bridge leg can have it is possible to get a close to sinusoidal averaged bridge leg output. The voltage between two phases, the line-to-line voltage can achieve five different voltage levels:

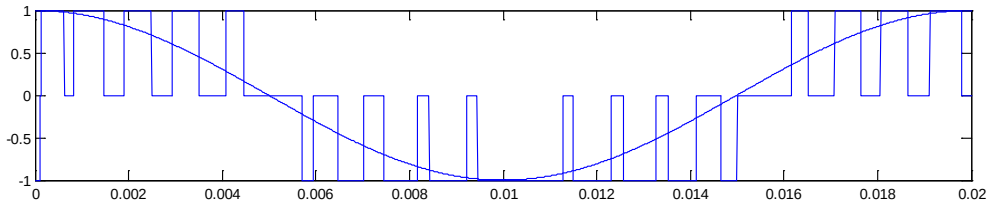

Figure 1.1-3: Bridge leg voltage

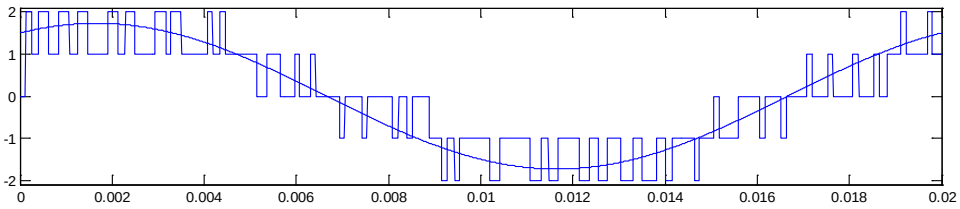

Figure 1.1-4: Line-to-line voltage

Converters with a higher number of levels will give a smother output of the converter. However it makes it more difficult to control and it's outside the scope of this master thesis.

In order to get the model as close as possible to real implementation parameters concerning minimum on/off-time and dead time are included. Dead time is included to avoid the possibility of short circuiting the DC-side. In other words will not the complementary switch be turned on before the other switch has been off for at least the dead time. Minimum on- and off-time is the minimum time a switch has to be on or off in order to switch. For instance if a switch is supposed to be turned on, but will not be on as long as the minimum time, then it should just be kept off. The gain of the output voltage to have the switch on for such a short time compared to the switching losses is very low or might be negative. With non-ideal switch there is also a limit of how fast a switch can be turned on and off, hence it might need the minimum on/off-time.

The control of the switches is done in periods named triangular periods. In one period there is a maximum of one turn on and one turn off of a switch. The time a switch is on in a period relative to the length of the period is the duty cycle of the switch.

$$d_{ij} = \frac{t_{on}}{T_{tri}}, i = \{a,b,c\},\ j = \{1,2\} \tag{1.1}$$

These duty cycles range between 0 and 1. The duty cycles of switch 3 and 4 for the bridge leg is not defined since they are complementary to switch 1 and 2. Meaning the duty cycle of switch 3 is one minus the duty cycle of switch 1. Modulation is done by calculations of these duty cycles. If it is assumed that each of the capacitors has the same voltage $U_{dc}/2$; the bridge leg voltage can be expressed as:

$$U_{a0} = \frac{U_{dc}}{2} d_{a2} + \frac{U_{dc}}{2} d_{a1}, d_{a2} > d_{a1} \tag{1.2}$$

However when there is only one power supply the voltages over each of the capacitors will fluctuate. This is due to the neutral point current, i_{NP} seen in Figure 1.1-1. By defining ΔU_{dc} as the voltage difference between the upper and lower capacitor voltage it was shown in [13] that the bridge leg voltage can be defined as

$$U_{i0} = \left(\frac{U_{dc}}{2} - \frac{\Delta U_{dc}}{2}\right) d_{i2} + \left(\frac{U_{dc}}{2} + \frac{\Delta U_{dc}}{2}\right) d_{i1}, i = \{a,b,c\} \tag{1.3}$$

The voltages of importance when it comes to output of the converter are the line-to-line voltages and the phase voltages. The line-to-line voltage from A to B is:

$$U_{ab} = U_{a0} - U_{b0} \tag{1.4}$$

From the equation it can be seen that due to the opposite sign any equal offset added to all the bridge leg voltages will be cancelled for the line-to-line voltages. This is utilized to get enhanced modulation in most of the modulation strategies as discussed in [13]. If the

expressions in (1.3) are inserted in (1.4) a line-to-line voltage as function of DC-bus unbalance and switch duty cycles is achieved:

$$U_{ab} = \frac{1}{2}U_{dc}(d_{a2} + d_{a1} - d_{b2} - d_{b1}) + \underbrace{\frac{1}{2}\Delta U_{dc}(d_{a1} - d_{a2} + d_{b2} - d_{b1})}_{\text{Voltage error}} \tag{1.5}$$

The first term on the right hand side is the line-to-line voltage at DC-bus balance. The modulating strategies base their calculations on DC-bus balance. Hence the output of the converters will have an error represented by the second term in the equation. To minimize this error there is a need for DC-bus balancing. This is done by control of the neutral point current. The control of the neutral point current is related to the choice and extent of the switching states. This is done by adding additional conditions to the calculation of switch duty cycles for the different modulation strategies.

2 Modulation Strategies

In [13] some of the different modulation methods for a three-level converter were studied in detail. Some of what was written in [13] will be repeated in this master thesis to get a better overall picture of this topic.

2.1 Pulse-Width Modulation

Pulse width modulation is a method of controlling the output voltage of an inverter. In this method a control signal is compared with a repetitive signal, typical a triangular signal. To make the converter work in an inverter mode the control signal should have a sinusoidal shape. This control signal can vary a bit and this will be discussed in [13]. At a constant switching frequency the time period of the triangular signal is also constant since this signal gives the switching frequency. This is given in equation (2.1).

$$f_{sw} = \frac{1}{T_{tri}} \tag{2.1}$$

The frequency of the control signal gives the frequency of the desired fundamental output voltage. For a two-level converter there are two switches in one bridge leg and the upper switch will be on when the control signal is greater than the triangular signal. If unipolar switching is chosen the lower switch will be off when the upper is on, which means that it will be off when the control signal is greater than the triangular signal. Switch number 2 will be on when the control signal is lower than the triangular and hence the upper switch will be off. This is shown in the figure below.

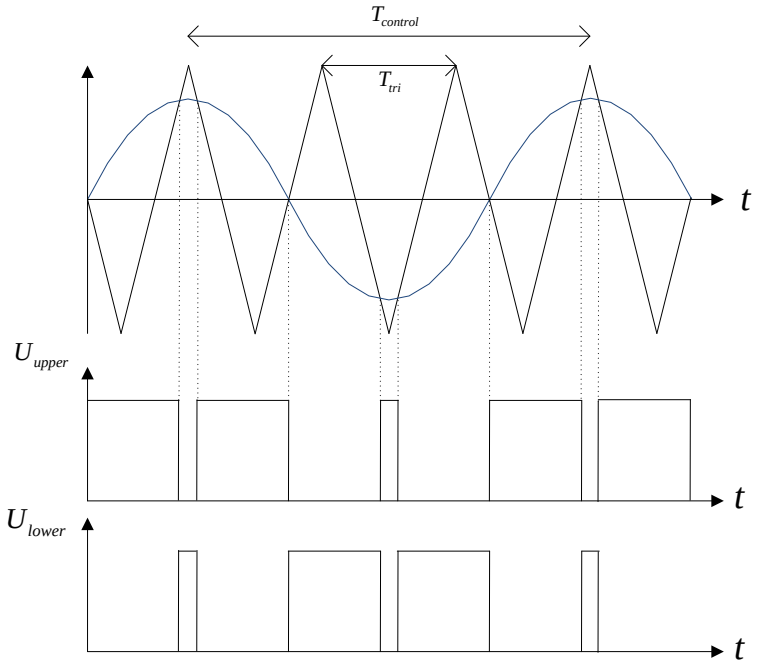

Figure 2.1-1: PWM with bipolar switching pattern

As it will be seen in the next subchapters the control is a bit more complicated when a three-level converter is being used. More about two-level converter control is to be found in [8]. There are a few parameters that need to be defined when PWM is discussed. The amplitude ratio is given as

$$m_a = \frac{\hat{U}_{cont}}{\hat{U}_{tri}} \tag{2.2}$$

This ratio tells the value of the amplitude of the bridge leg voltage compared to $U_{DC}/2$. This parameter is a part of the control signals which are given in the equation below.

$$\begin{aligned} U_{sta} &= m_a \cdot \cos(\omega t) \\ U_{stb} &= m_a \cdot \cos(\omega t - 2\pi/3) \\ U_{stc} &= m_a \cdot \cos(\omega t - 4\pi/3) \end{aligned} \tag{2.3}$$

These voltages are the bridge-leg voltages that are desired on the AC-side of the converter. When normal sinusoidal modulation is used these signals are also the control signals which are compared with the triangular signal. Other methods could be by injection the 3rd harmonic voltage to each phase or by adding a common offset, which are described in [3]. Space vector and Double-Signal are the two methods used in this master thesis and they are described in the next two subchapters.

The other parameter that is important to be defined is the ratio between the frequency of the control signal and the triangular signal.

$$m_f = \frac{f_{sw}}{f_{control}} \tag{2.4}$$

It is common to divide the modulation strategies into two strategies and which one that is preferred is depending on m_f. In [8] it is recommended to use synchronous modulation if m_f is lower or equal to 21 and asynchronous modulation if m_f is above this value. The definition of synchronous modulation is that m_f is an integer, which gives that the control signal is sampled at the same angles every fundamental period. The definition of asynchronous modulation is that m_f is not an integer. Asynchronous modulation will create undesirable subharmonics, but due to the high frequency the difference in amplitude between synchronous and asynchronous subharmonics will be marginal. This is according to [8].The major drawback of synchronous modulation is that it is not very flexible and hence there will be some challenges in applications with variable speed drives. With asynchronous modulation this should not cause problems as long as m_f is large.

The application studied in this report is to be used in the medium voltage range and the switching frequency will be in the area from 300 – 1100 Hz, which indicates that synchronous modulation should be used. Having a low switching frequency will increase the amplitude of the lower harmonics. This occurs because the harmonic distortion has the greatest values

around m_f, $2m_f$, $3m_f$ and so on, and since the switching frequency is reduced m_f is also reduced.

2.2 Space Vector PWM

Space vector PWM is a popular modulation method for converters, due to its low harmonics and increased linear range up to a m_a equal to 1.1547. The theory of space vector is that phase A, B and C has a permanent position to each other in the vector space, phase shifted with 120 degrees. This can be seen in Figure 2.2-1. U_a, U_b and U_c are varying as in equation (2.3). The reference voltage is defined as

$$\underline{U}_{ref}^{\zeta}(t) = U_{sta}(t)e^{j0} + U_{stb}(t)e^{j2\pi/3} + U_{stc}(t)e^{j4\pi/3} \tag{2.5}$$

For a two-level converter there exist eight switching states. Two of these states are zero vectors, which gives seven different states that can be used to generate the wanted output voltage. A zero vector is when all the bridge legs are connected to the same point and all of the line-to-line voltages are zero. The six non-zero vectors have all the same amplitude, but different angles. By using these vectors in a correct manner the average of them will be the reference vector, by saying that the switching frequency is much higher than the fundamental frequency. A three-level converter has 27 vectors that can be used to create the desired voltage, with 19 different states, which can be seen in Figure 2.2-1.

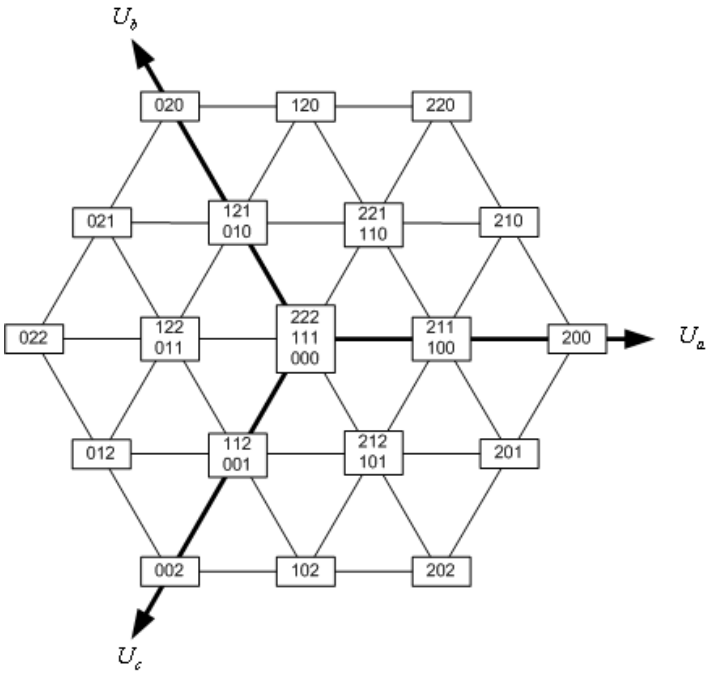

Figure 2.2-1: Space vector diagram for a three-level converter

There are four different groups the vectors can be divided into, and within each group the magnitude of the vectors are the same. The overview of the vectors is given in Table 2.2-1.

Table 2.2-1: Overview of space vectors

Zero vectors	Small vectors	Medium vectors	Large vectors
(000)	(100),(211),(110),(221),	(210),(120)	(200),(220)
(111)	(121),(010),(011),(122),	(021),(012)	(020),(022)
(222)	(001),(112),(101),(212)	(102),(201)	(002),(202)

The vectors are the following

$$U_s = \frac{1}{3} U_{DC} \cdot e^{j\theta}$$
$$U_m = \frac{1}{\sqrt{3}} U_{DC} \cdot e^{j\theta} \quad (2.6)$$
$$U_l = \frac{2}{3} U_{DC} \cdot e^{j\theta}$$

Where U_{DC} is the DC-link voltage.

There are a lot of vectors to choose among for a three-level converter, and the normal way of solving this is to choose the three vector states closest to the reference vector when using Space Vector modulation. The reason for this is that the harmonic distortion will be the lowest with this choice. By doing this, the vector space can be divided into 24 different sectors. How to find the correct sector can be done several ways, where they all lead to the same result. The method chosen for the simulations in this master thesis is the same as in [1] and [4]. Here the vector space is divided into six new hexagons as shown in the figure below.

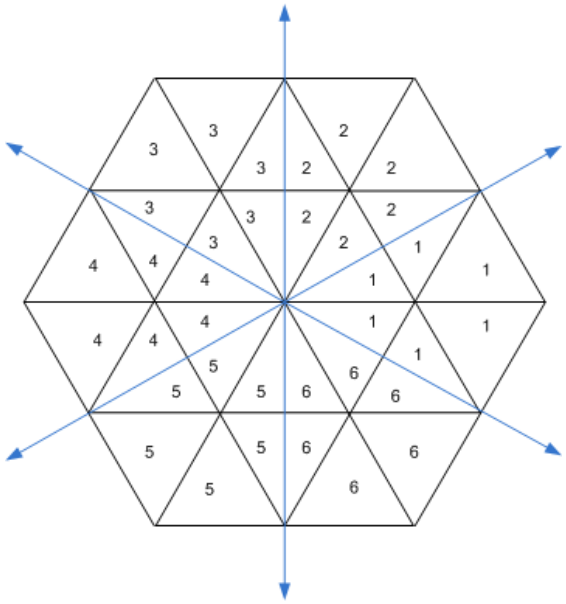

Figure 2.2-2: Overview of hexagons

When the correct sector has been found, the duty cycles of the vectors have to be calculated. Finding the duty cycles for a three-level converter is more complicated than for a two-level. As long as the reference vector stays within the six inner sectors, the duty cycles can be calculated the same way as for a two-level, which is shown in Figure 2.2-3.

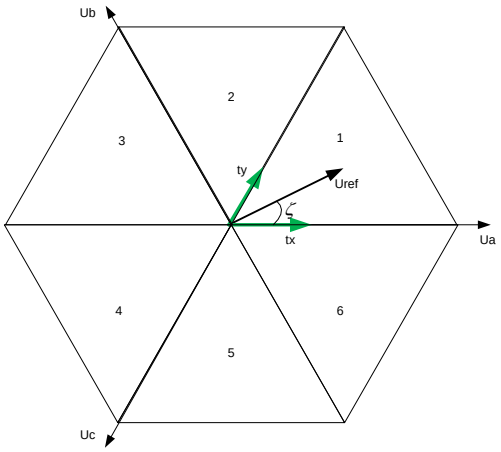

Figure 2.2-3: Duty cycle calculations for the six inner hexagons

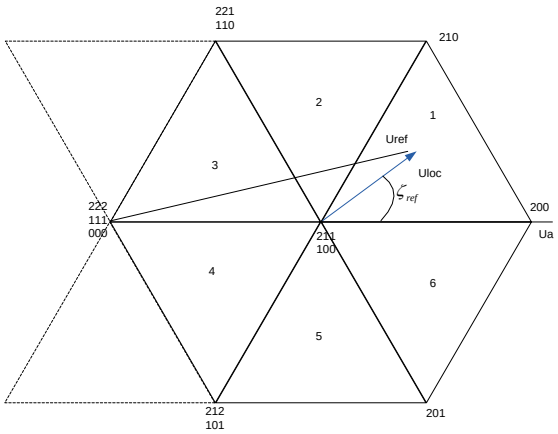

Figure 2.2-4: Duty cycle calculations outside the six inner hexagons

The equations are shown as the following

$$\begin{aligned} t_x &= \sqrt{3}\left|U_{ref}\right|\sin(60^o-(\zeta-(\text{sec\_}in-1)\cdot 60^o)) \\ t_y &= \sqrt{3}\left|U_{ref}\right|\sin(\zeta-(\text{sec\_}in-1)\cdot 60^o) \\ t_0 &= 1-t_x-t_y \end{aligned} \tag{2.7}$$

T_x is the duty cycle for the vector lagging the reference vector, while t_y is the duty cycle for the vector leading the reference vector. T_0 is the duty cycle for the zero vectors. If the reference vector is outside the six inner hexagons then one common method calculation the on-times is making a local reference vector as shown in Figure 2.2-4. The on-times will den be as shown below.

$$\begin{aligned} t_x &= \frac{2}{\sqrt{3}}\left|U_{loc}\right|\sin(60^o-(\zeta_{ref}-(\text{sec}-1)\cdot 60^o)) \\ t_y &= \frac{2}{\sqrt{3}}\left|U_{loc}\right|\sin(\zeta_{ref}-(\text{sec}-1)\cdot 60^o) \\ t_0 &= 1-t_x-t_y \end{aligned} \tag{2.8}$$

This is described more in detail in [13].

The switching pattern should be designed in a way which minimizes the number of switching transitions. In this report the aim has not been to minimize the number of switching transitions, but to be able to balance the DC-bus. Hence there are several switching patterns that can be used.

There are in total 7 vectors available if the reference vector is inside the first sector among the six inner hexagons. The switching pattern used in this report takes all of the vectors into use, the same approach as in [1]. The switching pattern will then be as shown below.

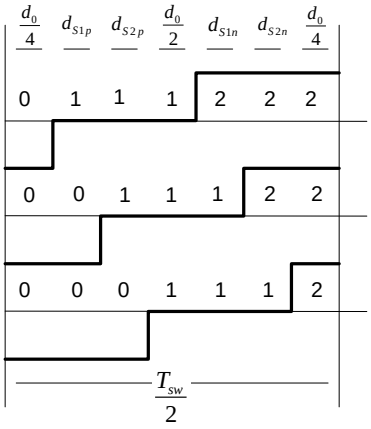

Figure 2.2-5: Switching pattern for space vector modulation

This figure is showing half of the switching sequences for a reference vector staying inside sector 1 among the six inner hexagons. It is starting off with vector 000 and moving on to 100 and so on, such that there is one switching transition between every new vector, for instance not to use the order 000, 200, 100 and 210. With this switching pattern all the vectors are being used, and the possibility of using the vector redundancy is maximized. The major drawback of using all of the vectors is that there will be an increase in the switching losses. At least should either 000 or 222 be removed since they give the same state. Hence other methods should be considered such that the switching losses may be reduced.

The method that would require the least amount of commutations having the reference vector inside sector 1 could be 222, 221, 211, 221 and 222 which is defined as modified space vector modulation according to [17], while the classical method is 222, 221, 211, 111, 211, 221 and 222. Even though the modified version has less switching transitions, it is concluded in [17] that the method produces more harmonics in the lower modulation area compared to classical space vector modulation, and thus the classical version is preferred. The very clear disadvantage with this switching scheme is that there is no possibility of DC-bus balancing. If it should be used with only one DC-source then other vectors must be used in order to have some redundancy. In [17] it is suggested that there are two switching patterns that could be used alternatively. First 111, 211, 221 and 222, and the second alternative is 111, 110, 100 and 000. It is shown in [18] and [19] that natural balancing occurs at steady-state if there is resistance in the phase loads and if correct switching frequency is chosen. Hence this last alternative could be used if the correct conditions are present. If not, then at least one vector pair should be used during one switching period. Then the switching pattern with the classical method would look like 222, 221, 211, 111 and 110. This switching pattern improves the balancing possibilities, but if the balancing algorithm should be optimized the switching pattern in Figure 2.2-5 has to be used, but 222 should be skipped.

2.2.1 Current Flow with Space Vector PWM

In this report there have been developed equations of the current flowing in this converter in order to get a better understanding of the two modulation methods. The mathematic expressions for the currents are quite long when using Space Vector.

Figure 2.2-6, Figure 2.2-7 and Figure 2.2-8 show the phase currents out of each of the levels 0, 1 and 2 due to a switch state in the vector space. The sum of currents i_a, i_b and i_c is treated as zero. Zero vectors [000], [111] and [222] are neglected in the calculations since they connect all currents to the same level and they cancel each other. Having the sum of the phase currents equal to zero also mean that the sum of two of them is equal to the negative of the third. As an example: Switch state [220] connects i_a and i_b to level 2. The sum of these two is equal to $-i_c$. Hence this current is treated when looking at the switch state [220]'s contribution to a current out of level 2.

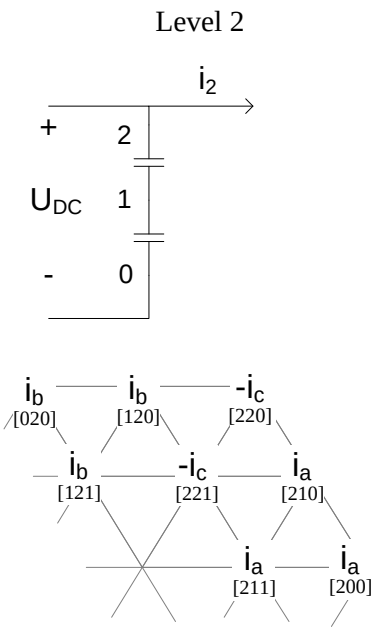

Figure 2.2-6 Phase currents out of level 2 due to switch state

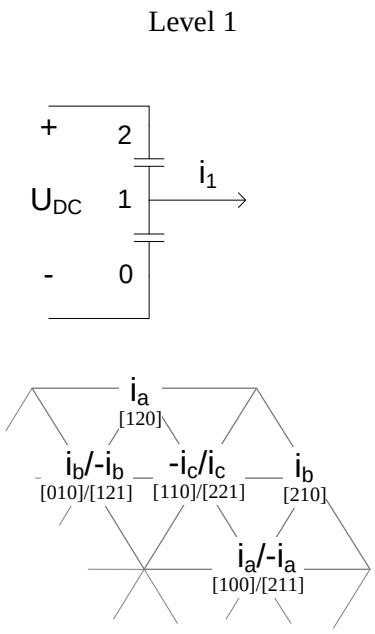

Figure 2.2-7 Phase current out of level 1 (neutral point) due to switch state

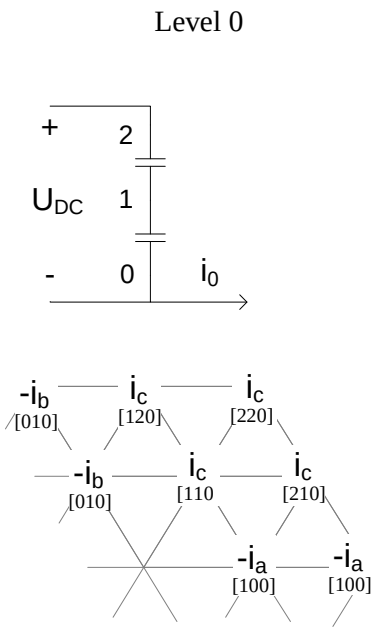

Figure 2.2-8 Phase current out of level 0 due to switch state

From [14] formulas for calculation of space vector duty cycles are found. These are seen in the sector diagram of Figure 2.2-9. Each of the sectors is numbered in the same manner as in [14]. Formula (2.9) relates these formulas to the reference index m and angle ζ.

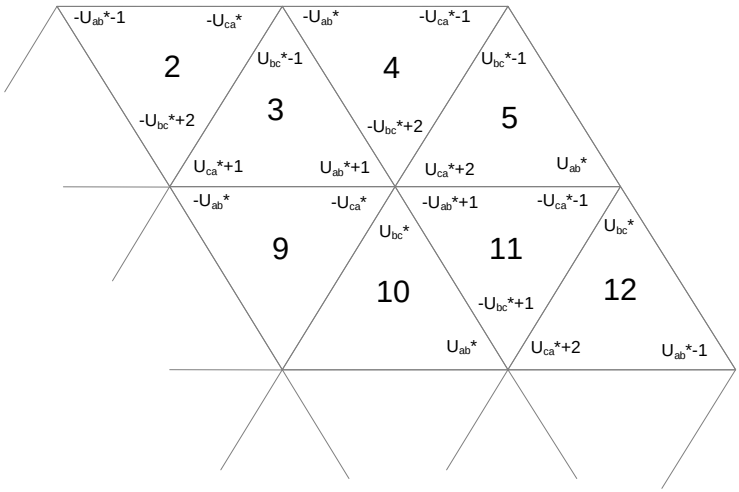

$$U_{ab}* = \sqrt{3}m\left(\frac{\sqrt{3}}{2}\cos\varsigma - \frac{1}{2}\sin\varsigma\right)$$
$$U_{bc}* = \sqrt{3}m\sin\varsigma \quad (2.9)$$
$$U_{ca}* = \sqrt{3}m\left(-\frac{\sqrt{3}}{2}\cos\varsigma - \frac{1}{2}\sin\varsigma\right)$$

Figure 2.2-9 Space vector Duty Cycles

The instantaneous current out of level 2 is expressed at infinite switching frequency as a function of the reference angle ζ, the phase delay φ and the modulation index m in formula (2.9). $i_{2[ABC]}$ is the phase current out of level 2 due to switch state [ABC]. $d_{[ABC]}$ is the duty cycle of this switch state. The instantaneous current is the sum of the currents in level 2 due to switch states in the current sector.

$$i_2(\zeta,\varphi,m) = \sum i_{2[ABC]}(\zeta,\varphi)d_{[ABC]}(\zeta,m) \quad (2.10)$$

As an example the current out of level 2 when the reference is in sector 10, the first inner sector is:

$$i_2(\zeta,\varphi,m) = i_a \cdot d_{[211]} - i_c \cdot d_{[221]} = \underbrace{\hat{I}_{phase}\cos(\zeta-\varphi)}_{\hat{i}_a}\cdot\underbrace{U_{ab}*\cdot f}_{d_{[211]}} - \underbrace{\hat{I}_{phase}\cos(\zeta-\varphi)}_{\hat{i}_c}\cdot\underbrace{U_{bc}*\cdot f}_{d_{[221]}} \quad (2.11)$$

f is a constant between [0,1] that shares the space vector duty cycles between two redundant states. When there is no DC-bus balancing this will imply that f is equal to ½. The sharing of redundant states depends on the DC-bus balancing strategy, the unbalance of the capacitors and the phase delay of the phase currents. It is unlikely that f will have the same value throughout a fundamental period. However f could have a constant value during a fundamental period if there is a large voltage unbalance.

The large and medium space vectors seen as the outermost space vectors in the space vector diagram and can only be produced by one switch state each. Hence there is no need for a sharing constant.

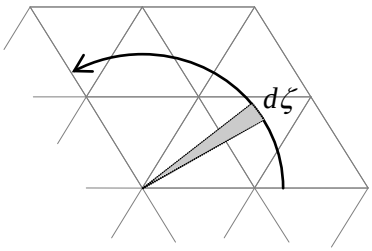

Figure 2.2-10 Variable of integral calculations

Calculation of average and RMS currents are in this report done by integral calculations in the vector space over the reference angle ζ. Only the first 1/3 of a fundamental period is looked at due to symmetries over a period. The integral over 1/3 of a period is the sum of integrals over each part of a sector that the reference crosses. The sectors that are crossed and the angle they are crossed at vary with modulation index m. The sector diagram is divided into modes as in [14] depending on what sectors that are crossed. This is shown in Figure 2.2-11. Mode four depends on the modulation strategy at overmodulation and neutral point current will be looked upon later in this report. M equals m_a in all of the calculations.

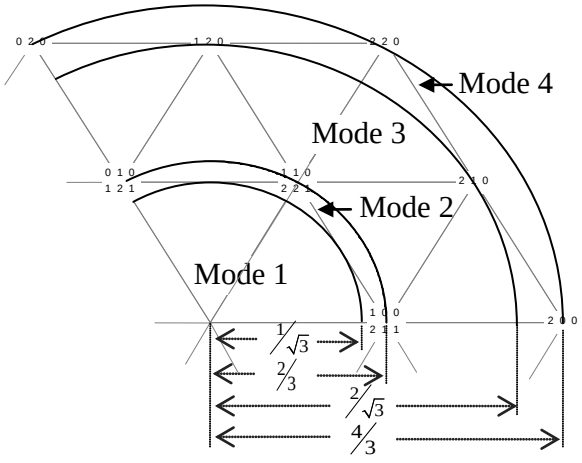

Mode 1: $0 < m < 1/\sqrt{3}$

Mode 2: $1/\sqrt{3} < m < 2/3$

Mode 3: $2/3 < m < 2/\sqrt{3}$

Mode 4: $2/\sqrt{3} < m < 4/3$

Figure 2.2-11: Separation of the vector space into modes

2.2.2 RMS Current Level 2

The RMS current out of level two is the square root of the sum of integrals over each of the sectors that are crossed:

$$I_{2rms} = \sqrt{\frac{1}{2\pi/3}\int_0^{2\pi/3} {i_2}^2(\zeta,\varphi,m)d\zeta} = \sqrt{\frac{1}{2\pi/3}\sum\int\sum {i_{2[ABC]}}^2(\zeta,\varphi)d_{[ABC]}(\zeta,m)d\zeta} \qquad (2.12)$$

Note that only expressions of phase currents are squared. The duty cycles are related to how long a phase current is connect to level 2 due to a switch state and should not be squared.

Mode 1 (0 < m < 1/√3)

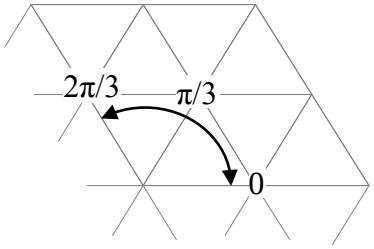

Figure 2.2-12: Reference vector mode 1

In this mode the RMS current is calculated in two integrals: from 0 to π/3 and from π/3 to 2π/3. The RMS expression is normalized by division of the phase current amplitude. The duty cycles of the switch states and the phase currents that are connected to level 2 is found in Figure 2.2-9. In this mode there are only small vectors and the reference vector will only stay within two sectors, and therefore the calculation only consists of two integrals.

$$\frac{I_{2\,rms}}{\hat{I}_{phase}} = \left(\frac{3}{2\pi} \left(\int_{0}^{\frac{\pi}{3}} \underbrace{\sqrt{3}m\left(\frac{\sqrt{3}}{2}\cos(\zeta) - \frac{1}{2}\sin(\zeta)\right)}_{d([211])} f \cdot \underbrace{\cos^2(\zeta-\varphi)}_{i_a^2} + \underbrace{\sqrt{3}m \cdot \sin(\zeta)}_{d([221])} f \cdot \underbrace{\left(-\cos\left(\zeta-\varphi-\frac{4\pi}{3}\right)\right)^2}_{(-i_c)^2} d\zeta + \int_{\frac{\pi}{3}}^{\frac{2\pi}{3}} \underbrace{-\sqrt{3}m\left(-\frac{\sqrt{3}}{2}\cos(\zeta) - \frac{1}{2}\sin(\zeta)\right)}_{d([221])} f \cdot \underbrace{\left(-\cos\left(\zeta-\varphi-\frac{4\pi}{3}\right)\right)^2}_{(-i_c)^2} + \int_{\frac{\pi}{3}}^{\frac{\pi}{3}} \underbrace{-\sqrt{3}m\left(\frac{\sqrt{3}}{2}\cos(\zeta) - \frac{1}{2}\sin(\zeta)\right)}_{d([121])} f \cdot \underbrace{\cos^2\left(\zeta-\varphi-\frac{2\pi}{3}\right)}_{i_b^2} d\zeta \right) \right)^{\frac{1}{2}} \tag{2.13}$$

The results are presented in (2.16)

Mode 2: (1/√3 < m < 2/3)

In this mode both small and medium vectors will be used to create the desired voltage. The angle where a sector border is crossed is expressed by β in addition to the π/3 intervals as illustrated in Figure 2.2-13. β is found in [14] and normalized to have the same the scaling of m as in the rest of this report.

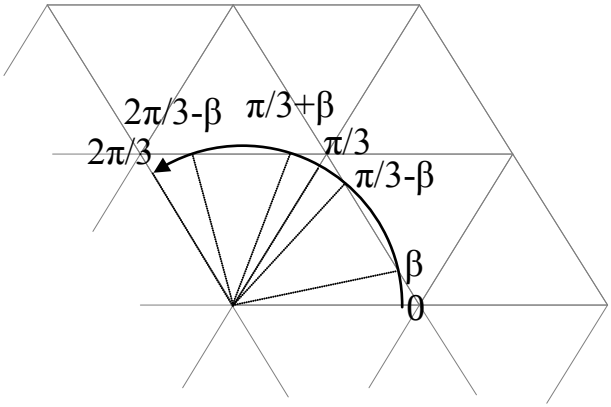

$$\beta = \sin^{-1}\left(\frac{1}{\sqrt{3}m}\right) - \frac{\pi}{3}$$

Figure 2.2-13: Reference vector in mode 2

In this mode the calculation will consist of six integrals. In the first part there will only be two small vector pairs while in the next part there will be two small vector pairs and one medium vector. The third integral will be equal the first one only with new integral calculations limits. The next three integrals will have the same pattern.

$$\frac{I_{2rms}}{\hat{I}_{phase}} = \frac{3}{2\pi}\left(\begin{array}{l}
\int_{0}^{\sin^{-1}\left(1/\sqrt{3m}\right)-\frac{\pi}{3}} \left(\begin{array}{l} \underbrace{\sqrt{3m}\left(\frac{\sqrt{3}}{2}\cos(\zeta)-\frac{1}{2}\sin(\zeta)\right)}_{d([211])} f\cdot\underbrace{\cos^2(\zeta-\varphi)}_{i_a^2} \\ +\underbrace{\sqrt{3m}\cdot\sin(\zeta)}_{d([221])} f\cdot\underbrace{\left(-\cos\left(\zeta-\varphi-\frac{4\pi}{3}\right)\right)^2}_{(-i_c)^2} \end{array}\right) d\zeta + \\
\int_{\sin^{-1}\left(1/\sqrt{3m}\right)-\frac{\pi}{3}}^{\frac{\pi}{3}-\left(\sin^{-1}\left(1/\sqrt{3m}\right)-\frac{\pi}{3}\right)} \left(\begin{array}{l} \left(\underbrace{\left(-\sqrt{3m}\cdot\sin(\zeta)+1\right)}_{d([211])} f\ \underbrace{-\sqrt{3m}\left(-\frac{\sqrt{3}}{2}\cos(\zeta)-\frac{1}{2}\sin(\zeta)\right)-1}_{d([210])}\right)\underbrace{\cos^2(\zeta-\varphi)}_{i_a^2} \\ +\left(\underbrace{-\sqrt{3m}\left(\frac{\sqrt{3}}{2}\cos(\zeta)-\frac{1}{2}\sin(\zeta)\right)+1}_{d([221])}\right) f\cdot\underbrace{\left(-\cos\left(\zeta-\varphi-\frac{4\pi}{3}\right)\right)^2}_{(-i_c)^2} \end{array}\right) d\zeta + \\
\int_{\frac{\pi}{3}-\left(\sin^{-1}\left(1/\sqrt{3m}\right)-\frac{\pi}{3}\right)}^{\frac{\pi}{3}} \left(\begin{array}{l} \underbrace{\sqrt{3m}\left(\frac{\sqrt{3}}{2}\cos(\zeta)-\frac{1}{2}\sin(\zeta)\right)}_{d([211])} f\cdot\underbrace{\cos^2(\zeta-\varphi)}_{i_a^2} \\ +\underbrace{\sqrt{3m}\cdot\sin(\zeta)}_{d([221])} f\cdot\underbrace{\left(-\cos\left(\zeta-\varphi-\frac{4\pi}{3}\right)\right)^2}_{(-i_c)^2} \end{array}\right) d\zeta + \\
\int_{\frac{\pi}{3}}^{\frac{\pi}{3}+\left(\sin^{-1}\left(1/\sqrt{3m}\right)-\frac{\pi}{3}\right)} \left(\begin{array}{l} \underbrace{-\sqrt{3m}\left(-\frac{\sqrt{3}}{2}\cos(\zeta)-\frac{1}{2}\sin(\zeta)\right)}_{d([221])} f\cdot\underbrace{\left(-\cos\left(\zeta-\varphi-\frac{4\pi}{3}\right)\right)^2}_{(-i_c)^2} \\ +\underbrace{-\sqrt{3m}\left(\frac{\sqrt{3}}{2}\cos(\zeta)-\frac{1}{2}\sin(\zeta)\right)}_{d([121])} f\cdot\underbrace{\cos^2\left(\zeta-\varphi-\frac{2\pi}{3}\right)}_{i_b^2} \end{array}\right) d\zeta + \\
\int_{\frac{\pi}{3}+\left(\sin^{-1}\left(1/\sqrt{3m}\right)-\frac{\pi}{3}\right)}^{\frac{2\pi}{3}-\left(\sin^{-1}\left(1/\sqrt{3m}\right)-\frac{\pi}{3}\right)} \left(\begin{array}{l} \left(\underbrace{\sqrt{3m}\left(\frac{\sqrt{3}}{2}\cos(\zeta)-\frac{1}{2}\sin(\zeta)\right)+1}_{d([221])}\right) f\cdot\underbrace{\left(-\cos\left(\zeta-\varphi-\frac{4\pi}{3}\right)\right)^2}_{(-i_c)^2} \\ +\left(\underbrace{\sqrt{3m}\cdot\sin(\zeta)-1}_{d([120])}+\left(\underbrace{\sqrt{3m}\left(-\frac{\sqrt{3}}{2}\cos(\zeta)-\frac{1}{2}\sin(\zeta)\right)+1}_{d([121])}\right) f\right)\cdot\underbrace{\cos^2\left(\zeta-\varphi-\frac{2\pi}{3}\right)}_{i_b^2} \end{array}\right) d\zeta + \\
\int_{\frac{2\pi}{3}-\left(\sin^{-1}\left(1/\sqrt{3m}\right)-\frac{\pi}{3}\right)}^{\frac{2\pi}{3}} \left(\begin{array}{l} \underbrace{-\sqrt{3m}\left(-\frac{\sqrt{3}}{2}\cos(\zeta)-\frac{1}{2}\sin(\zeta)\right)}_{d([221])} f\cdot\underbrace{\left(-\cos\left(\zeta-\varphi-\frac{4\pi}{3}\right)\right)^2}_{(-i_c)^2} \\ +\underbrace{-\sqrt{3m}\left(\frac{\sqrt{3}}{2}\cos(\zeta)-\frac{1}{2}\sin(\zeta)\right)}_{d([121])} f\cdot\underbrace{\cos^2\left(\zeta-\varphi-\frac{2\pi}{3}\right)}_{i_b^2} \end{array}\right) d\zeta
\end{array}\right) \tag{2.14}$$

Mode 3 (2/3 < m < 2/√3)

Mode 3 is the most complicated of the three modes. In this case the reference vector will be inside 6 sectors during the integral limits and 18 sectors during one fundamental period. Note that in this mode the expression of β is the same as in the previous section, but the signs have changed.

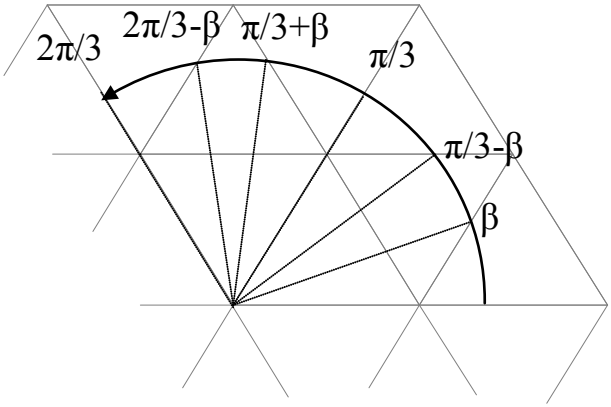

$$\beta = -\sin^{-1}\left(\frac{1}{\sqrt{3}m}\right) + \frac{\pi}{3}$$

Figure 2.2-14: Reference vector mode 3

In the first integral there will be a contribution from one small vector pair and one medium vector. The same goes for integral number 3, 4 and 6. In the two other integrals there are two vector pairs and one medium vector contribution to the current in level 2.

$$\frac{I_{2\,rms}}{\hat{I}_{phase}} = \frac{3}{2\pi}\left(\int_{0}^{-\sin^{-1}\left(\frac{1}{\sqrt{3m}}\right)+\frac{\pi}{3}}\left(\underbrace{\sqrt{3m}\left(\frac{\sqrt{3}}{2}\cos(\zeta)-\frac{1}{2}\sin(\zeta)\right)}_{d(\{200\})}-1+\underbrace{\sqrt{3m}\cdot\sin(\zeta)}_{d(\{210\})}+\left(\underbrace{\sqrt{3m}\left(-\frac{\sqrt{3}}{2}\cos(\zeta)-\frac{1}{2}\sin(\zeta)\right)+2}_{d(\{211\})}\right)f\right)\cdot\underbrace{\cos^2(\zeta-\varphi)}_{i_a^2}\,d\zeta+\right.$$

$$\int_{-\sin^{-1}\left(\frac{1}{\sqrt{3m}}\right)+\frac{\pi}{3}}^{\frac{\pi}{3}-\left(-\sin^{-1}\left(\frac{1}{\sqrt{3m}}\right)+\frac{\pi}{3}\right)}\left(\left(\underbrace{\left(-\sqrt{3m}\cdot\sin(\zeta)+1\right)}_{d(\{211\})}f\;\underbrace{-\sqrt{3m}\left(-\frac{\sqrt{3}}{2}\cos(\zeta)-\frac{1}{2}\sin(\zeta)\right)-1}_{d(\{210\})}\right)\underbrace{\cos^2(\zeta-\varphi)}_{i_a^2}\,d\zeta\right.$$

$$\left.\left.+\left(\underbrace{-\sqrt{3m}\left(\frac{\sqrt{3}}{2}\cos(\zeta)-\frac{1}{2}\sin(\zeta)\right)+1}_{d(\{221\})}\right)f\cdot\underbrace{\left(-\cos\left(\zeta-\varphi-\frac{4\pi}{3}\right)\right)^2}_{(-i_c)^2}\right)d\zeta+\right.$$

$$\int_{\frac{\pi}{3}-\left(-\sin^{-1}\left(\frac{1}{\sqrt{3m}}\right)+\frac{\pi}{3}\right)}^{\frac{\pi}{3}}\left(\underbrace{\sqrt{3m}\left(\frac{\sqrt{3}}{2}\cos(\zeta)-\frac{1}{2}\sin(\zeta)\right)}_{d(\{210\})}\cdot\underbrace{\cos^2(\zeta-\varphi)}_{i_a^2}+\right.$$

$$\left.\left(\underbrace{\sqrt{3m}\cdot\sin(\zeta)-1}_{d(\{220\})}+\left(\underbrace{\sqrt{3m}\left(-\frac{\sqrt{3}}{2}\cos(\zeta)-\frac{1}{2}\sin(\zeta)\right)+2}_{d(\{221\})}\right)f\right)\cdot\underbrace{\left(-\cos\left(\zeta-\varphi-\frac{4\pi}{3}\right)\right)^2}_{(-i_c)^2}\right)d\zeta+$$

$$\int_{\frac{\pi}{3}}^{\frac{\pi}{3}+\left(-\sin^{-1}\left(\frac{1}{\sqrt{3m}}\right)+\frac{\pi}{3}\right)}\left(\left(\underbrace{-\sqrt{3m}\left(-\frac{\sqrt{3}}{2}\cos(\zeta)-\frac{1}{2}\sin(\zeta)\right)}_{d(\{220\})}-1+\left(\underbrace{-\sqrt{3m}\cdot\sin(\zeta)+2}_{d(\{221\})}\right)f\right)\cdot\underbrace{\left(-\cos\left(\zeta-\varphi-\frac{4\pi}{3}\right)\right)^2}_{(-i_c)^2}\right.$$

$$\left.+\left(\underbrace{-\sqrt{3m}\left(-\frac{\sqrt{3}}{2}\cos(\zeta)-\frac{1}{2}\sin(\zeta)\right)}_{d(\{120\})}\right)\cdot\underbrace{\cos^2\left(\zeta-\varphi-\frac{2\pi}{3}\right)}_{i_b^2}\right)d\zeta+$$

$$\int_{\frac{2\pi}{3}-\left(-\sin^{-1}\left(\frac{1}{\sqrt{3m}}\right)+\frac{\pi}{3}\right)}^{\frac{\pi}{3}+\left(-\sin^{-1}\left(\frac{1}{\sqrt{3m}}\right)+\frac{\pi}{3}\right)}\left(\left(\underbrace{\sqrt{3m}\left(\frac{\sqrt{3}}{2}\cos(\zeta)-\frac{1}{2}\sin(\zeta)\right)+1}_{d(\{221\})}\right)f\cdot\underbrace{\left(-\cos\left(\zeta-\varphi-\frac{4\pi}{3}\right)\right)^2}_{(-i_c)^2}\right.$$

$$\left.+\left(\underbrace{\sqrt{3m}\cdot\sin(\zeta)-1}_{d(\{120\})}+\left(\underbrace{\sqrt{3m}\left(-\frac{\sqrt{3}}{2}\cos(\zeta)-\frac{1}{2}\sin(\zeta)\right)+1}_{d(\{121\})}\right)f\right)\cdot\underbrace{\cos^2\left(\zeta-\varphi-\frac{2\pi}{3}\right)}_{i_b^2}\right)d\zeta+$$

$$\int_{\frac{2\pi}{3}-\left(-\sin^{-1}\left(\frac{1}{\sqrt{3m}}\right)+\frac{\pi}{3}\right)}^{\frac{2\pi}{3}}\left(\left(\underbrace{-\sqrt{3m}\left(-\frac{\sqrt{3}}{2}\cos(\zeta)-\frac{1}{2}\sin(\zeta)\right)}_{d(\{120\})}+\underbrace{\left(-\sqrt{3m}\cdot\sin(\zeta)+2\right)}_{d(\{121\})}f\right)\right.$$

$$\left.\left.+\left(\underbrace{-\sqrt{3m}\left(\frac{\sqrt{3}}{2}\cos(\zeta)-\frac{1}{2}\sin(\zeta)\right)-1}_{d(\{020\})}\right)\right)\cdot\underbrace{\cos^2\left(\zeta-\varphi-\frac{2\pi}{3}\right)}_{i_b^2}\right)d\zeta \qquad (2.15)$$

The expressions of the RMS currents in the different modes are solved in MAPLE and the results are:

$$\frac{I_{2rms}}{\hat{I}_{phase}} = \begin{cases} \frac{1}{2\sqrt{\pi}}\sqrt{\sqrt{3m\left(4\cos^2(\varphi)+1\right)}\sqrt{2f}} & 0 < m < \frac{1}{\sqrt{3}} \\ \frac{1}{2\sqrt{\pi}}\sqrt{\sqrt{3m\left(4\cos^2(\varphi)+1\right)}2f + (2f-1)2\left(3\pi + \left(\left(\frac{2}{3m^2}-2\right)\cos^2(\varphi) - \left(5+\frac{1}{3m^2}\right)\right)\sqrt{3m^2-1} - 6\sin^{-1}\left(\frac{1}{\sqrt{3m}}\right)\right)} & \frac{1}{\sqrt{3}} < m < \frac{2}{3} \\ \frac{1}{2\sqrt{\pi}}\sqrt{m\sqrt{3}\left(4\cos(\varphi)^2+1\right) + \frac{(2f-1)}{m^2}\left(-\left(3m^2-1\right)\left(2\cos(\varphi)^2-1\right)\sqrt{3m^2-1}+2\pi m^2 + \sqrt{3}\left(-4m^3-\frac{3}{2}m^2+\frac{1}{3}+\left(2m^3+3m^2-\frac{2}{3}\right)\cos(\varphi)^2\right)\right)} & \frac{2}{3} < m < \frac{2}{\sqrt{3}} \end{cases} \quad (2.16)$$

As it can be seen from the equations the expression in the inner hexagon is clearly the easiest, and this is expected since there are only small vectors in the inner hexagon. By setting f equal to ½ for mode 1, 2 and 3 the results are the same:

$$\frac{I_{2rms}}{\hat{I}_{phase}} = \frac{1}{2\sqrt{\pi}}\sqrt{\sqrt{3}m\left(4\cos^2(\varphi)+1\right)}$$

Below are two plots of the current at f equal 1 and f equal 0. At normal operation condition will f not be stuck to one of these two values but oscillate around ½.

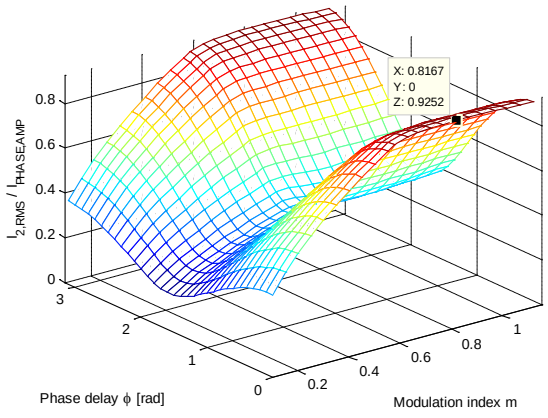

Figure 2.2-15 I_2 RMS at f=1

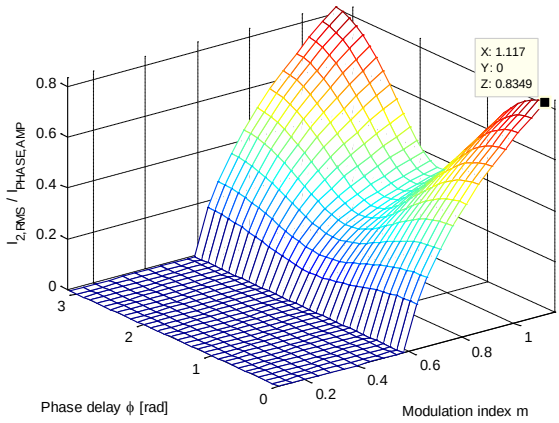

Figure 2.2-16 I_2 RMS at f=0

By having f equal to 0 there will be no current flowing in level 2 at a low modulation, which can be seen in Figure 2.2-16. The reason for this is that f is telling how much the small vector connected to the upper level should be on compared to the small vector connected to level 0, and since f is zero the vectors connected to level 2 will never be on. The simulations show that the RMS current is continuous in the modulation up to 1.1547.

Figure 2.2-17 and Figure 2.2-18 show analytical calculations and simulation results of the RMS current in level two respectively.

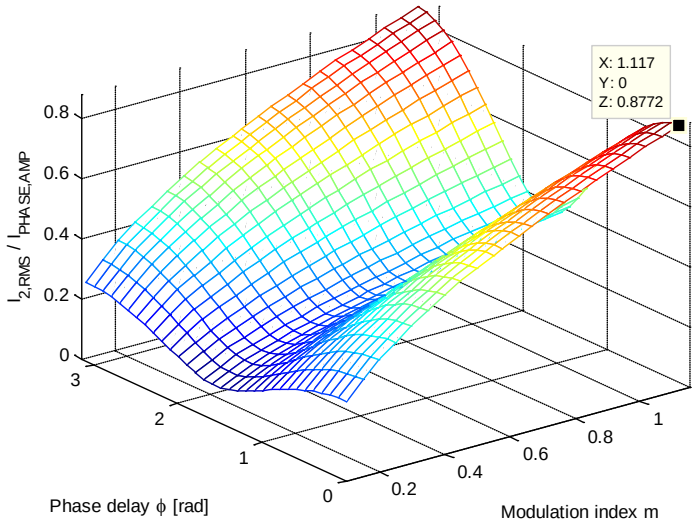

Figure 2.2-17 Analytical calculations of I_2 RMS current, f=1/2

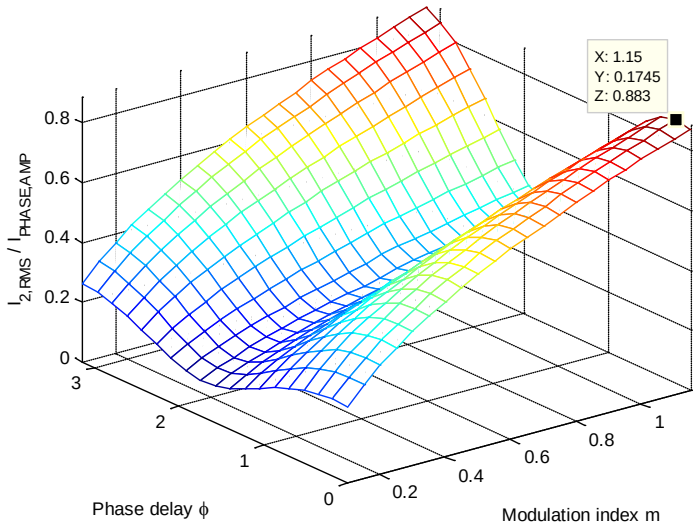

Figure 2.2-18 SIMULINK simulations of I_2 RMS current at 1050 Hz switching and 50 Hz fundamental, f=1/2

The results correlate very well despite that the analytical results has the premise of an infinite switching frequency while the simulation results are calculated with a switching frequency of 1050 Hz. Thus the analytical expressions developed in this thesis can be used to make an estimate of the actual RMS current.

2.2.3 Average Current Level 2

In [15] there is made an estimate of the average or DC current flowing into level 2 and the same calculations are made here. The difference is that in [15] the calculations are done with

sinusoidal modulation and not space vector as in this case. The expressions are developed exactly the same way as for the RMS current, the only exception is that the current is not squared.

The average current out of level 2:

$$I_{2,avg} = \frac{1}{2\pi/3}\int_0^{2\pi/3} i_2(\zeta,\varphi,m)d\zeta = \frac{1}{2\pi/3}\sum^{\substack{sector\\parts}}\int\sum^{\substack{switch\\states}} i_{2[ABC]}(\zeta,\varphi)d_{[ABC]}(\zeta,m)d\zeta \qquad (2.17)$$

The expressions of the RMS current in maple are changed such that the average current is calculated. The results are:

$$\frac{I_{2,avg}}{\hat{I}_{phase}} = \begin{cases} \frac{3}{4}\cos(\varphi)\, m\, 2f & 0 < m < \frac{1}{\sqrt{3}} \\ \frac{3}{4}\cos(\varphi)\, m\left(1+\frac{(2f-1)}{\pi}\left(-2\pi+6\sin^{-1}\left(\frac{1}{\sqrt{3}m}\right)+\frac{2}{m^2}\sqrt{3m^2-1}\right)\right) & \frac{1}{\sqrt{3}} < m < \frac{2}{3} \\ \frac{3}{4}\cos(\varphi)\, m\left(1+\frac{(2f-1)}{\pi}\left(-\pi+3\sin^{-1}\left(\frac{1}{\sqrt{3}m}\right)+\frac{1}{m^2}\sqrt{3m^2-1}+\frac{1}{m^2\sqrt{3}}\right)\right) & \frac{2}{3} < m < \frac{2}{\sqrt{3}} \end{cases} \qquad (2.18)$$

As for the RMS current the expressions for the average current will be equal if f is equal to ½.

$$\frac{I_{2,avg}}{\hat{I}_{phase}} = \frac{3}{4}\cos(\varphi)\, m$$

If f is not ½, the average current will still be continuous but the expressions will not be the same, and the two figures below show the cases with f equal 0 and f equal 1.

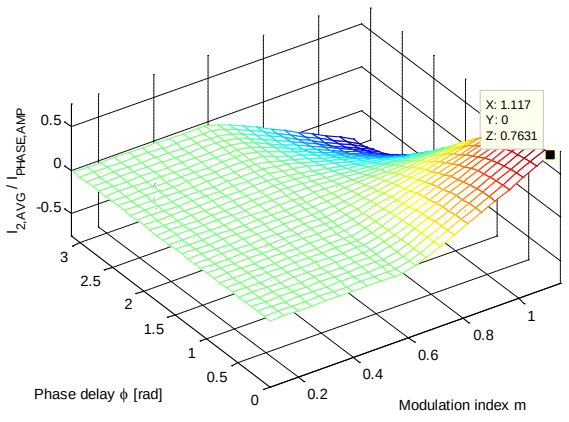

Figure 2.2-19 I2 Analytical average current, f=0

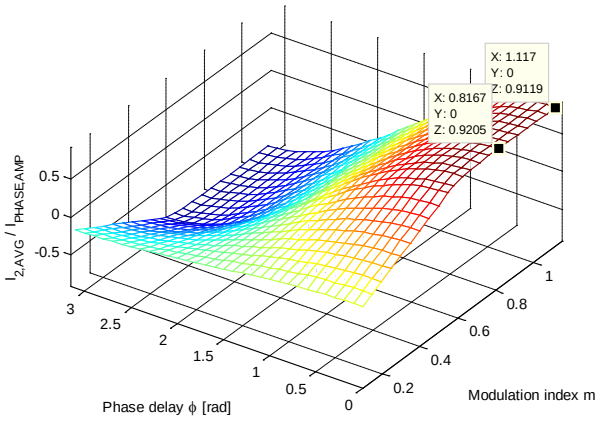

Figure 2.2-20 Analytical average current, f=1

Having f equal to zero gives zero average current at a low modulation and the explanation is the same as for the RMS current; none of the upper switches will be on.

As for RMS current it is also important to verify that the analytical expressions and the simulations give the same results for the average current in level 2.

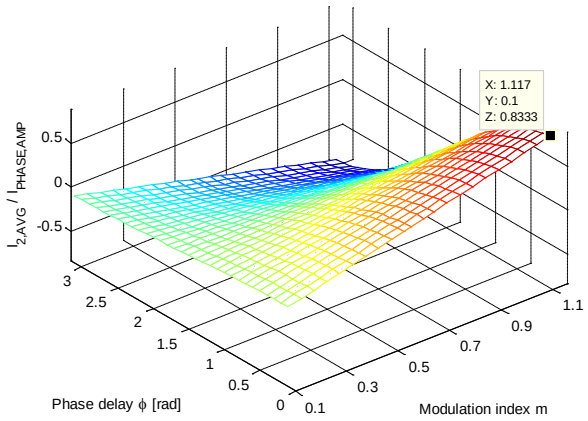

Figure 2.2-21 Analytical I_2 average current, f=½

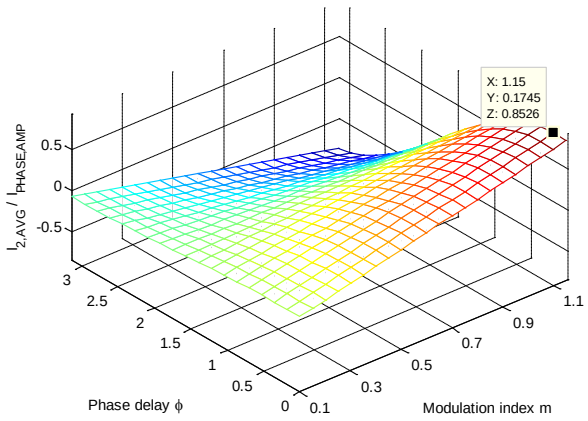

Figure 2.2-22 SIMULINK simulations of I_2 average current at 1050 Hz switching and 50 Hz fundamental, f=½

The results correlate well in this case too, but there are some minor errors. With an φ equal to 2π and a modulation index equal to 0.7 the simulated current is a bit above -0.5 while the calculated current is a bit below -0.5. The reason for the inaccuracy is probably the same as for RMS current; the switching frequency is much lower in the simulations than in the calculations.

2.2.4 Capacitor RMS Current

If it's presumed that the current into the DC link from the rectifier side is DC and the ripple current goes through the capacitors it is shown in [15] that the capacitor RMS current will be:

$$I_{C,rms} = \sqrt{I_{2rms}{}^2 - I_{2avg}{}^2} \tag{2.19}$$

From formula (2.16) and (2.18) the capacitor current is:

$$\frac{I_{C,rms}}{\hat{I}_{phase}} = \sqrt{m} \cdot \sqrt{\cos^2(\varphi)\left(\frac{\sqrt{3}}{\pi} - \frac{9}{16}m\right) + \frac{\sqrt{3}}{4\pi}} \tag{2.20}$$

This is the current when f=½. The plots from the calculations and from simulations are shown in Figure 2.2-21 and Figure 2.2-22. As seen the results are quite equal.

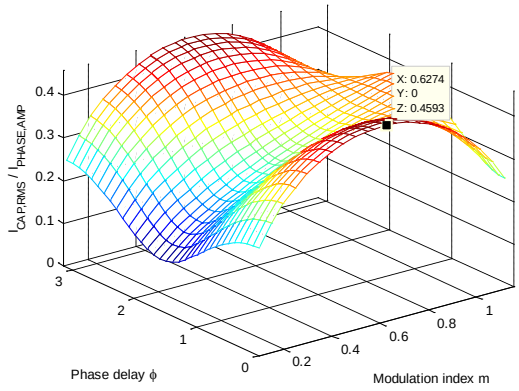

Figure 2.2-23 Analytical calculations of I capacitor RMS current

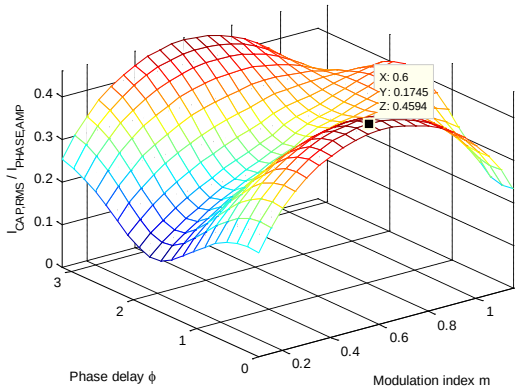

Figure 2.2-24 SIMULINK simulations of capacitor RMS current at 1050 Hz switching and 50 Hz fundamental

2.3 Double-Signal Modulation

This is a quite new method and the purpose of it is to control the DC-bus. The method is described in detail in [5]. It is based on some of the same theory as for common offset voltage addition, but only the first offset value will be added and this is to increase the linear range up to 1.1547. This is given as

$$U_{off} = -\frac{\max(U_{sta}, U_{stb}, U_{stc}) + \min(U_{sta}, U_{stb}, U_{stc})}{2} \tag{2.21}$$

The first approach to a new control signal will be to change the control signal as

$$U_i^{'} = U_a - U_{off} \tag{2.22}$$

When this is done, the next principle in this modulation technique is to split the control signal into two signals. The idea is to keep the voltage unbalance as small as possible, and at the same time as few switching transitions as possible. The optimal solution of this is found in [5] as

$$\begin{aligned} U_{ip} &= \frac{U_i - \min(U_a, U_b, U_c)}{2}, i = a,b,c \\ U_{in} &= \frac{U_i - \max(U_a, U_b, U_c)}{2}, i = a,b,c \end{aligned} \tag{2.23}$$

The positive signal will be compared to the upper triangular signal, while the negative signal will be compared with the lower triangular signal. By adding some offset signals to the new signals the DC-bus can be controlled. How this can be done will be described more in detail in the chapter about DC-bus balancing.

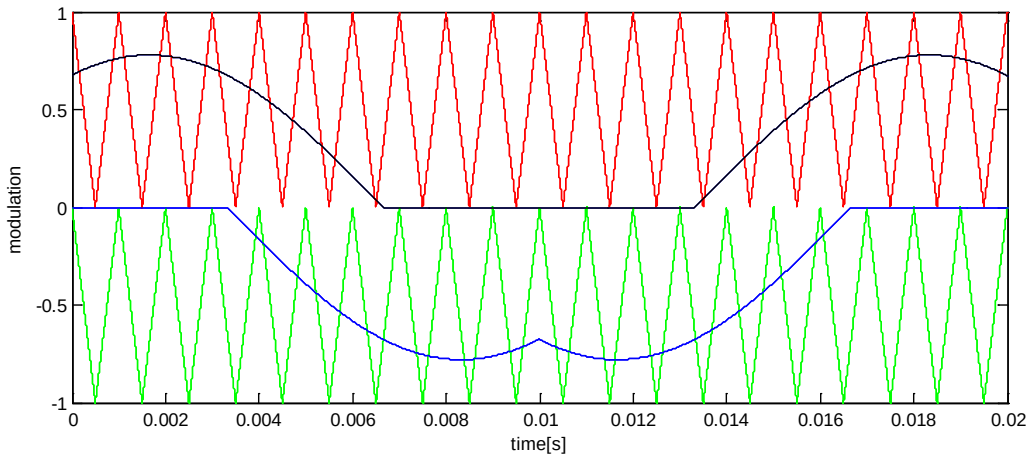

Figure 2.3-1: Control signals for Double-Signal PWM

2.3.1 Current Flow with Double-Signal

The calculations of the currents flowing when using Double-Signal is easier compared to Space Vector. It is enough to look at the upper control signals to calculate the average currents. The upper control signals tell how much each bridge leg is connected to level 2. Unlike Space Vector there is no need to divide into different modes. The upper control signals are given in the figure below for one fundamental period.

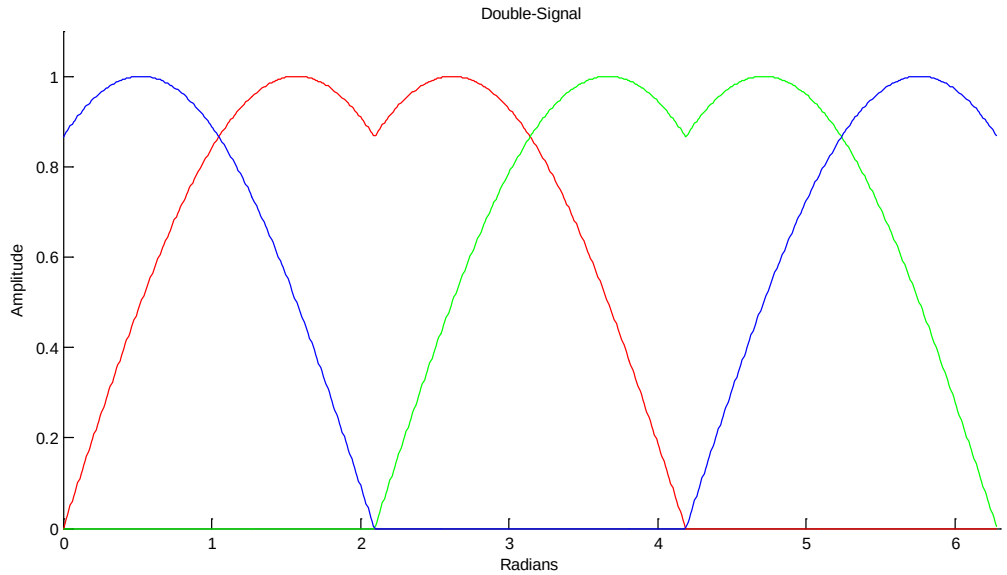

Figure 2.3-2: Upper control signals for Double-Signal

It is enough to calculate the current from 0 to $2\pi/3$ due to symmetry. The upper control signal for phase C is zero during this interval and hence there will be no current contribution from phase C. The calculations will then be as the following for the average current.

$$\frac{I_{2,avg}}{\hat{I}_{phase}} = \frac{3}{2\pi}\int_{0}^{\frac{2\pi}{3}} \left(\begin{array}{l} \frac{\left(m\cdot\cos(\zeta) - m\cdot\cos\left(\zeta+\frac{2\pi}{3}\right)\right)}{2}\cdot\cos(\zeta-\varphi) \\ -\frac{\left(m\cdot\cos\left(\zeta-\frac{2\pi}{3}\right) - m\cdot\cos\left(\zeta+\frac{2\pi}{3}\right)\right)}{2}\cdot\cos\left(\zeta-\frac{2\pi}{3}-\varphi\right) \end{array} \right) d\zeta \tag{2.24}$$

The result of the integral is given below.

$$\frac{I_{2,avg}}{\hat{I}_{phase}} = \frac{3}{4}\cdot m\cdot\cos(\varphi) \tag{2.25}$$

The result is the same as for Space Vector which it should be. The calculation of the RMS current is a bit more complicated than the average. In the period from 0 to π/3 the control signal for phase A is greater than for phase B, which means that phase A will always be connected to the upper level when phase B is connected. So when phase B is connected the total current flowing in level 2 will be $i_a(t)$ plus $i_b(t)$. This is important to remember since the total current will be squared, so that the calculations will be $(i_a(t) + i_b(t))^2$ and not $i_a(t)^2$ plus $i_b(t)^2$. From π/3 to 2π/3 the control signal for phase B will greater than for phase A and hence the situation is opposite compared to 0 to π/3. The calculations will then be as below.

$$\frac{I_{2,RMS}^2}{\hat{I}_{phase}^2} = \frac{3}{2\pi}\left(\begin{array}{l} \int_{0}^{\frac{\pi}{3}} \left(\begin{array}{l} \left(\frac{\left(m\cdot\cos(\zeta) - m\cdot\cos\left(\zeta+\frac{2\pi}{3}\right)\right)}{2} - \frac{\left(m\cdot\cos\left(\zeta-\frac{2\pi}{3}\right) - m\cdot\cos\left(\zeta+\frac{2\pi}{3}\right)\right)}{2} \right)\cdot\cos(\zeta-\varphi)^2 \\ + \left(\frac{\left(m\cdot\cos\left(\zeta-\frac{2\pi}{3}\right) - m\cdot\cos\left(\zeta+\frac{2\pi}{3}\right)\right)}{2} \right)\cdot\left(\cos(\zeta-\varphi) + \cos\left(\zeta-\frac{2\pi}{3}-\varphi\right)\right)^2 \end{array} \right) d\zeta \\ \int_{\frac{\pi}{3}}^{\frac{2\pi}{3}} \left(\begin{array}{l} \left(\frac{\left(m\cdot\cos\left(\zeta-\frac{2\pi}{3}\right) - m\cdot\cos\left(\zeta+\frac{2\pi}{3}\right)\right)}{2} - \frac{\left(m\cdot\cos(\zeta) - m\cdot\cos\left(\zeta+\frac{2\pi}{3}\right)\right)}{2} \right)\cdot\cos\left(\zeta-\frac{2\pi}{3}-\varphi\right) \\ + \frac{\left(m\cdot\cos(\zeta) - m\cdot\cos\left(\zeta+\frac{2\pi}{3}\right)\right)}{2}\cdot\left(\cos(\zeta-\varphi) + \cos\left(\zeta-\frac{2\pi}{3}-\varphi\right)\right)^2 \end{array} \right) d\zeta \end{array} \right) \tag{2.26}$$

The result of the integral is given below.

$$\frac{I_{RMS}^2}{\hat{I}_{phase}} = \frac{3}{2} \cdot \frac{\frac{2}{3} \cdot m \cdot \sqrt{3} \cdot \cos(\varphi)^2 + \frac{1}{6} \cdot m \cdot \sqrt{3}}{\pi}$$
$$\frac{I_{RMS}}{\hat{I}_{phase}} = \frac{1}{2} \cdot \frac{3^{1/4} \cdot \sqrt{m \cdot \left(4 \cdot \cos(\varphi)^2 + 1\right)}}{\sqrt{\pi}} \qquad (2.27)$$

By setting the f parameter in the equations for Space Vector to 1/2 it can be shown that Double-Signal and SV give the same result for RMS and average current, which is a good result. The capacitor current will be the same as for SV since both the average current and the RMS current are the same. In the next subchapter simulations will be done for different cos(φ) and different modulation factor to compare the theoretical current values with simulated values. The simulation results are shown in the figures below.

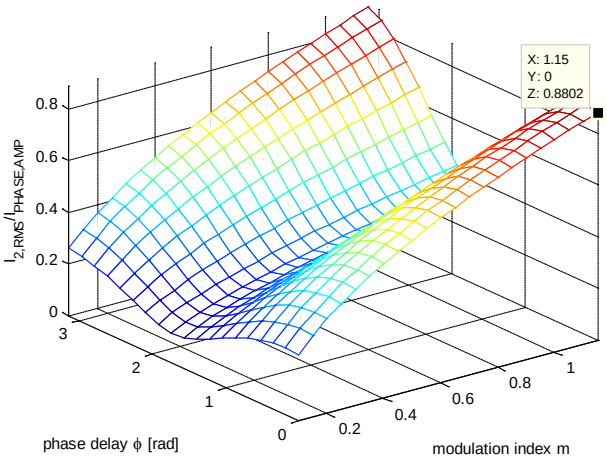

Figure 2.3-3: SIMULINK simulations of RMS current at 1050 Hz switching and 50 Hz fundamental

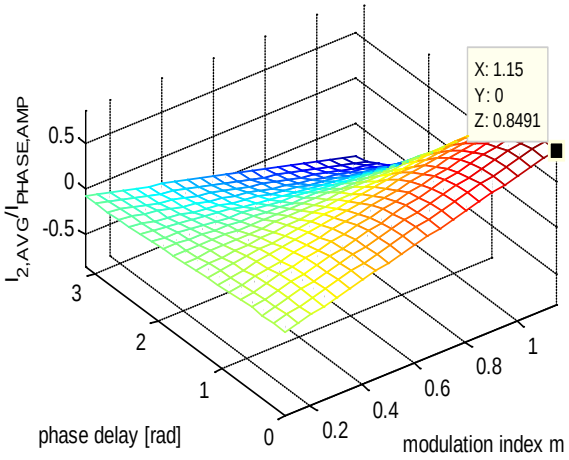

Figure 2.3-4: SIMULINK simulations of average current at 1050 Hz switching and 50 Hz fundamental

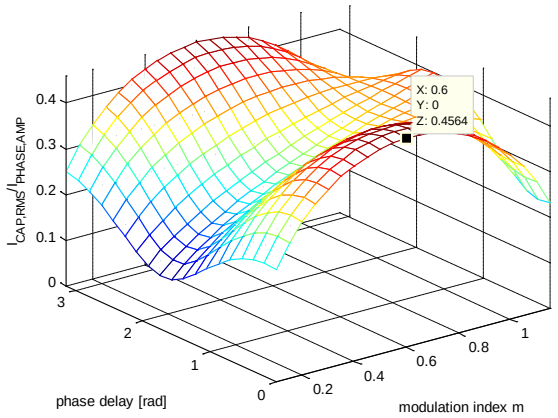

Figure 2.3-5: SIMULINK simulations of capacitor current at 1050 Hz switching and 50 Hz fundamental

The simulations correspond well with both Space Vector and the analytical results, which is expected due to the equations.

3 Overmodulation

3.1 Description of Overmodulation

Before DC-balancing is to be discussed there is one special area that needs to be studied and that is in the range of 2/sqrt(3) up to $4/\pi * U_{dc}/2$, which is called overmodualtion. This is a nonlinear region; the output of the converter is not proportional to the reference and $4/\pi * U_{dc}/2$ is the maximum reachable output voltage. As long as the reference vector has an amplitude lower than $2/\sqrt{3}$ it will not move into the area of overmodulation. The figure below shows the space vectors and the shaded area represents overmodulation area.

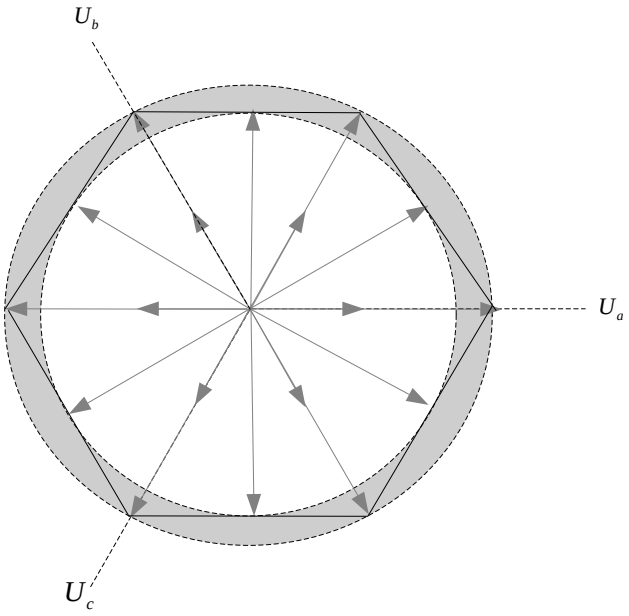

Figure 3.1-1: Space vector diagram showing the overmodulation area

The grey vectors show the space vectors that can be created from the different switching states to get the desired reference vector. Combinations of these switch states can only produce average space vectors inside the hexagon at a finite switching frequency. A reference vector can be produced as long as it stays within the hexagon. As it can be seen in the figure there are some of the areas that are defined as overmodulation that are inside the hexagon, but since the reference vector is rotating it will not be possible to produce this vector the entire time. The output will be a space vector that points to somewhere on the hexagon border but not of a length that is sufficient to have a linear response.

If the reference is $4/\pi$, a linear response would result in six-step operation. Only the six large vectors should be used and they should be used once per fundamental period. The switching sequence at six-step is shown in the figure below.

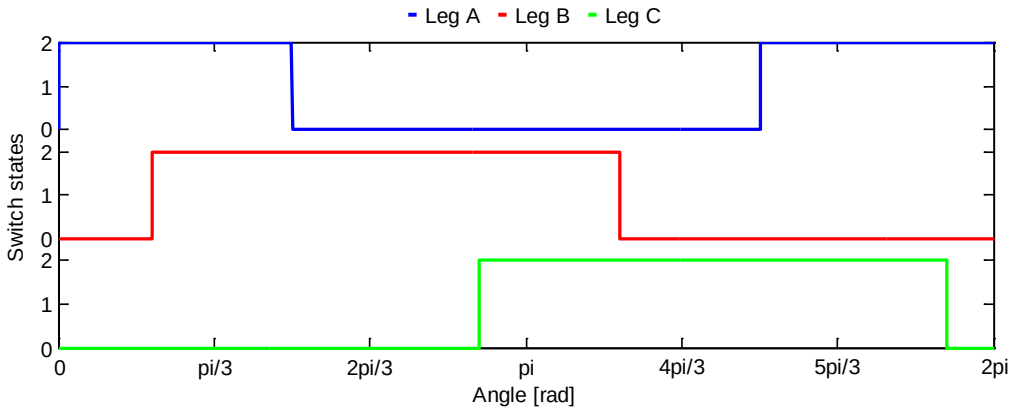

Figure 3.1-2: Six-step operation

Six-step is not reached for Double-Signal and Space Vector at this value, they take other vectors into use and hence the output voltage is less than wanted. Their switching patterns are shown in Figure 3.1-3 and Figure 3.1-4. Harmonic analysis of the line-to-line voltages show that Space Vector gives 2.0845 in output with an m_a of $4/\pi$. With a linear response the result should have been 2.2053. Double-Signal gives the output of 2.0860, which is close to the value of Space Vector. Hence the two methods have a quite similar response. The simulations show that the m_a needs to be several times $4/\pi$ to reach six-step. Thus methods to improve the response in the nonlinear region should be implemented.

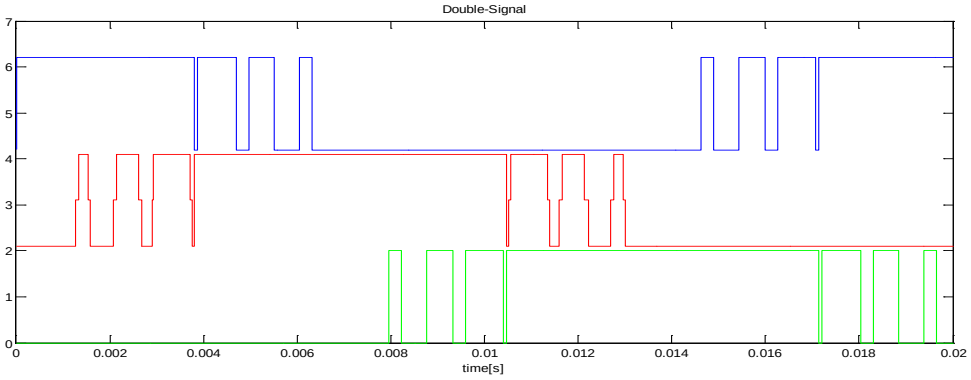

Figure 3.1-3: Double signal switching states with a modulation index of 4/ π

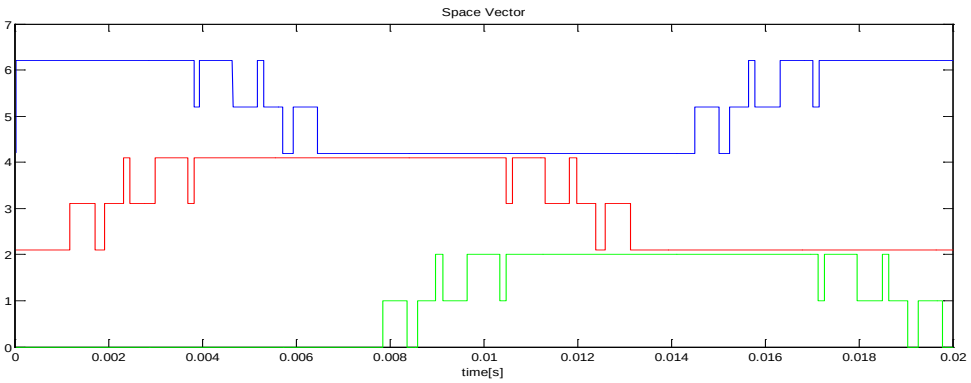

Figure 3.1-4: Space vector switching states with a modulation index of 4/ π

Overmodulation algorithm

One method to improve the response in the nonlinear region is to be found in [11]. The method is based on a simple principle of keeping the reference vector to the point where it crosses the border of the hexagon. Hence the reference vector is rotated back or forth to the point where it crosses the hexagon border if it's outside this border. This is illustrated in the figure below.

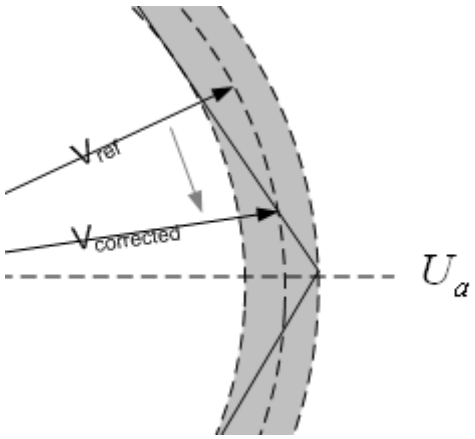

Figure 3.1-5: Correction of reference vector in overmodulation

The figure shows that the reference vector is rotated back to the point where it crosses the hexagon border. With this method six-step will be reached when the amplitude of the reference vector is equal to the length of the large vectors, which is 4/3. Hence the method is improved, but it is not linear. With this method it is needed to find the place where the reference vector is crossing the hexagon border. Calculations of average currents when using space vector are done in [14], and here a convenient method for finding the angle where the reference vector crosses the area for the non-linear region is presented. Below is a flow chart of how to find the correct angle.

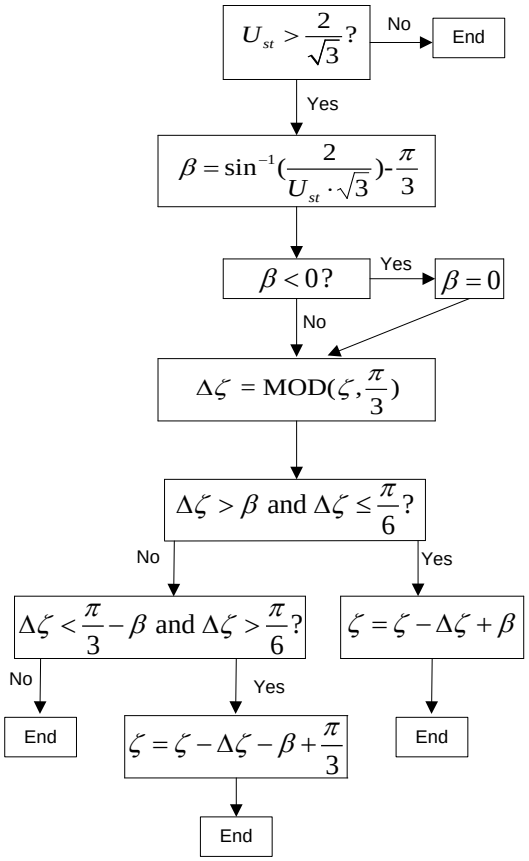

Figure 3.1-6: Flowchart of overmodulation algorithm

Where β is the angle where the reference vector is crossing the hexagon border. So far this method is working the same way for both Space Vector and Double-Signal. The Space Vector algorithm is always using the three closest vector states. In very high modulation the use of small vectors is very limited, and hence the balancing possibilities are small.

3.2 Simulation Results

Previous in this report it has been discussed the importance of choosing a switching frequency which lower the total harmonic distortion and that three phase symmetry is achieved. The switching frequency was decided to be 1050 Hz and both Space Vector and Double-Signal were simulated. The maximum reachable line-to-line output voltage is 2.205 with ideal conditions and this should be reached with a modulation index of 4/3, which in line-to-line voltage is 2.309. The results are presented in Table 3.2-1 and Table 3.2-2. The total harmonic distortion is defined as

$$\%THD_i = 100 \cdot \sqrt{\sum_{h \neq 1} \left(\frac{I_{sh}}{I_{s1}} \right)^2}, I_{sh} = \frac{V_h}{j\omega L} \tag{3.1}$$

Table 3.2-1: 1st harmonic line-to-line output voltage with m_f equal to 21

	Line-to-line voltage modulation			
Signal	**2.078**	**2.165**	**2.252**	**2.309**
Space vector	2.0562	2.1157	2.1666	2.1981
Double-Signal	2.0488	2.1087	2.1597	2.1923

Table 3.2-2: THD_i with m_f equal to 21

	Line-to-line voltage modulation			
Signal	**2.078**	**2.165**	**2.252**	**2.309**
Space vector	3.0%	4.01%	5.31%	6.06%
Double-Signal	3.32%	4.11%	5.34%	6.07%

Space Vector has a bit better 1st harmonic output and THD_i but the differences are not very big. Both methods have improved their response and hence the method of locking the reference vector to the angle β has been successfully implemented. To show how sensitive the output voltage can be when six-step is reached there were made several simulations with different switching frequency and the results are collected in the table below.

Table 3.2-3: 1st harmonic line-to-line output voltage with m equal 1.333

m_f	Switching frequency	1st harmonic output	THD_i
15	750Hz	2.1865	7.17%
18	900Hz	2.1985	4.65%
19	950Hz	2.2252	5.19%
20	1000Hz	2.0534	6.80%
21	1050Hz	2.1923	6.07%
22	1100Hz	2.1353	5.38%
23	1150Hz	2.1638	5.30%

The table is showing how critical it is to choose a switching frequency which creates three phase symmetry. Even with an m_f equal 23, which is synchronized switching, the 1st harmonic output is far from the wanted value. These results show that it should be aimed for having synchronized switching and three phase symmetry when the operation point is in overmodulation.

4 Symmetrical and Asymmetrical Modulation

4.1 Comparison of Symmetrical and Asymmetrical Modulation

Figure 4.1-1 and Figure 4.1-2 shows how a continuous control signal is sampled and the switch response in the bridge leg for symmetrical and asymmetrical modulation. In symmetrical modulation the control signals are sampled when the triangular waves reach their tops. These values are used to determine when switches 1 and 2 are turned on and switches 3 and 4 are turned off in the first half of a triangular period. Since there is no new sample, the same values are also used to determine when switches 1 and 2 are turned off and 3 and 4 are turned on in the last half of the triangular period. In asymmetric modulation however there is an extra sampling at the bottom of the triangular waves. Hence there are new sampled values of the control signals to determine the turn off of switch 1 and 2 and turn on of switch 3 and 4 in the last half period.

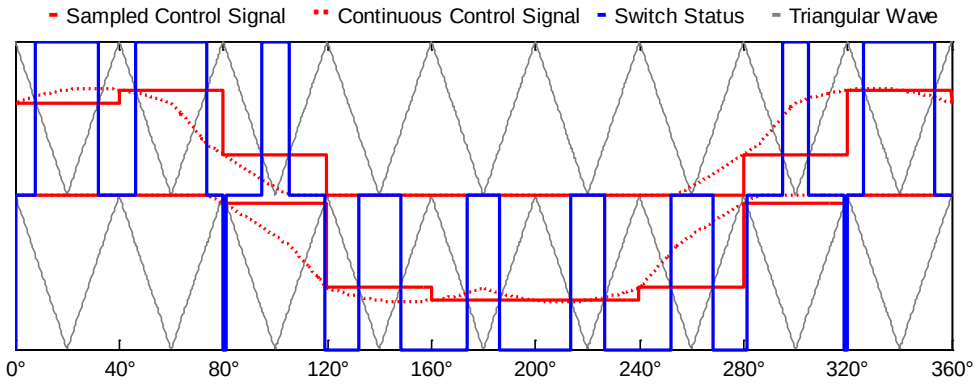

Figure 4.1-1: Sampling with symmetrical modulation

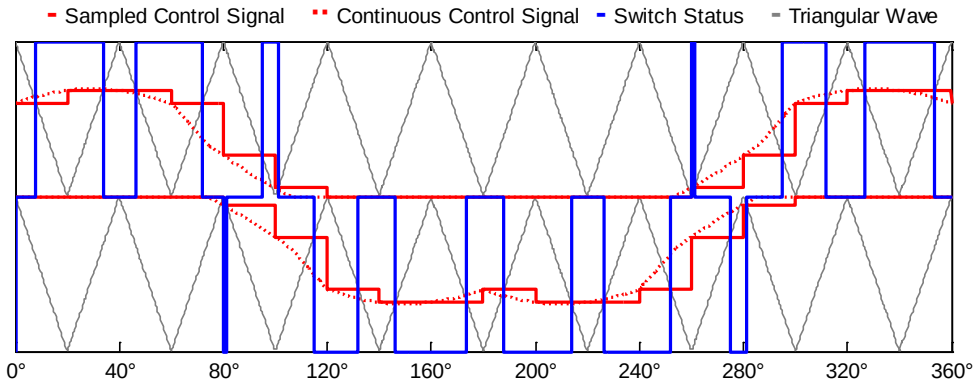

Figure 4.1-2: Sampling with asymmetrical modulation

In the asymmetrical modulation it can be seen that there is turn on of switch 1 at 260°. This is in the last half period of the triangular signal. Extra turn on is added since there has been no switching in the first half period. In other words there is a turn on and a turn off of a switch in one half period. It's worth noting that the extra sampling will result in additional calculation.

In Figure 4.1-3 and Figure 4.1-4 THD_i of current at inductive load is simulated for asymmetric and symmetric modulation for Double-Signal and Space Vector. Asymmetrical modulation has a better THD than symmetric in general. The difference is however only significant when the switching frequency is low compared to the fundamental.

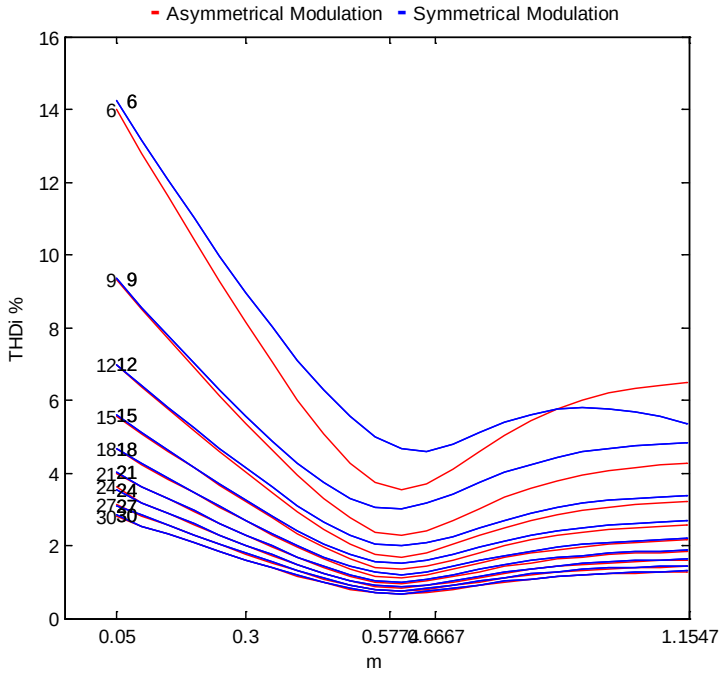

Figure 4.1-3: THD_i of inductive load at different m_f with Double-Signal

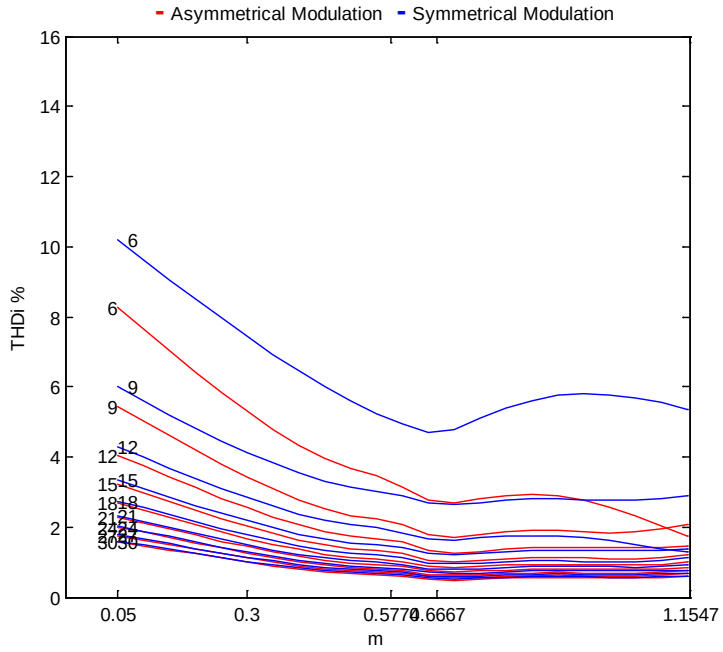

Figure 4.1-4: THD_i of inductive load at different m_f with Space Vector

In Figure 4.1-5 harmonics from simulations it is shown that some of the harmonics are considerably reduced by the use of asymmetrical modulation.

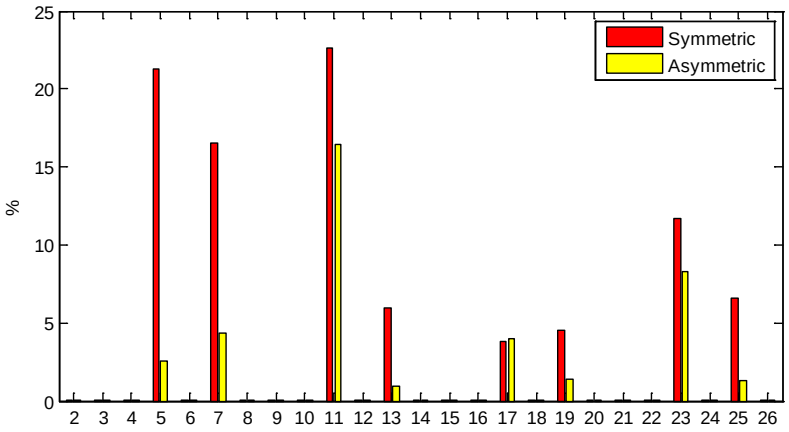

Figure 4.1-5: Harmonic spectra with m_f equal to 6

Figure 4.1-6 and Figure 4.1-7 show the change of switching pattern going from symmetrical to asymmetrical modulation. The switching half periods are separated by a grey line.

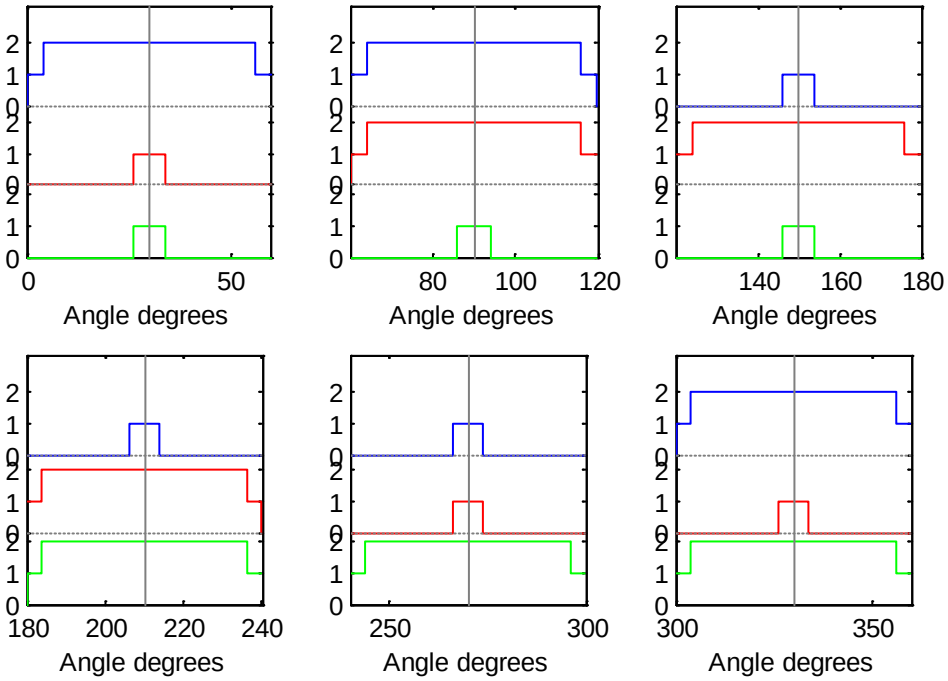

Figure 4.1-6: Switching vectors with symmetrical modulation during one fundamental period, m_f equal 6

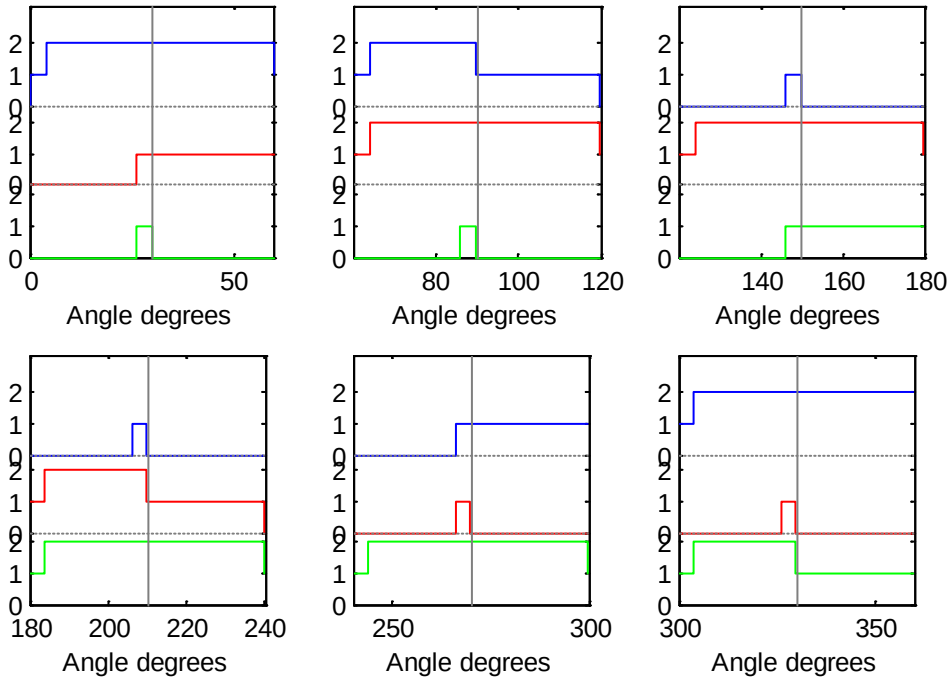

Figure 4.1-7: Switching vectors with symmetrical modulation during one fundamental period, m_f equal 6

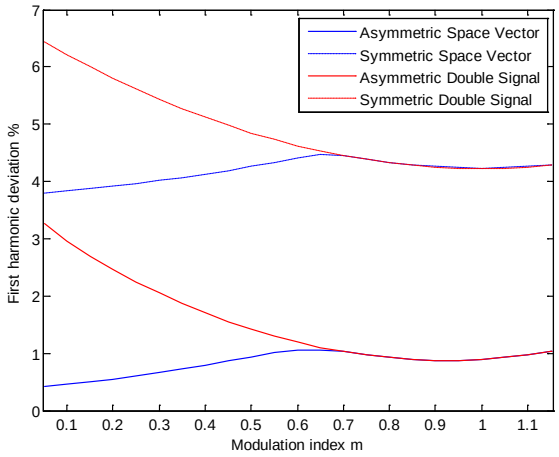

Figure 4.1-8 First harmonic deviation at m_f equal 6

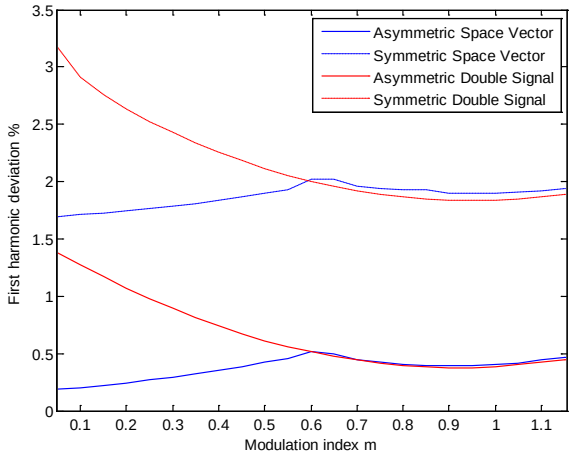

Figure 4.1-9 First harmonic deviation at m_f equal 6

In Figure 4.1-8 it can be seen that the deviation from the desired output for the first harmonic is much better for asymmetric modulation. The main advantage of asymmetric is the reduction of THD_i at low switching frequency. Figure 4.1-9 shows that there is a decline in error as the switching frequency relative to the fundamental is increased when compared to Figure 4.1-8.

All the simulations listed in this section have until now been done with the first sampling of control voltage at angle 0. However the THD will be affected of what angle the samplings are done at.

Figure 4.1-10 and Figure 4.1-11 shows the THDi for space vector modulation as a function of the angle the first sample of the control voltage is taken at. Only low switching frequencies relative to the fundamental are shown since higher frequencies do not vary to any considerable degree. The plots are of different length due to that the maximum delay of the first sample is limited by the length of the switching period. Asymmetrical modulation has a much better THDi in general than the symmetrical. But it also seems that it has the best potential for minimizing THD by better sampling. When the switching frequency is 6 times the fundamental the minimum THDi is less than half of the maximum.

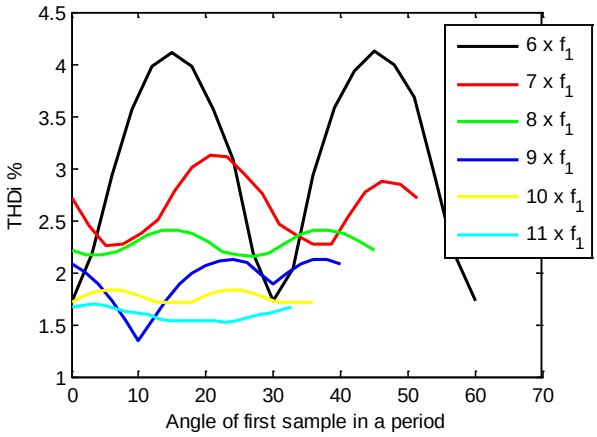

Figure 4.1-10 THDi at asymmetrical SV modulation m_a=1.1547

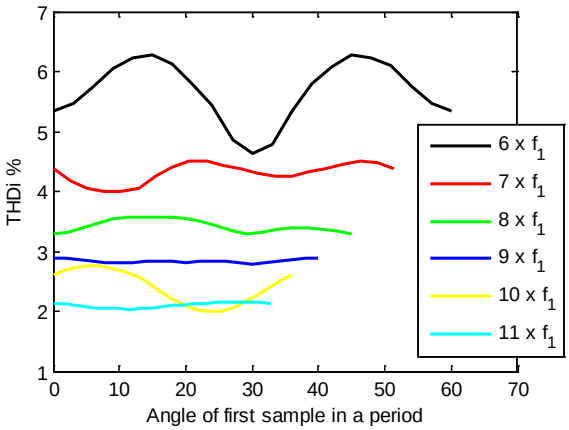

Figure 4.1-11 THDi at symmetrical SV modulation m_a=1.1547

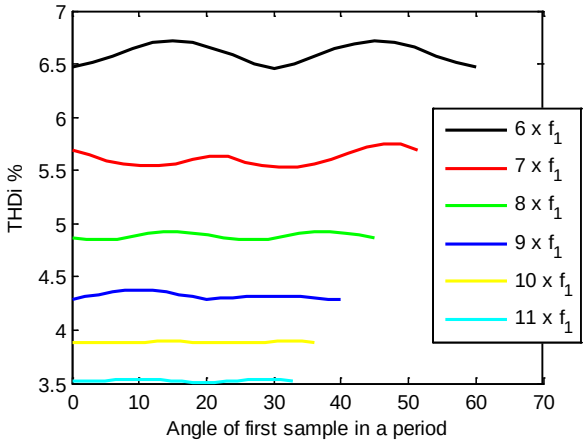

Figure 4.1-12 THDi at asymmetrical DS modulation m_a=1.547

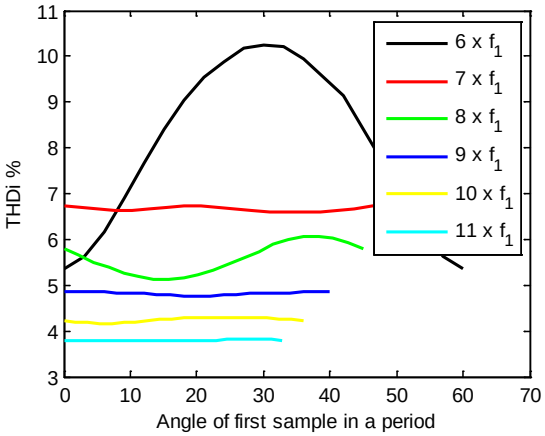

Figure 4.1-13 THDi at symmetrical DS modulation m_a=1.1547

The worst case compared to the best case for modulation with a switch frequency six times the fundamental will now be discussed in detail. In [16] cancelling even harmonics by the use of complementary switch states every 180 degrees is discussed. An example of using complementary switch states is having the switch state [1 0 0] and then switch state [1 2 2]

180 degrees later. State 1 is the neutral point of the bridge leg. Its complementary state is 1. The negative state 0 has the complementary positive state 2. In Figure 4.1-14 and Figure 4.1-15 the space vector diagram for the best and the worst case scenario is shown with reference vectors marked where sampling is conducted. The red vector illustrates sampling at the beginning of the first half of a switch period while the blue vector illustrates sampling at the beginning of the last half. Asymmetric modulation obviously. The switch states for two switching periods that should have complementary switching to cancel even harmonics are shown below the space vector diagrams and the switching periods are marked in the diagrams. In the best case scenario in the first switching period it can be seen that the switch state [1 0 0] is used. However the complementary state [1 2 2] is not to be seen 180 degrees later but closer to 210 degrees later. However the switch states [2 0 0] have its complementary switch state [0 2 2] at exactly 180 degrees later, in other words perfect cancellation. In the last half periods only complementary medium vectors are used and they match by 180 degrees. In the worst case scenario it can be seen there is very little match by 180 degrees of complementary switch states.

BEST CASE SCENARIO

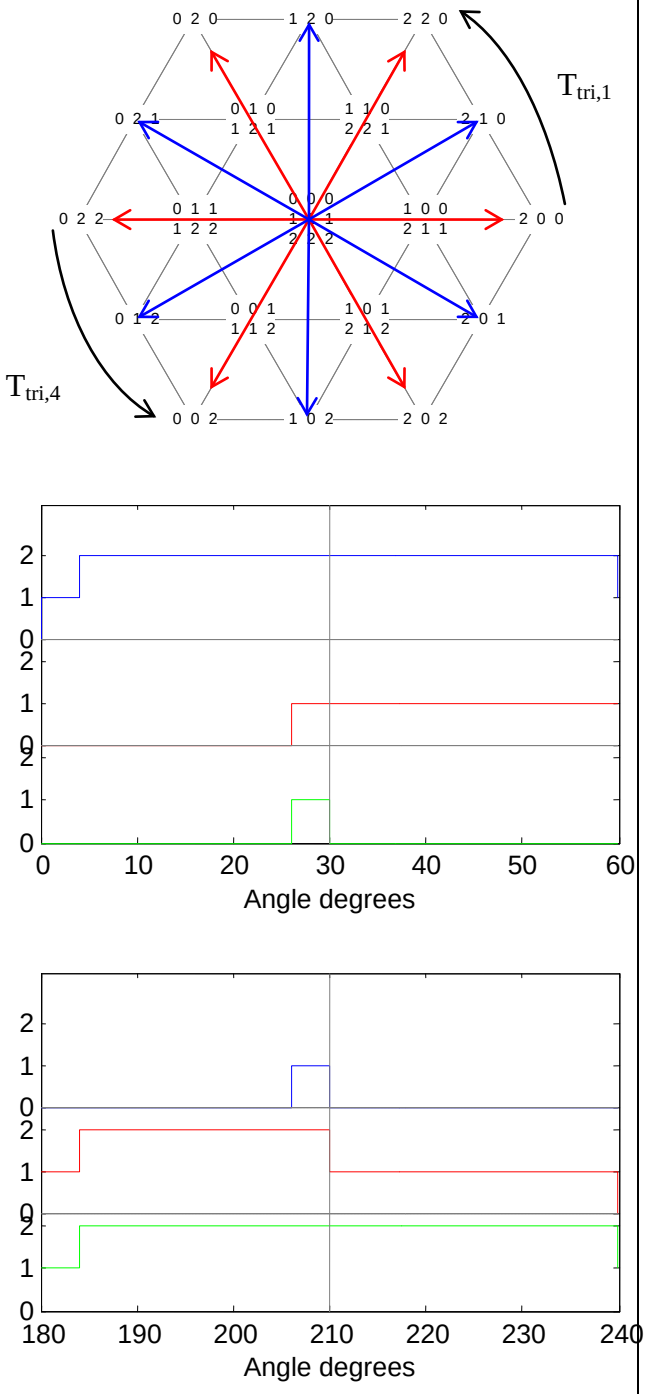

Figure 4.1-14: Best case scenario with m_f equal 6 and m_a equal 1.1547

WORST CASE SCENARIO

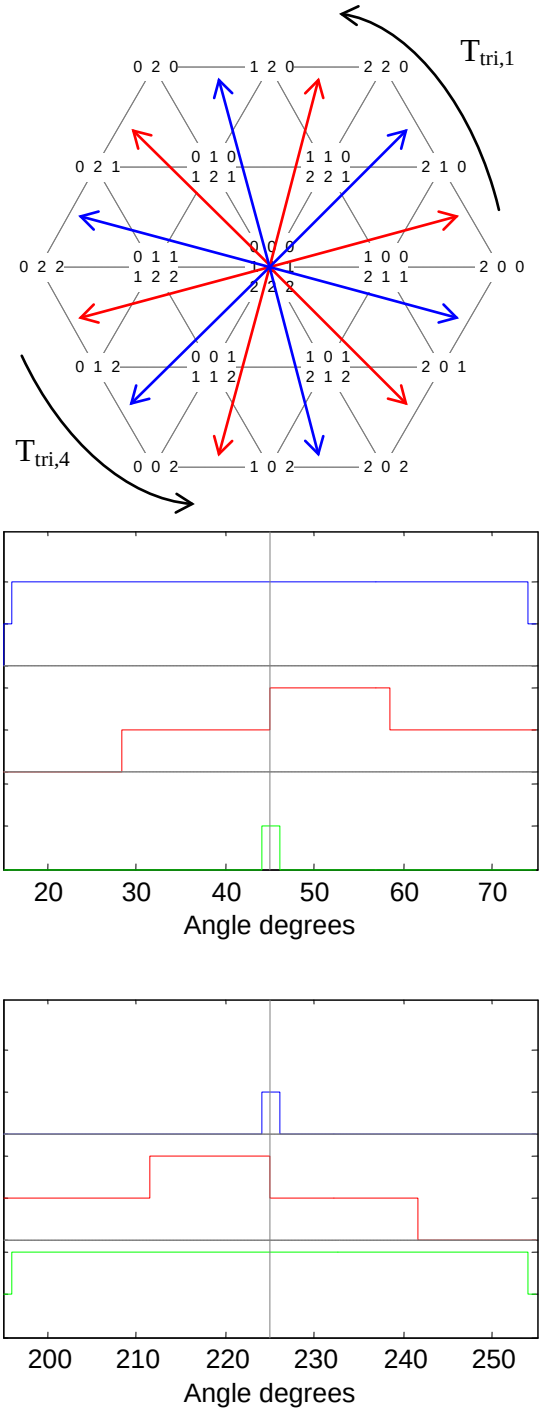

Figure 4.1-15: Worst case scenario with m_f equal 6 and m_a equal 1.1547

In Figure 4.1-16 lower order voltage harmonics as percentage of the fundamental is shown for the two scenarios. It's clear that there is very good cancellation of even harmonics in the case with the best sampling. Only variation of first sampling at a fixed modulation degree of

1.1547 has been discussed. In Figure 4.1-16 THD at fixed frequency and varied delay and modulation degree is shown. The switching frequency is 6 times the fundamental.

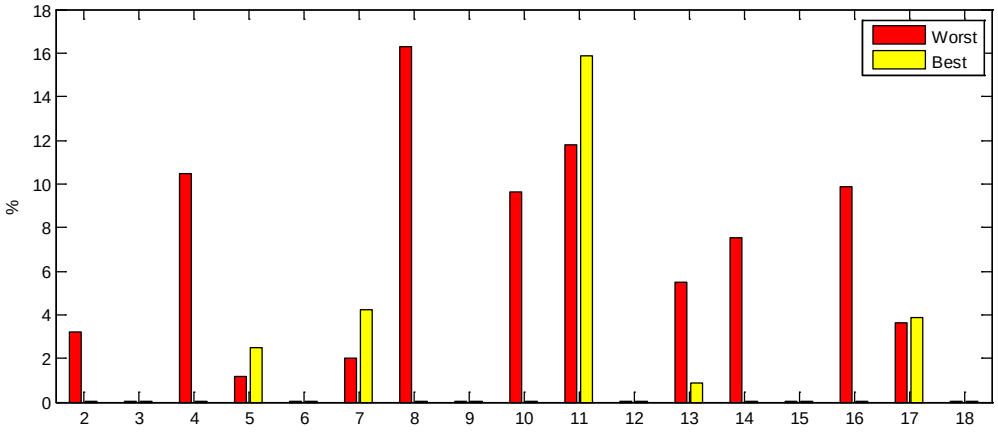

Figure 4.1-16: Harmonic spectra for best and worst case of asymmetrical modulation m_f equal 6 and m_a equal 1.1547

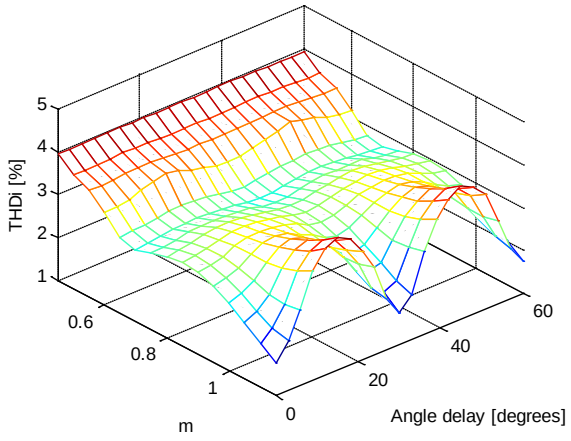

Figure 4.1-17: THD_i with m_f equal 6

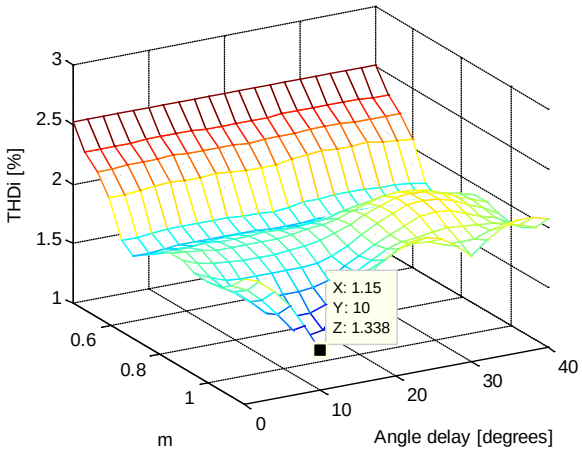

Figure 4.1-18: THD_i with m_f equal 9

In Figure 4.1-17 and Figure 4.1-18 the THD_i at varied modulation and delay of first sample at fixed frequencies are plotted. At the lower modulation indexes there is little variation in THD_i for different angles of first sampling. These values are not plotted. From the figures it can be seen that the best delay of sampling is the same for all modulation indexes when the sampling frequency is six times the fundamental. The best angles are 0 and 30 degrees. When it is 9 times the fundamental the best angle of first sampling varies with modulation, however it is quite good at 10 degrees for all modulation indexes.

5 DC-bus Balancing

Some of this topic was treated in [13] and more has been added here. Because of this some of the text from [13] will be repeated in this master thesis.

In a three-level neutral clamped converter DC-bus balancing is necessary to keep the voltage difference between the two capacitors small, such that the equipment connected to the capacitors don't get too high voltage stresses. With no balancing, all of the DC-link voltage could be across only one of the capacitors. Another problem that occurs with an unbalance in the capacitor voltages is that the output voltage will not follow the reference value. This will also increase the harmonic distortion. Due to these two main problems with a voltage unbalance the problem must be solved, otherwise this converter topology cannot be use. As it was mentioned in the previous chapter, it is Space Vector and Double-Signal PWM that has the most well documented methods of controlling the voltage across the capacitors. How these two methods should be used will be discussed in the next subchapters. Studies have also been made about using a PI controller for Space Vector. Since Space Vector is actively deciding which vectors that should be used while Double-Signal is calculating duty cycles for each phase it seems natural to describe the effect of the different vectors in the chapter of Space Vector. In addition there will be a separate subchapter regarding DC-bus balancing in overmodulation.

5.1 DC-bus Balancing with Space Vector PWM

In a NPC converter there are 27 vectors that give 19 different vector states. The three zero vectors and the big vectors don't have any influence on the DC-bus balance. There exist six medium vectors that could and will influence the voltage balance. How to control this influence and a possible initial voltage unbalance is by use of the six small vector pairs with a total of 12 vectors. Which phase current that will go through the neutral point is depending on which vector that is being used. Table 5.1-1 gives an overview of the NP current with the different space vectors. This table is found in [2].

Table 5.1-1: Overview of the relation between space vectors and neutral current

Positive small vectors	i_{NP}	Negative small vectors	i_{NP}	Medium vectors	i_{NP}
100	$\mathbf{i_a}$	211	$\mathbf{-i_a}$	210	$\mathbf{i_b}$
221	$\mathbf{i_c}$	110	$\mathbf{-i_c}$	120	$\mathbf{i_a}$
010	$\mathbf{i_b}$	121	$\mathbf{-i_b}$	021	$\mathbf{i_c}$
122	$\mathbf{i_a}$	011	$\mathbf{-i_a}$	012	$\mathbf{i_b}$
001	$\mathbf{i_c}$	112	$\mathbf{-i_c}$	102	$\mathbf{i_a}$
212	$\mathbf{i_b}$	101	$\mathbf{-i_b}$	201	$\mathbf{i_c}$

All of the positive and medium vectors will discharge the lower capacitor as long as the belonging phase current is positive, hence U_{dcu} will increase while U_{dcl} will decrease. If the phase current is negative, the upper capacitor will be discharged and the lower charged. The negative vectors act the opposite way of positive and medium vectors. A table can be made to clearly see what happens with the two capacitors.

Table 5.1-2: Overview of capacitor charging with small, medium and large vector

Type of vector	Phase current > 0	Phase current < 0
Positive small	Charge upper, discharge lower	Discharge upper, charge lower
Negative small	Discharge upper, charge lower	Charge upper, discharge lower
Medium	Charge upper, discharge lower	Discharge upper, charge lower
Large	No change in charge	No change in charge
Zero	No change in charge	No change in charge

In Figure 5.1-1 an overview of the vectors influencing the capacitor voltages is given. In the figure the belonging phase currents are shown with a plus and minus sign. A plus sign is representing a positive vector, while a negative sign is representing a negative vector.

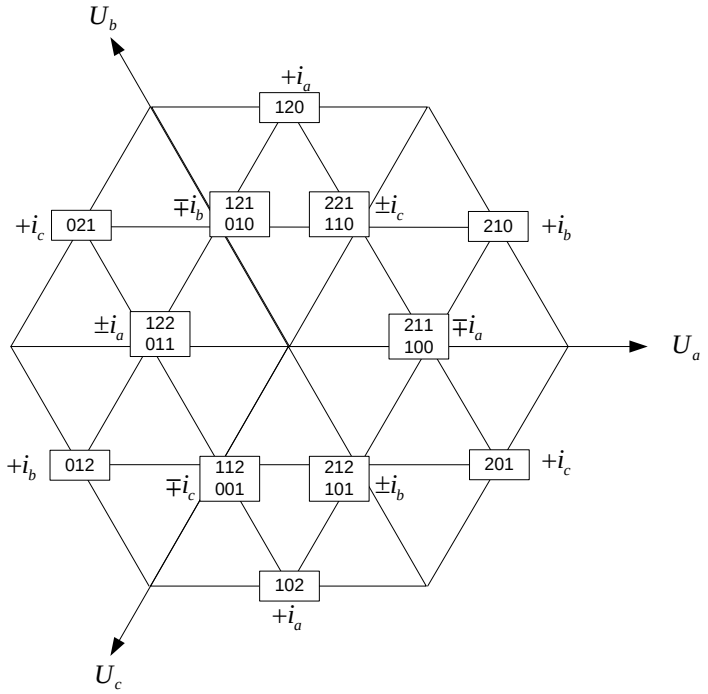

Figure 5.1-1: Small and medium vectors with their belonging phase currents

Only medium and small vector contribute to charging of the capacitors. There is an important phenomenon to understand when Space Vector is being used and this phenomenon is that there will be third harmonic oscillations as long as medium vectors are being used. This does not need to be looked upon as an unbalance which has to be removed, but rather as natural oscillations. At ideal conditions the small vectors will cancel each other in every switching period, while the medium vectors will cancel each other during one fundamental period. The challenge with the DC-bus balancing is that the converter will never operate at ideal conditions. There are several factors that might create unbalance.

- Finite switching frequency
- The phase currents change during a fundamental period.
- The reference change during a fundamental period
- The electrical parameters of the load are not perfectly symmetrical.
- The switches are not ideal

Even though there will be no unbalance at ideal situation there will be unbalances in real life unless balancing algorithms are implemented. In this report three different methods for Space Vector balancing will be presented. The technique of balancing is to differentiate the on-time for each vector within a small vector pair. In the part of PI controller the controlling parameter f is defined the same way as in the calculations for RMS currents in chapter 2. For proportional and prediction balancing there will be presented two controlling parameters.

5.1.1 DC-bus Balancing with Proportional Controller

To reduce the unbalances that occur it is necessary to control the use of the six small vector pairs. When a small vector pair is involved a total duty cycle of d_1 is calculated, where d_1 is a duty cycle of T_{tri}. Due to DC-bus balancing this duty cycle is divided into two:

$$d_1 = d_{1,p} + d_{1,n} \tag{5.1}$$

Here $d_{1,n}$ is the duty cycle off the negative vector, while $d_{1,p}$ is the duty cycle of the positive vector. In a case where the voltage is balanced between the capacitors, these two duty cycles will be equal, but in most cases they will not. Due to this, a controlling parameter is needed, named f_1. By introducing f_1, the expression for $d_{1,n}$ and $d_{1,p}$ will be as the following:

$$\begin{aligned} d_{1,p} &= f_1 \cdot d_1 \\ d_{1,n} &= (1 - f_1) \cdot d_1 \end{aligned} \tag{5.2}$$

If the reference vector is located in a sector with two small vector pair, another controlling parameter is needed, named f_2. The expression for the duty cycles for the second vector pair will be exactly the same as for the first one. The easiest way to balance the voltage is to have a proportional regulator. To decide the values of f_1 and f_2 there are some parameters that have to be found. By measuring the phase currents and capacitor voltages, the ratio between the two small vectors can be decided. Having a situation where U_{dcu} is greater than U_{dcl}, a vector that discharges the upper capacitor and charges the lower one has to be chosen. In [7] a table is given of which vectors that should be used in different cases. The value of f_1 and f_2 should be 0.5 at balanced situations and it should be regulated depending on the voltage difference and direction of the current. The equations of f_1 and f_2 are then as shown below.

$$\begin{aligned} f_1 &= 0.5 - k \cdot \frac{abs(U_{dcu} - U_{dcl})}{(U_{dcu} + U_{dcl})} \\ f_1 &= 0.5 + k \cdot \frac{abs(U_{dcu} - U_{dcl})}{(U_{dcu} + U_{dcl})} \end{aligned} \tag{5.3}$$

K is in this case a constant which has to be given a proper value. As it can be seen from the formula, the value of f_1 is depending on the difference in capacitor voltage. Depending on the sign of the current and whether the vector is a positive or negative vector one of the equations above has to be chosen.

5.1.2 DC-bus Balancing with Prediction

A method which in some cases could give a better result than proportional regulation is by predicting the change in ΔU_{dc} due to the medium vector, and by adding this change in voltage to the existing unbalance, the on-times of the small vectors can be calculated. According to where the reference vector is, three cases could occur:

- one small vector pair, one medium vector and one large vector(case 1)
- two small vector pairs and a medium vector(case 2)
- two small vector pairs and zero vectors (case 3).

Prediction gives a bit more complex situation than proportional regulation, because in each different case there will be different voltage contributions. With this method the small vectors are used to damp the oscillations from the medium vectors.

Case 1:

As described earlier, the way to control the medium vector's influence on the voltage balance between the two capacitors is by use of the small vectors. To find the most correct value of the controlling parameter f_1, the change in voltage due to medium vector has to be calculated. When this voltage and the voltage difference between the capacitors are known, the small vector pair can be regulated. It is not sure that the vector pair can neutralize the unbalance; it depends on the on-time and the current. The voltage contribution from the medium vector is given by

$$U_{medium} = i_{medium} \cdot \frac{t_{medium}}{C} \tag{5.4}$$

Here i_{medium} is equal the neutral point current when the medium vector is being used and t_{medium} is the on-time for the medium vector. U_{medium} will increase U_{dcu} if the neutral point current is positive and this voltage has to be added to the initial ΔU_{dc} before deciding the value of the control parameter. The conditions will therefore be

$$\begin{aligned} (U_{dcu} - U_{dcl} + U_{medium}) \cdot i_{small} > 0 \\ (U_{dcu} - U_{dcl} + U_{medium}) \cdot i_{small} < 0 \end{aligned} \tag{5.5}$$

The neutral point current is i_{small} when the positive small vector is on and $-i_{small}$ when the negative small vector is used. The total voltage contribution that is possible to get from the small vectors is

$$U_{small} = i_{small} \cdot \frac{t_{small}}{C} \tag{5.6}$$

U_{small} is the maximum change in voltage that one of the small vectors can give either positive or negative. If the absolute value of $U_{dcu} - U_{dcl} + U_{medium}$ is greater than the absolute value of U_{small}, then only one of the small vectors should be used during a switching period to reduce

this voltage unbalance. In the opposite situation the small vector is able to remove the unbalance and it should be on until balance is reached. The rest of t_{small} should be shared equal between the two vectors when voltage equilibrium is reached. A flowchart of the code is shown in the figure below.

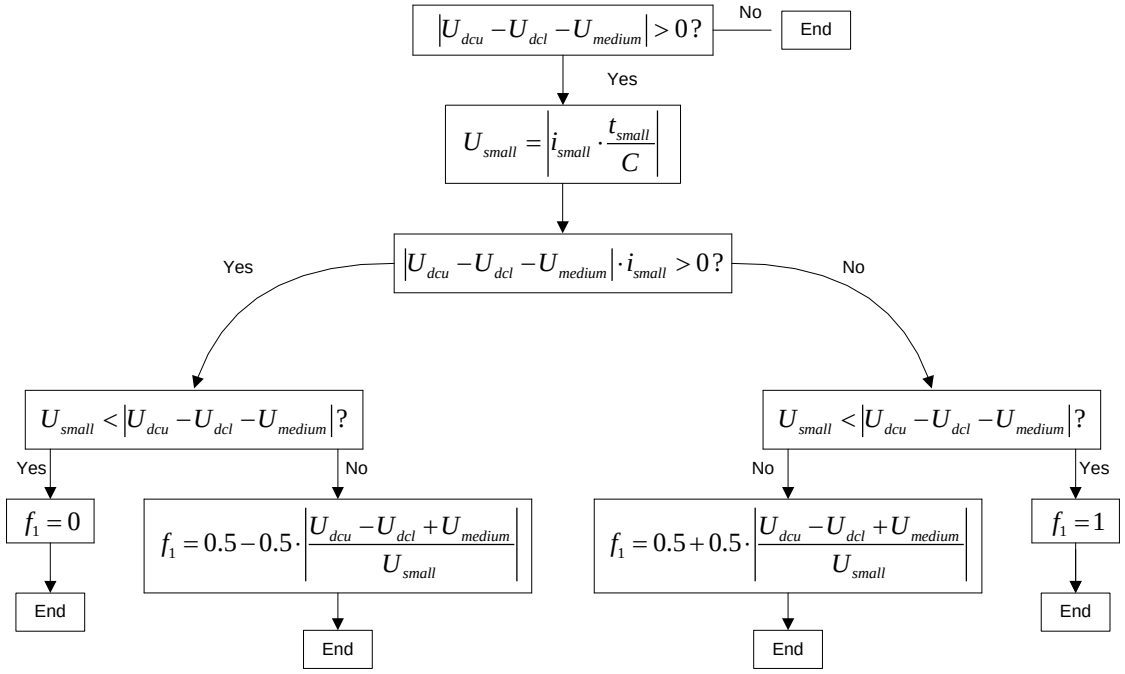

Figure 5.1-2: Flowchart for deciding the values of f_1 and f_2 with SV prediction

As it can be seen in the calculations of f_1, U_{small} is the denominator and if U_{small} have a value close to 0, f_1 can get a higher/lower value than wanted. This will not cause any big problems due to the fact that U_{small} has a low value and a change in f_1 will not have a big influence on ΔU_{dc}.

Case 2:

In this case there is one additional small vector pair compared to previous case. This gives a better chance of balancing the voltage unbalance. In a situation where f_1 is unequal 0 or 1 there is no need to actively control the second small vector pair and f_2 is equal 0.5. U_{small} is not big enough to bring ΔU_{dc} to zero if f_1 is equal 0 or 1, and in that case f_2 needs to be actively controlled. The code for deciding f_2 will be the same as for f_1, the only difference is the following:

$$U_{dcu} - U_{dcl} + U_{medium} \Rightarrow U_{dcu} - U_{dcl} + U_{medium} + U_{small}$$

By having f_2 equal to 0 or 1 both vector pairs are used to their maximum to balance the capacitor voltages. If there is still an unbalance, this has to be balanced in the upcoming switching periods.

Case 3:

In this case there will be no voltage contribution from a medium vector, so it will be easier to control the voltage in this case. Staying inside the six inner sectors will only require small adjustments of f_1 and f_2. As in case 2, f_1 is controlled first. If only controlling f_1 is not enough to bring the voltage to an equilibrium, then f_2 also has to be controlled. According to the current and on-time to the small vectors, as in the other cases, it is not sure that the voltage unbalance is brought to equilibrium within only one switching period.

5.1.3 Space Vector Balancing with PI Controller

In order to get a good understanding of the response of the DC-bus voltages an analysis of the neutral point current should be made. As it has been described earlier in this report it is the use of small vectors and medium vectors that create a neutral point current which again influence the DC-bus voltages. In [10] the expression for the neutral point current is given as the following for Space Vector

$$i_{NP} = i_{small1}(t)\cdot(1-2f_1)\cdot t_{small1} + i_{small2}(t)\cdot(1-2f_2)\cdot t_{small2} + i_{medium}(t)\cdot t_{medium} \tag{5.7}$$

This is a very general expression and in order to find the average current it is needed to evolve expressions for the duty cycles for the different vectors in the modulation modes. In an ideal situation the neutral point current should be zero during one switching period in order to keep the DC-bus voltage close to equilibrium. In [14] the average neutral point current is given, but the calculations are not shown and the scaling is also different compared to this master thesis. Some errors also occurred when the results were plotted. It was therefore decided to calculate the neutral point current in this thesis to certify the results from [14]. In [13] and [1] there were used two balancing parameters. In [14] only one is used and that will also be the case in the equations derived here. The f parameter is the duty cycle of the small vector connected to level 2. To be able to calculate the average NP current it is necessary to divide the integral into different regions, as it was for the average and RMS currents calculated earlier in this report. The calculation for mode 1 which is the six inner hexagons is given as the following

$$\frac{I_{NP,avg}}{\hat{I}_{phase}} = \frac{3}{2\pi}\left(\begin{array}{l}\int_0^{\frac{\pi}{3}}\left(\begin{array}{l}\sqrt{3}m\cdot\sin\left(\frac{\pi}{3}-\zeta\right)\cdot f\cdot(-\cos(\zeta-\varphi))+\sqrt{3}m\cdot\sin\left(\frac{\pi}{3}-\zeta\right)\cdot(1-f)\cdot\cos(\zeta-\varphi)\\ +\sqrt{3}m\cdot\sin(\zeta)\cdot f\cdot\cos\left(\zeta+\frac{2\pi}{3}-\varphi\right)-\sqrt{3}m\cdot\sin(\zeta)\cdot(1-f)\cdot\cos\left(\zeta+\frac{2\pi}{3}-\varphi\right)\end{array}\right)d\zeta\\ +\int_{\frac{\pi}{3}}^{\frac{2\pi}{3}}\left(\begin{array}{l}\sqrt{3}m\cdot\sin\left(\frac{2\pi}{3}-\zeta\right)\cdot f\cdot\cos\left(\zeta+\frac{2\pi}{3}-\varphi\right)-\sqrt{3}m\cdot\sin\left(\frac{2\pi}{3}-\zeta\right)\cdot(1-f)\cdot\cos\left(\zeta+\frac{2\pi}{3}-\varphi\right)\\ \sqrt{3}m\cdot\sin\left(\zeta-\frac{\pi}{3}\right)\cdot(1-f)\cdot\cos\left(\zeta-\frac{2\pi}{3}-\varphi\right)-\sqrt{3}m\cdot\sin\left(\zeta-\frac{\pi}{3}\right)\cdot f\cdot\cos\left(\zeta-\frac{2\pi}{3}-\varphi\right)\end{array}\right)d\zeta\end{array}\right) \tag{5.8}$$

The duty cycles are to be found in chapter 2 and the result of this integral is given below

$$\frac{I_{NP,avg}}{\hat{I}_{phase}} = \frac{3}{2}\cdot m\cdot(1-2f)\cdot\cos\varphi \tag{5.9}$$

As it can be seen the neutral point current will be equal to zero in the six inner sectors if the sharing function is 0.5. In a practical situation it is not sure that i_{NP} will be equal to zero by having f equal to 0.5. This equation is derived by setting the switching frequency equal to infinity, but for this type of application it is more likely that it will be in the area of 1000 Hz. In mode 2 the calculations are more complicated because the reference vector is partly in the six inner hexagons and partly outside.

As in the calculations in chapter 2 it is necessary to introduce the angle β. β is in this case given as the following

$$\beta = \sin^{-1}\left(\frac{1}{\sqrt{3}\cdot m}\right) - \frac{\pi}{3} \tag{5.10}$$

At this angle the reference vector crosses the border of the six inner hexagons and between β and π/3 the reference will use medium and large vectors. Due to this the current calculation has to be divided into regions as shown below in this mode.

$$\frac{I_{NP,avg}}{\hat{I}_{phase}} = \frac{3}{2\pi}\left(\begin{array}{l}
\int_{0}^{\sin^{-1}\left(\frac{1}{\sqrt{3}\cdot m}\right)-\frac{\pi}{3}} \begin{pmatrix} \sqrt{3}\cdot m\left(\frac{\sqrt{3}}{2}\cdot\cos(\zeta)-\frac{1}{2}\cdot\sin(\zeta)\right)\cdot(2f-1)\cdot(-\cos(\zeta-\varphi))+ \\ \sqrt{3}\cdot m\cdot\sin(\zeta)\cdot(2f-1)\cdot\cos\left(\zeta+\frac{2\pi}{3}-\varphi\right) \end{pmatrix} d\zeta \\
+\int_{\sin^{-1}\left(\frac{1}{\sqrt{3}\cdot m}\right)-\frac{\pi}{3}}^{\frac{2\pi}{3}-\sin^{-1}\left(\frac{1}{\sqrt{3}\cdot m}\right)} \begin{pmatrix} \left(-\sqrt{3}\cdot m\cdot\sin(\zeta)+1\right)\cdot(2f-1)\cdot(-\cos(\zeta-\varphi)) \\ +\left(-\sqrt{3}\cdot m\cdot\left(-\frac{\sqrt{3}}{2}\cdot\cos(\zeta)-\frac{1}{2}\cdot\sin(\zeta)\right)-1\right)\cdot\cos\left(\zeta-\frac{2\pi}{3}-\varphi\right) \\ +\left(-\sqrt{3}\cdot m\cdot\left(\frac{\sqrt{3}}{2}\cdot\cos(\zeta)-\frac{1}{2}\cdot\sin(\zeta)\right)+1\right)\cdot(2f-1)\cdot\cos\left(\zeta+\frac{2\pi}{3}-\varphi\right) \end{pmatrix} d\zeta \\
+\int_{\frac{2\pi}{3}-\sin^{-1}\left(\frac{1}{\sqrt{3}\cdot m}\right)}^{\frac{\pi}{3}} \begin{pmatrix} \sqrt{3}\cdot m\cdot\left(\frac{\sqrt{3}}{2}\cdot\cos(\zeta)-\frac{1}{2}\cdot\sin(\zeta)\right)\cdot(2f-1)\cdot(\cos(\zeta-\varphi)) \\ +\sqrt{3}\cdot m\cdot\sin(\zeta)\cdot(2f-1)\cdot\cos\left(\zeta+\frac{2\pi}{3}-\varphi\right) \end{pmatrix} d\zeta \\
+\int_{\frac{\pi}{3}}^{\sin^{-1}\left(\frac{1}{\sqrt{3}\cdot m}\right)} \begin{pmatrix} -\sqrt{3}\cdot m\cdot\left(-\frac{\sqrt{3}}{2}\cdot\cos(\zeta)-\frac{1}{2}\cdot\sin(\zeta)\right)\cdot(2f-1)\cdot\cos\left(\zeta+\frac{2\pi}{3}-\varphi\right) \\ -\sqrt{3}\cdot m\cdot\left(\frac{\sqrt{3}}{2}\cdot\cos(\zeta)-\frac{1}{2}\cdot\sin(\zeta)\right)\cdot(2f-1)\cdot\left(-\cos\left(\zeta-\frac{2\pi}{3}-\varphi\right)\right) \end{pmatrix} d\zeta \\
+\int_{\sin^{-1}\left(\frac{1}{\sqrt{3}\cdot m}\right)}^{\pi-\sin^{-1}\left(\frac{1}{\sqrt{3}\cdot m}\right)} \begin{pmatrix} \left(\sqrt{3}\cdot m\cdot\left(\frac{\sqrt{3}}{2}\cdot\cos(\zeta)-\frac{1}{2}\cdot\sin(\zeta)\right)+1\right)\cdot(2f-1)\cdot\cos\left(\zeta+\frac{2\pi}{3}-\varphi\right) \\ +\left(\sqrt{3}\cdot m\cdot\sin(\zeta)-1\right)\cdot\cos(\zeta-\varphi)+\left(\sqrt{3}\cdot m\cdot\left(-\frac{\sqrt{3}}{2}\cdot\cos(\zeta)-\frac{1}{2}\cdot\sin(\zeta)\right)+1\right)\cdot \\ (2f-1)\cdot\left(-\cos\left(\zeta-\frac{2\pi}{3}-\varphi\right)\right) \end{pmatrix} d\zeta \\
+\int_{\pi-\sin^{-1}\left(\frac{1}{\sqrt{3}\cdot m}\right)}^{\frac{2\pi}{3}} \begin{pmatrix} -\sqrt{3}\cdot m\cdot\left(-\frac{\sqrt{3}}{2}\cdot\cos(\zeta)-\frac{1}{2}\cdot\sin(\zeta)\right)\cdot(2f-1)\cdot\cos\left(\zeta+\frac{2\pi}{3}-\varphi\right)- \\ \sqrt{3}\cdot m\cdot\left(\frac{\sqrt{3}}{2}\cdot\cos(\zeta)-\frac{1}{2}\cdot\sin(\zeta)\right)\cdot(2f-1)\cdot\left(-\cos\left(\zeta-\frac{2\pi}{3}-\varphi\right)\right) \end{pmatrix} d\zeta
\end{array}\right) \tag{5.11}$$

The result of this integral is given below

$$\frac{I_{NP,avg}}{\hat{I}_{phase}} = \frac{3\cdot\cos\varphi}{\pi}\cdot(1-2f)\cdot\left(3\cdot m\cdot\sin^{-1}\left(\frac{1}{\sqrt{3}\cdot m}\right)+\sqrt{\frac{3\cdot m^2-1}{m^2}}-m\cdot\pi\right) \tag{5.12}$$

By having f equal to 0.5 the average current will be zero, which means that the influence from the medium vectors will cancel each other. The next mode is when the reference vector is outside the six inner hexagons and inside overmodulation. Overmodulation will be treated in another chapter in this report. The integral for mode 3 is given below.

$$\frac{I_{NP,avg}}{\hat{I}_{phase}} = \frac{3}{2\pi}\left(\begin{array}{l}
\int_{0}^{\frac{\pi}{3}-\sin^{-1}\left(\frac{1}{\sqrt{3}\cdot m}\right)} \left(\begin{array}{l}\sqrt{3}\cdot m\cdot\sin(\zeta)\cdot\cos\left(\zeta-\frac{2\pi}{3}-\varphi\right)+\\ \left(\sqrt{3}\cdot m\cdot\left(-\frac{\sqrt{3}}{2}\cdot\cos(\zeta)-\frac{1}{2}\cdot\sin(\zeta)\right)+2\right)\cdot(2f-1)\cdot(-\cos(\zeta-\varphi))\end{array}\right)d\zeta \\
\int_{\frac{\pi}{3}-\sin^{-1}\left(\frac{1}{\sqrt{3}\cdot m}\right)}^{\sin^{-1}\left(\frac{1}{\sqrt{3}\cdot m}\right)} \left(\begin{array}{l}\left(-\sqrt{3}\cdot m\cdot\sin(\zeta)+1\right)\cdot(2f-1)\cdot(-\cos(\zeta-\varphi))+\\ \left(-\sqrt{3}\cdot m\cdot\left(-\frac{\sqrt{3}}{2}\cdot\cos(\zeta)-\frac{1}{2}\cdot\sin(\zeta)\right)-1\right)\cdot\cos\left(\zeta-\frac{2\pi}{3}-\varphi\right)\\ +\left(-\sqrt{3}\cdot m\cdot\left(\frac{\sqrt{3}}{2}\cdot\cos(\zeta)-\frac{1}{2}\cdot\sin(\zeta)\right)+1\right)\cdot(2f-1)\cdot\cos\left(\zeta+\frac{2\pi}{3}-\varphi\right)\end{array}\right)d\zeta \\
\int_{\sin^{-1}\left(\frac{1}{\sqrt{3}\cdot m}\right)}^{\frac{\pi}{3}} \left(\begin{array}{l}\sqrt{3}\cdot m\cdot\left(\frac{\sqrt{3}}{2}\cdot\cos(\zeta)-\frac{1}{2}\cdot\sin(\zeta)\right)\cdot\cos\left(\zeta-\frac{2\pi}{3}-\varphi\right)+\\ \left(\sqrt{3}\cdot m\cdot\left(-\frac{\sqrt{3}}{2}\cdot\cos(\zeta)-\frac{1}{2}\cdot\sin(\zeta)\right)+2\right)\cdot(2f-1)\cdot\cos\left(\zeta+\frac{2\pi}{3}-\varphi\right)\end{array}\right)d\zeta \\
\int_{\frac{\pi}{3}}^{\frac{2\pi}{3}-\sin^{-1}\left(\frac{1}{\sqrt{3}\cdot m}\right)} \left(\begin{array}{l}\left(-\sqrt{3}\cdot m\cdot\sin(\zeta)+2\right)\cdot(2f-1)\cdot\cos\left(\zeta+\frac{2\pi}{3}-\varphi\right)+\\ \left(-\sqrt{3}\cdot m\cdot\left(\frac{\sqrt{3}}{2}\cdot\cos(\zeta)-\frac{1}{2}\cdot\sin(\zeta)\right)\right)\cdot\cos(\zeta-\varphi)\end{array}\right)d\zeta \\
\int_{\frac{2\pi}{3}-\sin^{-1}\left(\frac{1}{\sqrt{3}\cdot m}\right)}^{\frac{\pi}{3}+\sin^{-1}\left(\frac{1}{\sqrt{3}\cdot m}\right)} \left(\begin{array}{l}\left(\sqrt{3}\cdot m\cdot\left(\frac{\sqrt{3}}{2}\cdot\cos(\zeta)-\frac{1}{2}\cdot\sin(\zeta)\right)+1\right)\cdot(2f-1)\cdot\cos\left(\zeta+\frac{2\pi}{3}-\varphi\right)+\\ \left(\sqrt{3}\cdot m\cdot\sin(\zeta)-1\right)\cdot\cos(\zeta-\varphi)+\\ \left(\sqrt{3}\cdot m\cdot\left(-\frac{\sqrt{3}}{2}\cdot\cos(\zeta)-\frac{1}{2}\cdot\sin(\zeta)\right)+1\right)\cdot(2f-1)\cdot\left(-\cos\left(\zeta-\frac{2\pi}{3}-\varphi\right)\right)\end{array}\right)d\zeta \\
\int_{\frac{\pi}{3}+\sin^{-1}\left(\frac{1}{\sqrt{3}\cdot m}\right)}^{\frac{2\pi}{3}} \left(\begin{array}{l}-\sqrt{3}\cdot m\cdot\left(-\frac{\sqrt{3}}{2}\cdot\cos(\zeta)-\frac{1}{2}\cdot\sin(\zeta)\right)\cdot\cos(\zeta-\varphi)+\\ \left(-\sqrt{3}\cdot m\cdot\sin(\zeta)+2\right)\cdot(2f-1)\cdot\left(-\cos\left(\zeta-\frac{2\pi}{3}-\varphi\right)\right)\end{array}\right)d\zeta
\end{array}\right) \quad (5.13)$$

The result of the integral is given below

$$\frac{I_{NP,avg}}{\hat{I}_{phase}} = \frac{\cos(\varphi)}{2\cdot\pi\cdot m}\cdot(1-2f)\cdot\left(\sqrt{3}+3\cdot\sqrt{\frac{3\cdot m^2-1}{m^2}}\cdot m+9\cdot m^2\cdot\sin^{-1}\left(\frac{1}{\sqrt{3}\cdot m}\right)-3\cdot\pi\cdot m^2\right) \quad (5.14)$$

A 3D plot in MATLAB can verify that the results are continuous. This is shown for an f equal to 0 and 1.

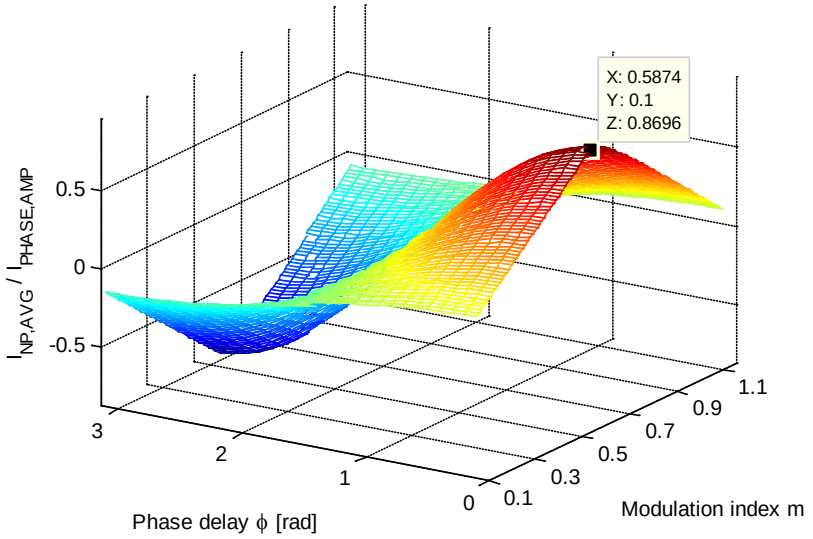

Figure 5.1-3: Average neutral point current with f equal to 0

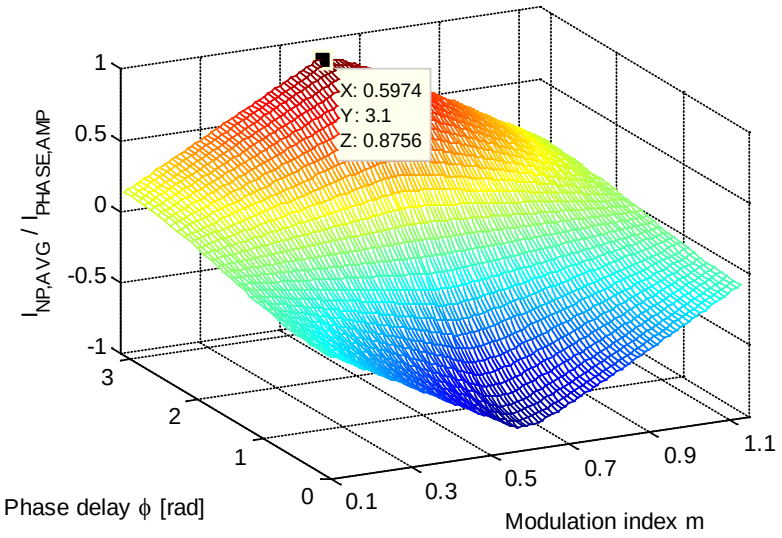

Figure 5.1-4: Average neutral point current with f equal to 1

As it can be seen in both figures the current is continuous in the whole spectra. Hence the calculations seem correct. The response is the same for f equal 0 and 1; it is only the sign that is changed. The figures show that the highest average neutral point current is reached at a modulation index in the area around 0.6, which is natural since the small vectors have the longest on-time in this area. It is also in this area space vector has the best regulation possibilities, due to little influence from the medium vector and the small vectors have maximum on-time.

The best way of deciding the parameters in the DC-bus regulators is by studying the effect of changing the parameters in the equations for the neutral point current. Since this is a non-linear system, linearization is needed in order to decide the values in the regulators. The approach in this report will be the same as in [14], and more details regarding linearization is

to be found in [20]. For this converter a positive neutral point current will increase the voltage in the upper capacitor voltage and a negative i_{NP} will decrease the upper capacitor voltage. The following expression can then be written:

$$C\frac{d\Delta U_{dc}}{dt} = i_{NP} \tag{5.15}$$

i_{NP} has the three variables m, φ and f. To make this system linear around a working point the expressions for i_{NP} needs to be differentiated with respect to the three variables. The value of f in the working point area will be 0.5. It can be shown that the value of the derivation of m and φ will be zero for all the modes having f equal to 0.5. Hence it is only the derivation of f that needs to be taken into consideration when deciding the parameters in the chosen regulator. The total transfer system with regulator will then be as shown in the figure below.

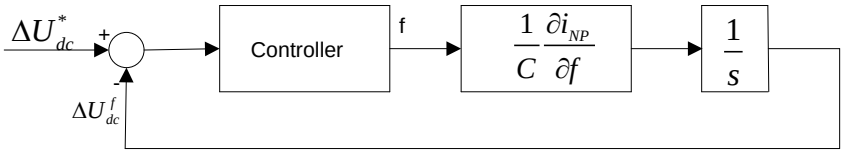

Figure 5.1-5: Block diagram for PI controller

When the system is given then the parameters in the regulator can be chosen. What need to be decided are the crossing frequency and an optimization of the parameters by simulations.

In [13] two different control strategies of balancing the DC-bus voltage were presented. Proportional regulation gave slightly better THD_i than prediction. One problem that might occur with proportional regulation is that a stationary error may take place. To be able to remove a stationary error it is necessary to have a PI controller. Then integrator part of the controller will then be able to remove a possible stationary error. The drawback of having a PI controller compared to a proportional regulator is that it makes the system slower. Thus it is important to check with simulations whether a PI controller is necessary or not and how the response will be.

The parameters of the PI controller were decided from the calculations of the neutral point currents. Hence the values in the controller will be adaptive. The same goes for the proportional controller. The method of deciding the parameter values for the PI controller is found in [21]. From the block diagram above the following criteria can be given for the transfer function.

PI controller: $\frac{k_i}{s}\left(1+\frac{s}{k_i/k_p}\right)$

$$\left| \left(\frac{k_i \frac{\partial i_{NP}}{\partial f}}{C} \right) \frac{1+s/(k_i/k_p)}{s^2} \right|_{s=j\omega_c} = 1$$
$$\angle \left(\frac{k_i \frac{\partial i_{NP}}{\partial f}}{C} \frac{1+s/(k_i/k_p)}{s^2} \right)_{s=j\omega_c} = -180^o + \phi_{pm} \tag{5.16}$$

By setting the crossover frequency to 100 Hz and the phase margin to 60 degrees, a suggestion of the parameter values can be given for the different modes. By solving these two equations the expressions of k_i and k_p are as the following.

$$k_i = \frac{C \cdot \omega_c^2}{\frac{\partial i_{NP}}{\partial f} \sqrt{1+\tan^2 \phi_{pm}}} \tag{5.17}$$

$$k_p = \frac{k_i}{\omega_c} \tan \phi_{pm} \tag{5.18}$$

The next step from this is to find the different derivatives of i_{NP} with respect to f for the different modes. The results are given in the table below.

Table 5.1-3: Derivatives of neutral point current

Mode	$\partial i_{NP} / \partial f$
1	$-3 \cdot m \cdot i \cdot \cos(\varphi)$
2	$\frac{-6 \cdot i \cdot \cos(\varphi)}{\pi} \cdot \left(3 \cdot m \cdot \sin\left(\frac{1}{\sqrt{3} \cdot m} \right) + \sqrt{\frac{3 \cdot m^2 - 1}{m^2}} - m \cdot \pi \right)$
3	$-\frac{i \cdot \cos(\varphi)}{\pi \cdot m} \cdot \left(\sqrt{3} + 3 \cdot \sqrt{\frac{3 \cdot m^2 - 1}{m^2}} \cdot m + 9 \cdot m^2 \cdot \sin^{-1}\left(\frac{1}{\sqrt{3} \cdot m} \right) - 3 \cdot m^2 \cdot \pi \right)$

As it can be seen from the table above the values of k_i and k_p will be dependent on the modulation index and cos(φ), hence they will probably work more dynamically compared to fixed values. To get the best values small adjustments by simulations are needed. One problem that will occur at pure inductive load and with very low current is that the denominator in k_i will go to zero and hence k_i will go to infinity. Because of this there should be some limitations when φ approaches π/2.

5.2 DC-bus Balancing with Double-Signal

Double-Signal PWM is the other method where active DC-bus balancing can be used. As it was described earlier; the method is to split the control signal into two signals. The idea behind splitting the control signal into two is that the average neutral point current should be zero during one switching period. In [5] the average neutral point current is given by

$$\bar{i}_{np} = d_{anp}\bar{i}_a + d_{bnp}\bar{i}_b + d_{cnp}\bar{i}_c \tag{5.19}$$

Where d_{inp} is the duty cycles for the bridge legs when switch 2 and 3 is on. It is defined as

$$d_{inp} = \left| v_{in} + 1 - v_{ip} \right|, i = \{a, b, c\} \tag{5.20}$$

The solution to keep the average neutral point current equal to zero and to have a minimum switching transitions is derived in [5] (in [10] an expression for the i_{NP} is presented for Space Vector modulation). Hence the control signals are given as in (2.23). In theory it should be enough to keep this average value equal to zero to prevent voltage unbalance. However, the operation of the converter and response of the converter and load will not be ideal in real operation. This will lead to drift of the capacitor voltages if there is no balancing.

Splitting the control signal into two signals is not enough to control the DC-bus. Proper offset signals needs to be added to keep the capacitor voltages close to equilibrium. In [5] proportional regulation is presented and in [6] regulation with prediction of the phase currents influence is presented. Both methods will be described more in detail in the next two chapters.

5.2.1 DC-bus Balancing with Proportional Regulation

One of the goals when the DC-bus should be balanced is to reach voltage equilibrium without increasing the switching frequency of the devices. For DSPWM the control signal is split into two signals, and due to this each signal is clamped to zero during one third of a fundamental period. It is not wanted to change the control signals when one of them is zero because this would increase the number of switching transitions dramatically. In other words there is only a possibility to change the control signals in one third of a fundamental period for each phase. Hence the offset signal can only be added to one bridge leg at all times. The drawback of this method is that the dynamics of the system is slow and it will take some time to balance the voltage. The offset signal which is proposed in [5] is given as

$$U_{ioff} = k\left|\Delta U_{dc}\right| \cdot sign(\Delta U_{dc} i_i) \cdot sign(U_{ip} - U_{in} - 1) \tag{5.21}$$

ΔU_{dc} is the voltage difference of U_{dcu}-U_{dcl}. This offset signal should be added to U_{ip} and subtracted from U_{in} The reason for the expression sign(U_{ip} – U_{in} – 1) is that one special situation could occur when the signal is split into two and this is shown in the figure below, which is showing the same as fig. 4 in [5].

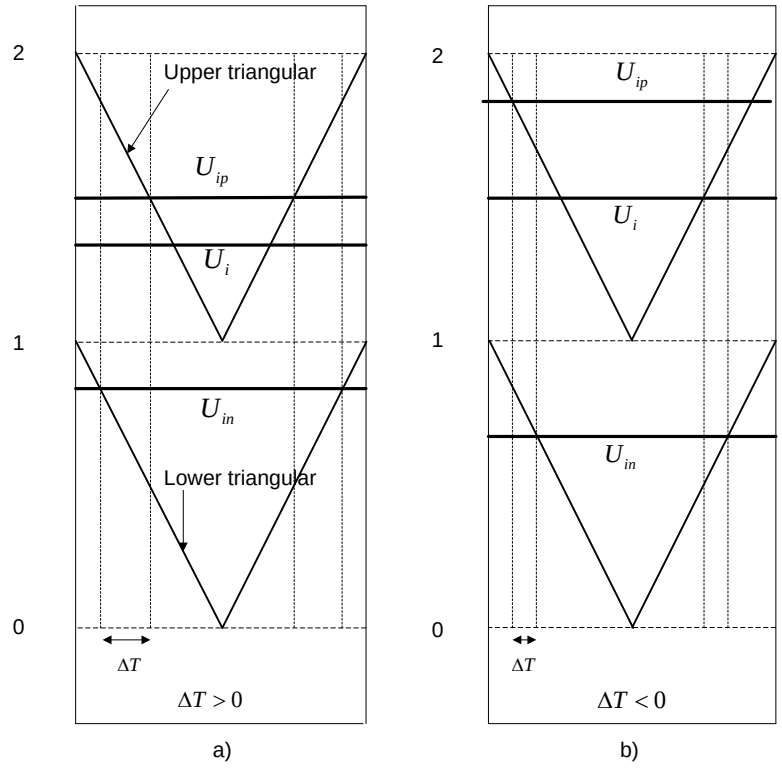

Figure 5.2-1: Two possible situations that may occur by adding an offset signal. A) Normal switching situation. B) Too big offset signal is added

ΔT is defined as $t_{on,upper} - t_{on,lower}$ and a positive value is a normal operational situation. Figure 5.2-1 a) is showing such a situation where switch 2 is turned on before switch 1, which is wanted. In b) a too big offset is added and due to this switch 1 turning on before switch 2. Because of this situation the expression $sign(U_{ip} - U_{in} - 1)$ is added, but as they conclude in [6], it is not necessary with it. $Sign(U_{ip} - U_{in} - 1)$ will always return -1 since v_{in} +1 will always be greater than v_{ip} when no offset signal is added. Since (4.10) is added to U_{ip} and subtracted to U_{in} equation (2.11) is still valid.

It is important to avoid that switch 1 is turned on before switch 2 and switch 2 should not be turned off before switch 1. Due to this the offset signal has some limitations. If a situation as in Figure 5.2-1 b) occurs it is important that the offset signal is reduced. The control statement is the following.

$$U_{ip} + U_{off} > U_{in} - U_{off} + 1 \tag{5.22}$$

If this is the case, then the offset signal has to be reduced to the following

$$U_{off} = \frac{U_{in} - U_{ip} + 1}{2} \tag{5.23}$$

An offset that is too large will make either the lower or the higher control signal or the both of them go into saturation. For the higher control signal it means that it has a value higher than 1

(positive saturation) or lower than 0 (negative saturation). For the lower control signal it means that it has a value higher than 0 (positive saturation) or lower than -1 (negative saturation). In these cases the output voltage of the bridge leg will not be what is desired. However the upper control signal will not go into positive saturation because the previous test has already made sure that the duty cycle of the upper switch is lower than the duty cycle of the lower switch. For the same reason the lower control signal will not go into negative saturation. How to solve this is given in Table 5.2-1.

Table 5.2-1: Limits for saturation of Double-Signal DC-bus balancing

Case	Problem description	Condition	Final offset
1	Negative saturation on the upper control signal and this is of a greater magnitude than a potential positive saturation on the lower control signal	$U_{ip}+U_{off}<0$ and $U_{ip}+U_{off}<-U_{in}+U_{off}$	$U_{off}=-U_{ip}$
2	Positive saturation on the lower control signal and this if of a greater magnitude than a potential negative saturation on the upper control signal	$U_{in}+1-U_{off}>1$ and $U_{ip}+U_{off}\geq -U_{in}+U_{off}$	$U_{off}=U_{in}$

5.2.2 Dc-bus Balancing with Prediction

This method is based on predicting the neutral point current needed to balance the capacitors and then calculate the offset needed on the upper and lower control signal to achieve this current. The method is published in [6]. The desired neutral point current is expressed as:

$$i_{NP}=C\frac{U_{cl}-U_{cu}}{T_{tri}} \tag{5.24}$$

The offset is added to the upper and lower control signal of only one leg at time. Table 4.2-2 lists the solution obtained in [6] and in what intervals the control signals are added.

Table 5.2-2: Offset signals for Double-Signal with prediction

Phase with either U_{upper} or U_{lower} clamped to zero	Offset
U_b and U_c	$U_{aoff} = \pm\frac{1}{2}\left\lvert\frac{i_{NP}\lvert U_{an}-U_{ap}+1\rvert}{-\lvert U_{bn}-U_{bp}+1\rvert i_b-\lvert U_{cn}-U_{cp}+1\rvert i_c}\right\rvert$
U_a and U_c	$U_{boff} = \pm\frac{1}{2}\left\lvert\frac{i_{NP}\lvert U_{bn}-U_{bp}+1\rvert}{-\lvert U_{an}-U_{ap}+1\rvert i_a-\lvert U_{cn}-U_{cp}+1\rvert i_c}\right\rvert$
U_a and U_b	$U_{coff} = \pm\frac{1}{2}\left\lvert\frac{i_{NP}\lvert U_{cn}-U_{cp}+1\rvert}{-\lvert U_{an}-U_{ap}+1\rvert i_a-\lvert U_{bn}-U_{bp}+1\rvert i_b}\right\rvert$

The sign of the solution is decided with the same test as in the previous section. The limitations to the offset signals are also the same as in the previous section. If the denominator is close to zero the offset could get too high. This will happen very seldom and the limitations to the offset signal will limit this effect. The phase current which the offset will be added to will have a small value in the cases when the denominator goes to zero. This can be seen in [6].

5.3 Simulations Results

In this part simulations of the PI controller have been made and there have also been made several simulations for the different controlling methods and they are compared.

5.3.1 Simulations PI Controller for Space Vector

Due to limitations in the simulation programs it is not possible to simulate for a long time with short time steps. Hence it is hard to see what will happen with the contribution from the integral part. If the time steps are increased too much the accuracy is not good enough and strange results occur.

The approach shown above was used to determine the parameters for the PI controller. Some very interesting results were found and the simulations below show what happened. When using the same sign as in the calculations for k_i the value of the contribution increased throughout the entire time interval and made the system unstable. With smaller values of k_i the contribution still increased, but not as steep as for higher values. This is shown in the figure below.

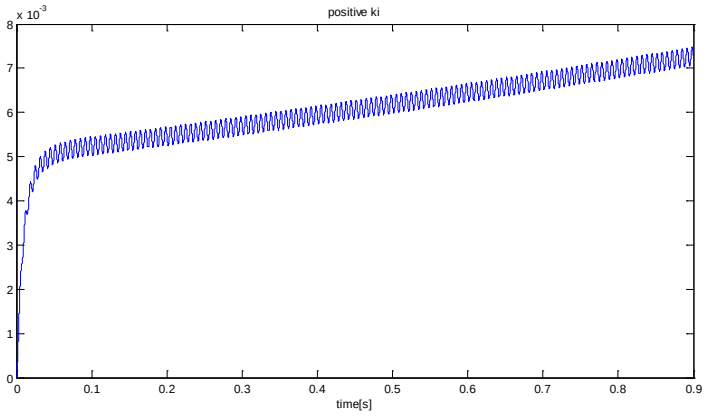

Figure 5.3-1: Response with positive k_i

This figure shows the contribution from the integral part of the PI controller. The figure is only showing up to 0.9 seconds due to limited data capability at this high resolution, but the graph continues with the same slop until it becomes unstable and increases rapidly. Hence it is not wanted to operate with the same sign for k_i as found in the table.

Because of the bad result the sign was changed. This gave a much better result than in previous case and is shown below.

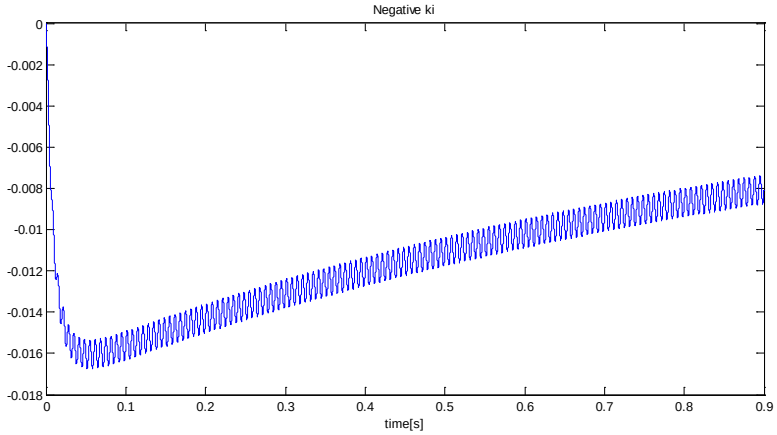

Figure 5.3-2: Response with negative k_i

With a higher value of k_i the contribution from the integral part will go faster to zero, but will also make the system more sensitive. What is really interesting to see here is that this value is very low. It has not a big influence on f, most of f is depending on the contribution from the proportional part. The simulations are showing that there seems to be few advantages of having a PI controller compared to a P controller for the setup used in the simulations. In real life implementation there might be a need for a PI controller due to the fact that there might be some disturbances that will work against f. This is something that needs to be tested in the laboratory.

5.3.2 Simulation Results of 1st Harmonic Output Voltage, THD_i and Maximum Voltage Unbalance at Stationary Operation

In this part there have been done some simulations in order to compare the different balancing strategies. In all the simulations the amplitude has been 1000 amps for all of the phase currents. In [13] the switching frequency was set to be 1000 Hz, while in this report it will be 1050 Hz. As it has been discussed previous in this report this could give a better result since there are three-phase symmetry with 1050 Hz.

Table 5.3-1: 1st harmonic line-to-line output voltage with DC-bus balancing. Cos(φ) equal to 1

	Line-to-line voltage modulation			
Signal	**0.8660**	**1.3856**	**1.7320**	**2.0**
Space vector proportional	0.8513	1.3713	1.7165	1.9844
Space vector prediction	0.8517	1.3714	1.7169	1.9836
Space vector PI	0.8515	1.3712	1.7167	1.9844
Double-Signal proportional	0.8534	1.3714	1.7165	1.9844
Double-Signal prediction	0.8527	1.3708	1.7161	1.9847

Table 5.3-2: 1st THD_i with DC-bus balancing. Cos(φ) equal to 1

	Line-to-line voltage modulation			
Signal	**0.8660**	**1.3856**	**1.7320**	**2.0**
Space vector proportional	1.05%	0.86%	0.88%	0.92%
Space vector prediction	1.06%	0.89%	0.99%	0.96%
Space vector PI	1.05%	0.87%	0.90%	0.92%
Double-Signal proportional	1.21%	1.48%	1.79%	1.89%
Double-Signal prediction	1.22%	1.47%	1.79%	1.88%

The values in Table 5.3-1 show that there are very little differences in the 1st harmonic output voltage. It can be concluded that all of the modulation methods works the way they should and the same results were found in [13]. In Table 5.3-2 the THD_i results are collected. The PI-controller for Space Vector has values very close to the proportional version, which is expected since it has been shown that the integral part of the PI-controller has a low contribution compared to the proportional part. The values are also better compared to having a switching frequency of 1000 Hz.

5.3.3 Simulation Results with Different Capacitor Values

When this model is to be implemented in real life the designer will always try to find two capacitors with as equal capacitances as possible, but they will not be exactly the same. As time goes by there will also be some fluctuation in the values. Hence it is important to find out whether the balancing strategies are able to balance conditions with different capacitor values. The simulations are done with a capacitor value of 1900 microfarad on the upper capacitor

and 1700 microfarad on the lower capacitor. A situation with such a big capacitor difference will most likely not occur in a real life implementation but it shows very well the balancing possibilities of the algorithms. The modulation index is 1.0 and the cos(φ) is 1.

The first simulation is done with the PI controller and is shown in the figure below.

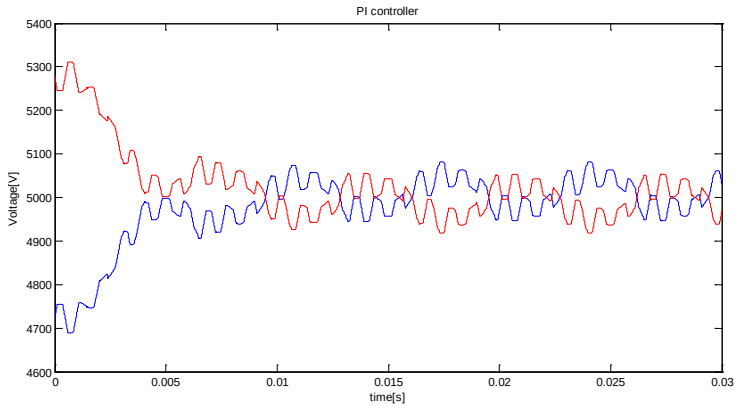

Figur 5.3-3: Space Vector PI controller with different capacitor values

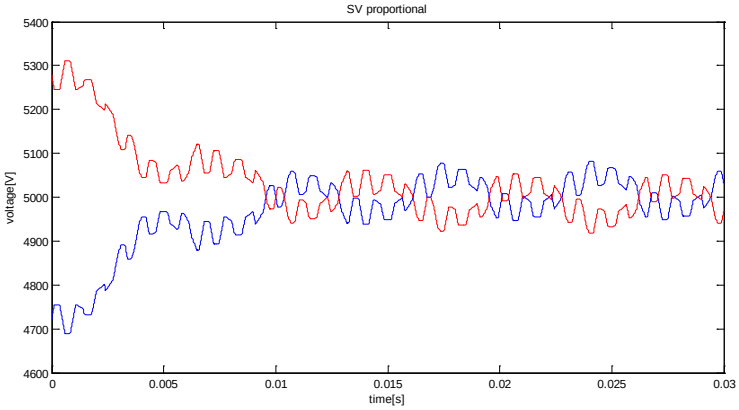

Figur 5.3-4: Space Vector proportional balancing with different capacitor values

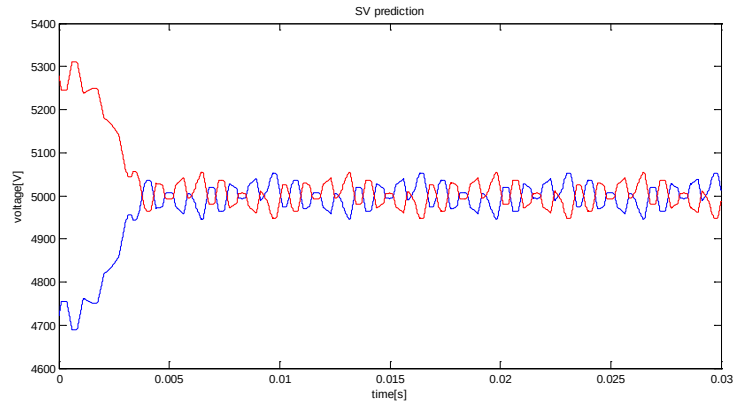

Figur 5.3-5 Space Vector prediction balancing with different capacitor values

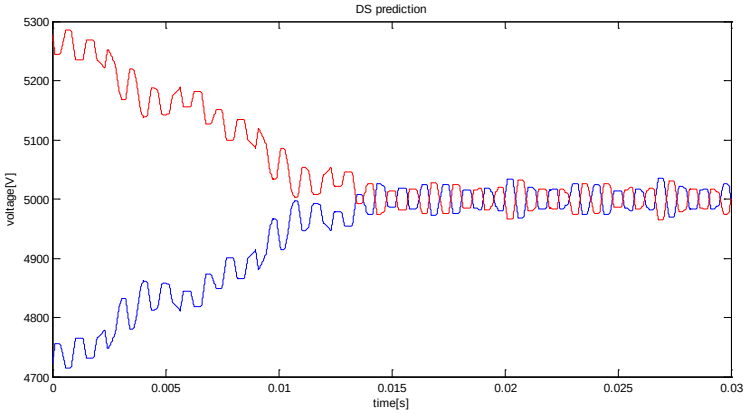

Figur 5.3-6: Double-Signal prediction balancing with different capacitor values

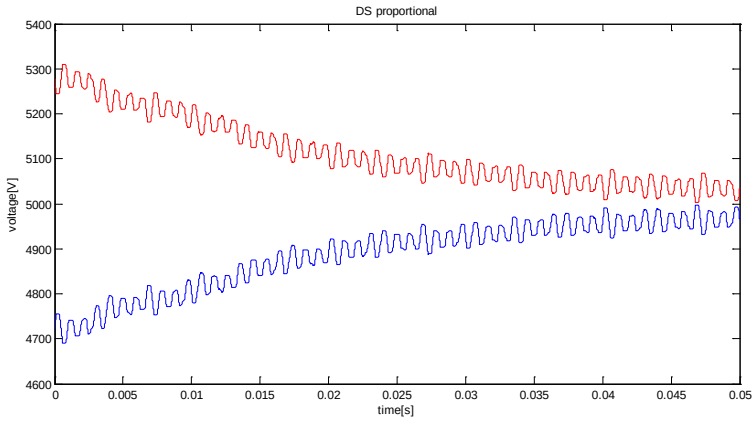

Figur 5.3-7: Double-Signal proportional balancing with different capacitor values

The simulations show that all of the methods are able to balance the DC-bus with a situation with different capacitor values. The method that struggle the most is Double-Signal with proportional regulation. From [13] it is found that Double-Signal has better balancing opportunities at a Cos(φ) equal to zero than one, while it is opposite for Space Vector. The reason for the voltage difference in the beginning is that PSCAD divides the voltage equal to

the ratio in capacitor voltage. Hence the initial voltage on the upper capacitor is 10 000*1900/(1900 + 1700) = 5278 V which can be read from the figures. It can from this be concluded that all of the modulation methods are able to handle such a situation.

In a real life implementation it is not sure that the load in every case will be equal for all of the phases. Thus it should be simulated and tested whether the control algorithms are able to handle this type of situation. In this report there have been done simulations with two current sources as load and with 1000 A as amplitude on phase A current source and 707.1 A as amplitude on phase B current source.

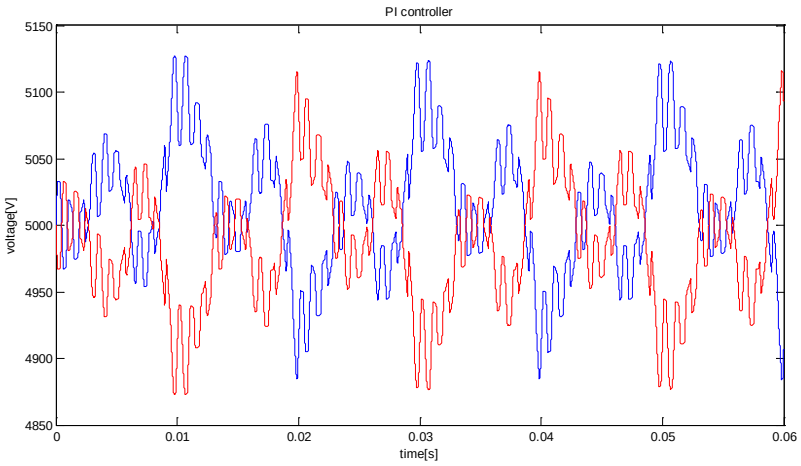

Figure 5.3-8: Space Vector PI controller balancing with unsymmetrical load

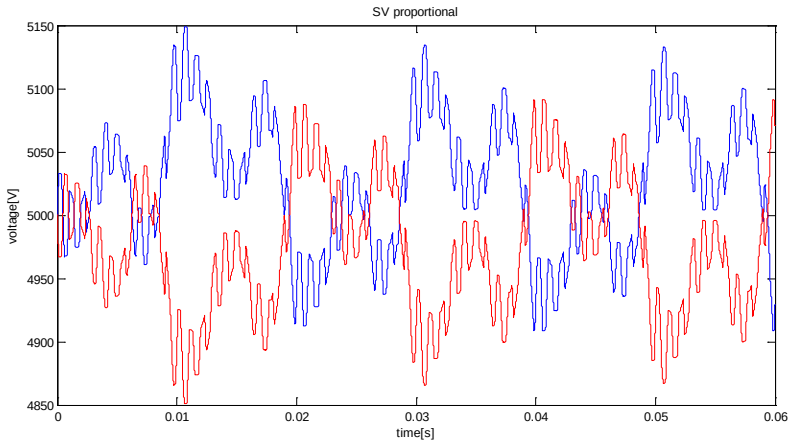

Figure 5.3-9: Space Vector proportional balancing with unsymmetrical load

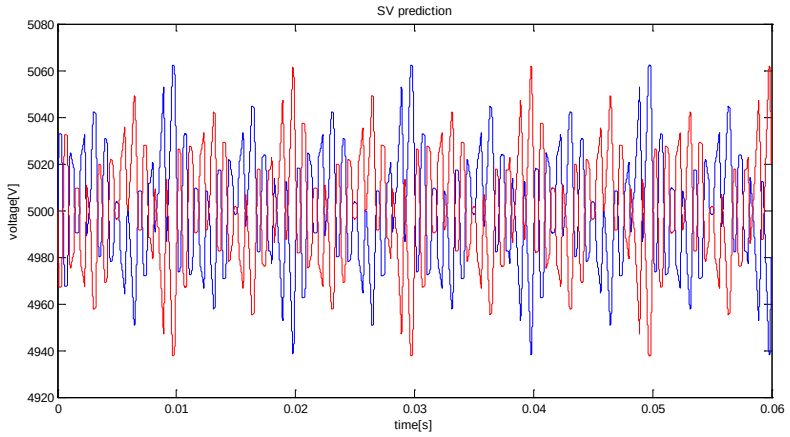

Figure 5.3-10: Space Vector prediction balancing with unsymmetrical load

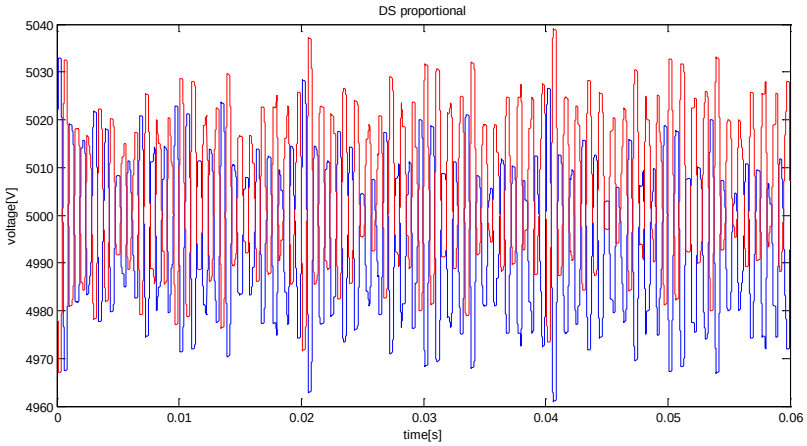

Figure 5.3-11: Double-Signal proportional balancing with unsymmetrical load

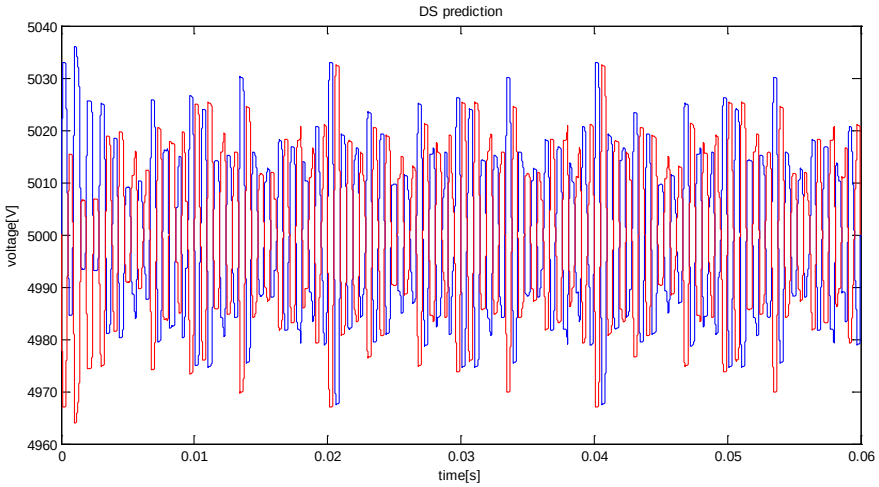

Figur 5.3-12: Double-Signal prediction balancing with unsymmetrical load

The simulations are showing that all of the modulation methods are able to balance the DC-bus while having unsymmetrical load. Simulations are also done with having unsymmetrical load and different capacitor values at the same time and all of the method handle that as well.

Hence it can be concluded that the methods balance the DC-bus with such errors at normal operation conditions. If the phase current is very low the balancing possibilities are more limited and it will also take much longer time to remove a possible voltage offset.

5.4 Balancing in Overmodulation with Space Vector

In overmodulation the use of medium vectors decrease from a maximum use at a modulation index of $2/\sqrt{3}$ to no use at $4/\pi$. This is because the angle is locked closer and closer to the large vectors while the reference is in overmodulation. Hence the 3rd harmonic DC-bus oscillation due to the medium vectors reduces from maximum to zero when increasing the modulation index in overmodulation.

DC-bus balancing with small vectors is possible only when the reference vector is inside the hexagon. The use of small vectors when inside the hexagon decreases as the modulation increases. At the same time the number of instances the reference is inside the hexagon decreases as the modulation increases. At six-step no small vectors are used. Hence the capability for DC-bus balancing with small vectors is reduced to none as the modulation increases to the absolute limit of modulation.

In [13] it is shown that at a high modulation index in the linear region and highly reactive load will create large 3rd harmonic oscillations. It is also shown that this does not necessary create a considerable harmonic distortion on the output voltage of the converter.

Even if the third harmonic oscillations on the DC-bus are accepted there is still a need to balance other unbalances. As mentioned the capability of the small vectors to remove an unbalance decreases with modulation index in the overmodulation region and is gone at six-step, a new balancing strategy for the region outside the hexagon is necessary. Figure 5.4-1 shows a technique proposed for balancing.

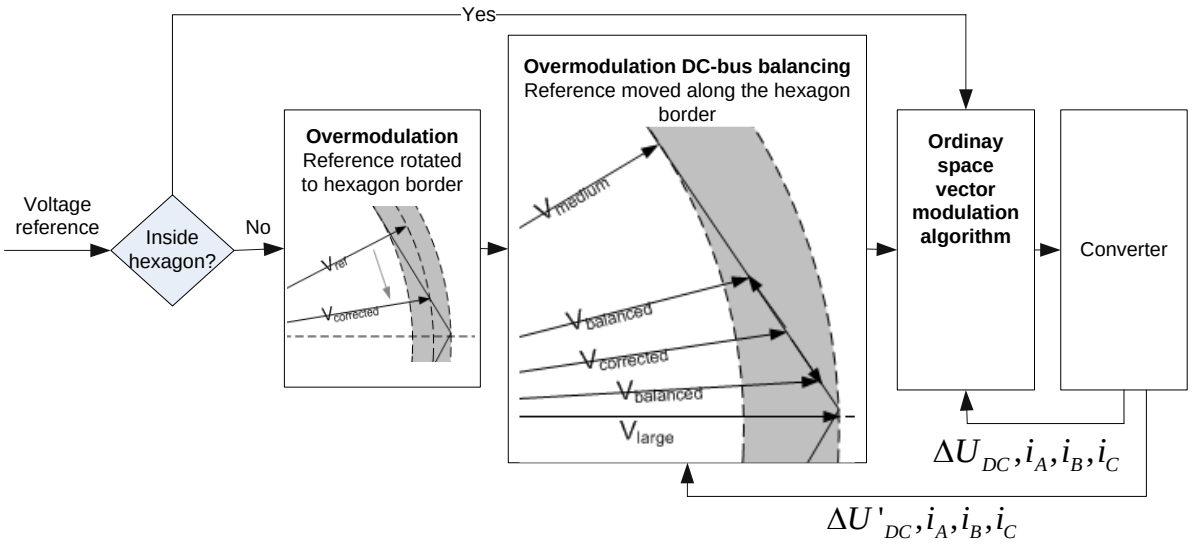

Figure 5.4-1: Flowchart of balancing in overmodulation

The balancing strategy is based on control of the neutral point current by controlling the medium vectors duty cycles. If the medium vector closest to the reference vector has a positive influence on the DC-bus balance, the reference vector is shifted along the hexagon border so it is closer to the medium vector. If the medium vector has a negative influence on the dc bus balance the reference is shifted further away. This will reduce the accuracy of the modulation since the medium vector is shorter than the large vector. With reactive load a shift closer to the medium vector will occur every other π /3 intervals, while a shift away from the medium vector will occur the other intervals. This is because the phase current the medium vector controls is equal but with opposite sign every π/3 interval as illustrated by Figure 5.4-2. The phase current this overmodulation balancing scheme uses for balance control is the same as double signal uses.

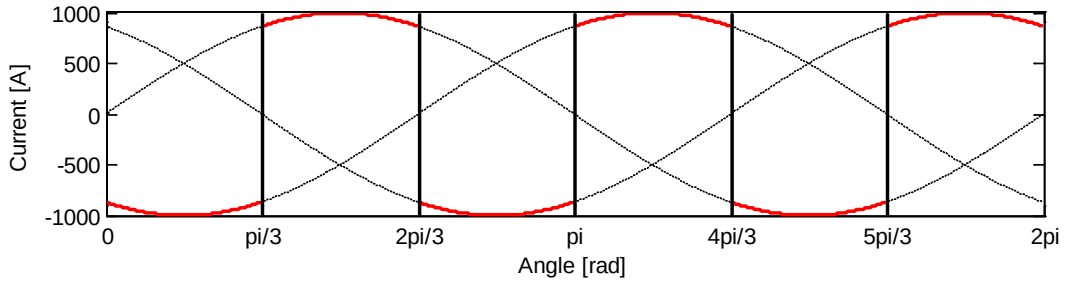

Figure 5.4-2: Currents that can be used for balancing at inductive load

Shifting along the hexagon border should be done by proportional regulation depending on ΔU_{dc}. Some limitations might be added such that the medium vector duty cycle cannot be changed more than a maximum of ± a limit that makes sure that the distortion does not get too big. Further the duty cycle cannot become lower than zero or higher than one. It is not desired to shift the reference beyond the medium vector or beyond the large vector, the absolute upper and lower limit of the shift.

In order to get a better understanding of how the voltages acts when operating in overmodulation there has been developed equations of the current in the following subchapter.

5.4.1 Calculations of Neutral Point RMS Current

As it has been discussed earlier in this report there are natural 3rd harmonic oscillations that occur in the NPC. In this chapter an analysis has been made of the RMS values of the neutral point current. This result can be used in order to get a better understanding of the oscillations.

$$\frac{I_{NP,RMS}^2}{\hat{I}_{phase}^2} = \frac{3}{2\pi}\cdot\left(\begin{array}{l}
\int_{0}^{a\sin\left(\frac{2}{m\cdot\sqrt{3}}\right)-\frac{\pi}{3}}\left(\begin{array}{l}\sqrt{3}\cdot m\cdot\sin(\zeta)\cdot\cos\left(\zeta-\frac{2\pi}{3}-\varphi\right)^2+\\ \left(\sqrt{3}\cdot m\cdot\left(-\frac{\sqrt{3}}{2}\cdot\cos(\zeta)-\frac{1}{2}\cdot\sin(\zeta)\right)+2\right)\cdot(2f-1)\cdot(-\cos(\zeta-\varphi))^2\end{array}\right)d\zeta\\
\int_{a\sin\left(\frac{2}{m\cdot\sqrt{3}}\right)-\frac{\pi}{3}}^{\frac{\pi}{6}}\left(\sqrt{3}\cdot m\cdot\sin\left(a\sin\left(\frac{2}{m\cdot\sqrt{3}}\right)-\frac{\pi}{3}\right)\cdot\cos\left(\zeta-\frac{2\pi}{3}-\varphi\right)^2\right)d\zeta\\
\int_{\frac{\pi}{6}}^{\frac{2\pi}{3}-a\sin\left(\frac{2}{m\cdot\sqrt{3}}\right)}\left(\sqrt{3}\cdot m\cdot\left(\frac{\sqrt{3}}{2}\cdot\cos\left(\frac{2\pi}{3}-a\sin\left(\frac{2}{m\cdot\sqrt{3}}\right)\right)\right)-\frac{1}{2}\cdot\sin\left(\frac{2\pi}{3}-a\sin\left(\frac{2}{m\cdot\sqrt{3}}\right)\right)\right)\cdot\cos\left(\zeta-\frac{2\pi}{3}-\varphi\right)^2\right)d\zeta\\
\int_{\frac{2\pi}{3}-a\sin\left(\frac{2}{m\cdot\sqrt{3}}\right)}^{\frac{\pi}{3}}\left(\begin{array}{l}\left(\sqrt{3}\cdot m\cdot\left(\frac{\sqrt{3}}{2}\cdot\cos(\zeta)-\frac{1}{2}\cdot\sin(\zeta)\right)\cdot\cos\left(\zeta-\frac{2\pi}{3}-\varphi\right)^2\right.\\ \left.+\left(\sqrt{3}\cdot m\cdot\left(-\frac{\sqrt{3}}{2}\cdot\cos(\zeta)-\frac{1}{2}\cdot\sin(\zeta)\right)+2\right)\cdot(2f-1)\cdot\cos\left(\zeta+\frac{2\pi}{3}-\varphi\right)^2\right)\end{array}\right)d\zeta\\
\int_{a\sin\left(\frac{2}{m\cdot\sqrt{3}}\right)}^{\frac{\pi}{3}}\left(\begin{array}{l}\left(-\sqrt{3}\cdot m\cdot\sin(\zeta)+2\right)\cdot(2f-1)\cdot\cos\left(\zeta+\frac{2\pi}{3}-\varphi\right)^2\\ +\left(-\sqrt{3}\cdot m\cdot\left(\frac{\sqrt{3}}{2}\cdot\cos(\zeta)-\frac{1}{2}\cdot\sin(\zeta)\right)\right)\cdot\cos(\zeta-\varphi)^2\end{array}\right)d\zeta\\
\int_{a\sin\left(\frac{2}{m\cdot\sqrt{3}}\right)}^{\frac{\pi}{2}}\left(\left(-\sqrt{3}\cdot m\cdot\left(\frac{\sqrt{3}}{2}\cdot\cos\left(a\sin\left(\frac{2}{m\cdot\sqrt{3}}\right)\right)\right)-\frac{1}{2}\cdot\sin\left(a\sin\left(\frac{2}{m\cdot\sqrt{3}}\right)\right)\right)\cdot\cos(\zeta-\varphi)^2\right)d\zeta\\
\int_{\frac{\pi}{2}}^{\pi-a\sin\left(\frac{2}{m\cdot\sqrt{3}}\right)}\left(-\sqrt{3}\cdot m\cdot\left(-\frac{\sqrt{3}}{2}\cdot\cos\left(\pi-a\sin\left(\frac{2}{m\cdot\sqrt{3}}\right)\right)-\frac{1}{2}\cdot\sin\left(\pi-a\sin\left(\frac{2}{m\cdot\sqrt{3}}\right)\right)\right)\cdot\cos(\zeta-\varphi)^2\right)d\zeta\\
\int_{\pi-a\sin\left(\frac{2}{m\cdot\sqrt{3}}\right)}^{\frac{2\pi}{3}}\left(\begin{array}{l}-\sqrt{3}\cdot m\cdot\left(-\frac{\sqrt{3}}{2}\cdot\cos(\zeta)-\frac{1}{2}\cdot\sin(\zeta)\right)\cdot\cos(\zeta-\varphi)^2\\ +\left(-\sqrt{3}\cdot m\cdot\sin(\zeta)+2\right)\cdot(2f-1)\cdot\left(-\cos\left(\zeta-\frac{2\pi}{3}-\varphi\right)\right)^2\end{array}\right)d\zeta
\end{array}\right) \tag{5.25}$$

As it can be seen the integral is divided into four integrals between 0 and π/3 and it will be described here. In the first integral the space vector is inside the big hexagon, and hence it can be calculated as normal. In the second integral some modifications need to be done. This

integral goes from where the reference vector crosses the hexagon border and this angle should be used to calculate the duty cycles in this integral. After π/6 the locked angle is changed to π/3 – β, and this will be the new angle used to calculate the duty cycles until the reference vector once again is inside the hexagon border. The last four integrals have the same approach as the first four. The result of the integral above is shown in Figure 5.4-3.

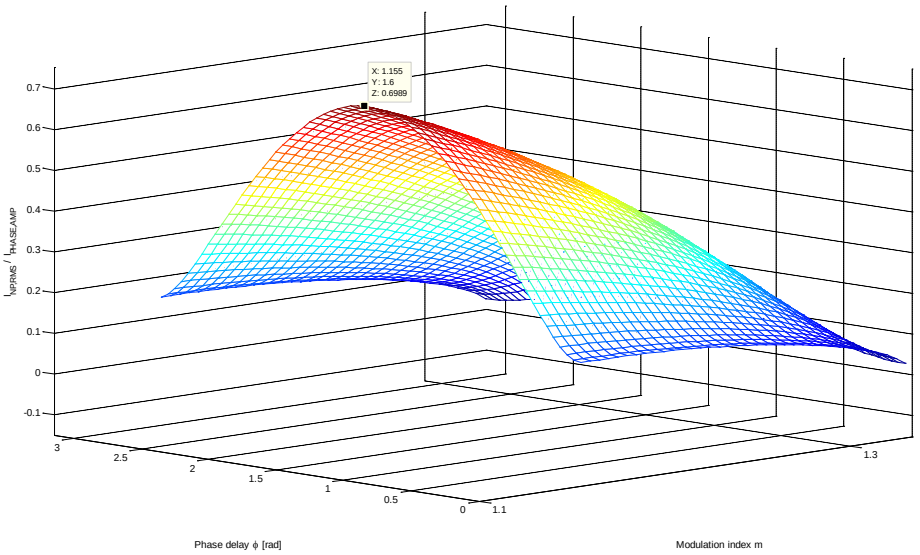

Figure 5.4-3: Analytical calculation of the neutral point RMS current in overmodulation

From simulations it seems like the calculated RMS value and the simulated RMS value of the neutral point current is close in value for some Cos(φ). With a Cos(φ) close to 1 the error between the calculated RMS and the simulated RMS is increased. With an m equal to 1.2 the calculated RMS with an f equal 0.6 is 175 A, while the simulated is 280 A. With the same m but with a Cos(φ) equal 0 the simulated RMS current was 590 A while the calculated was 607 A. One possible explanation why good results are achieved with Cos (φ) equal to zero could be that the medium vector current is the largest current as found in [13]. The small vectors are controlled by f and f is constantly changing during the simulations. In the theoretical plots f is kept constant and the changing f could lead to more distorted current and this again could distort the RMS current.

The integral solved above finds the RMS, and thus it cannot be used to calculate the 3rd harmonic oscillations accurate enough. If the 3rd harmonic component is to be calculated the answer will be very long and not very practical to use. As long as the f is not 0.5 in average there will be a DC part in the RMS current which also will influence the RMS current used in the calculations. This equation is also only developed for the case where there is only one f, such that the case where there are two balancing parameters could not use this approach. Thus there should be looked to alternative balancing strategies.

5.4.2 Implementation of Balancing Algorithm

Simulations have shown how critical it is to choose a switching frequency which ensures three phase sampling symmetry, otherwise the output voltage might be far from the wanted value. This will create symmetry which can be used in the balancing algorithm. Since the current is having 3rd harmonic oscillations the voltage difference should be zero three times during one fundamental period with infinite switching frequency. The capacitor voltage with SV PI controller is shown in the figure below.

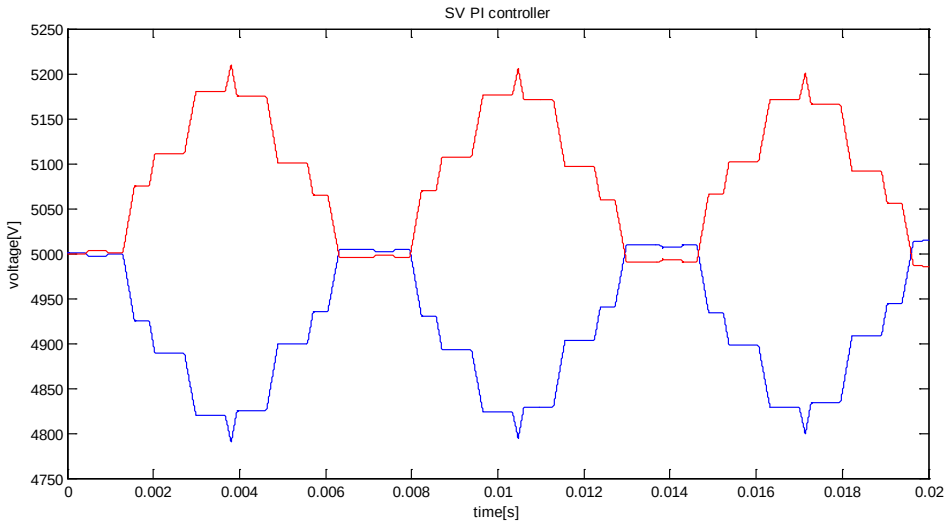

Figure 5.4-4: Voltage oscillations in overmodulation

The figure is showing the voltage on the upper and lower capacitor during one fundamental period which lasts 0.02s. As it can be seen there is a very clear third harmonic component which should not be removed. There are two different ways of solving the balancing by saying that the voltage difference should be zero for certain angles. If it is accepted that the upper capacitor will have the highest values and the lower capacitor the lowest values as in the figure then there should be zero voltage difference at the reference angles $2\pi/3$, $4\pi/3$ and 0 or 2π. By measuring the voltage difference at these points the extra voltage balancing can be added. The small vectors will be regulated as usual when the reference vector is inside the hexagon, but due to their limitations the β might have to be changed and this is decided according to the voltage difference at the mentioned angles. This is a fast method of deciding whether there are some unbalances or not.

As it can be seen in Figure 5.4-4 the average voltage of the upper capacitor is a bit higher than 5kV and the lower capacitor has an average voltage lower than 5kV. This means that ΔU_{DC} will not oscillate around zero, but it will have a DC component. For most of the methods studied in this report and in [13] there are some DC-offsets in most situations. If this DC-offset should be removed the parameters need to be optimized in all situations. The DC-offset can be removed in overmodulation but then ΔU_{DC} will not be zero at 0, $2\pi/3$ and $4\pi/3$. If there is a margin where the extra balancing in overmodulation is disabled the small vectors will do some balancing and the DC-offset can be removed.

The balancing algorithm is implemented such that there will be a measurement of the unbalance at 0, 120 and 240 degrees. At these angles there should be no voltage unbalance at ideal conditions. If the voltage difference is within a limit there will be no change in the β value and the needed balancing will be taken care of by the small vectors. The other situation is that the voltage unbalance is greater than a certain limit, and then there is a need to change the angle β. This is shown in the figure below.

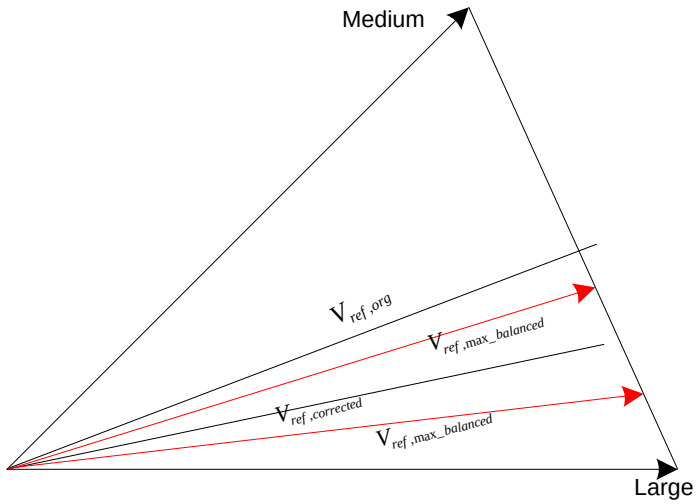

Figure 5.4-5: Maximum balancing in overmodulation

In the figure there is a maximum value of how much the corrected reference vector can be moved back and forth, this is done in order to not change the output value to much. There have been made simulations with a stiff DC-bus offset to find the THD_i. In these simulations fixed shift to/from medium vector is used instead of proportional balancing. The results are shown in Figure 5.4-6.

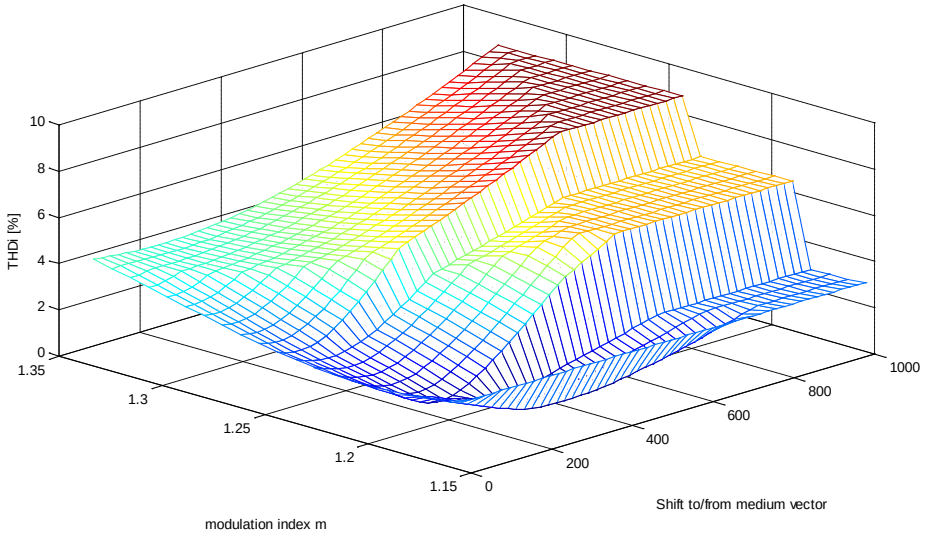

Figure 5.4-6: THD_i in overmodulation with balancing algorithm and a switching frequency of 1050 Hz

From the figure there is one parameter that goes from 0 to 1000 named shift of medium vector. The distance from the medium vector to the large vector is decided to be 1000, and the shift parameter is telling how much the originally locked angle can be moved toward or away from the medium vector. The reason for the flat areas is that for the particular modulation index the locked reference vector cannot be shifted more because then it will pass the medium or large vector. The steep steps from some of the modulation indexes is due to how many times it is sampled outside the hexagon and have the possibility to be shifted. With a m_a equal to 1.333 the distance can be shifted from 0 to 1000, which is natural since it is locked to every large vector.

There have been made simulations in order to see how the response time of removing an initial voltage offset of 4000 V for different m_a and cos(φ). With this method the reference vector cannot be moved more than a distance of 100, when the total distance between medium and large vector is 1000. In this case it is asymmetrical modulation that has been used and the switching frequency was 1050 Hz.

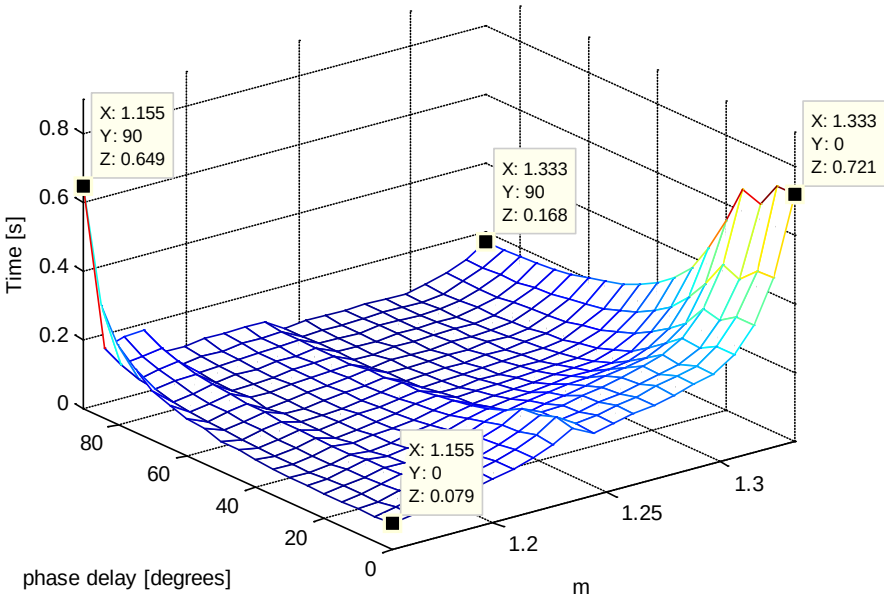

Figure 5.4-7: Time to remove an unbalance of 4000 V (c=1.8mF, Î=1000A) in overmodulation for asymmetrical Space Vector

As it has been discussed the medium vector has a great influence on the voltage balance in overmodulation. In general there are better possibilities of balancing when the current is inductive than active and this is because the value of the current flowing when using medium vector is at its maximum. By adjusting this vector it will have a greater influence on the voltage compared to adjusting it when the current has a low value. There are two areas that have the highest values. With a m_a equal to 1.155 and 90 degrees lagging current the only balancing opportunities are the small vectors, and thus it will need more time to balance. The small vectors also have the least influence on the DC-bus balance at this cos(φ). The other area where the response is slow is when the current is active or close to active and the

modulation index is high. Then the small vectors have very limited on-time and the i_{medium} is having a low value. The only possibility of reducing the balancing time at this area is to increase the limit of how much the reference vector can be adjusted.

To see how much the balancing algorithm is influencing the 1st harmonic output the voltages across each capacitor were given a constant value. Then it was simulated for different modulation indexes and different adjustment limits. The results are given in Figure 5.4-8.

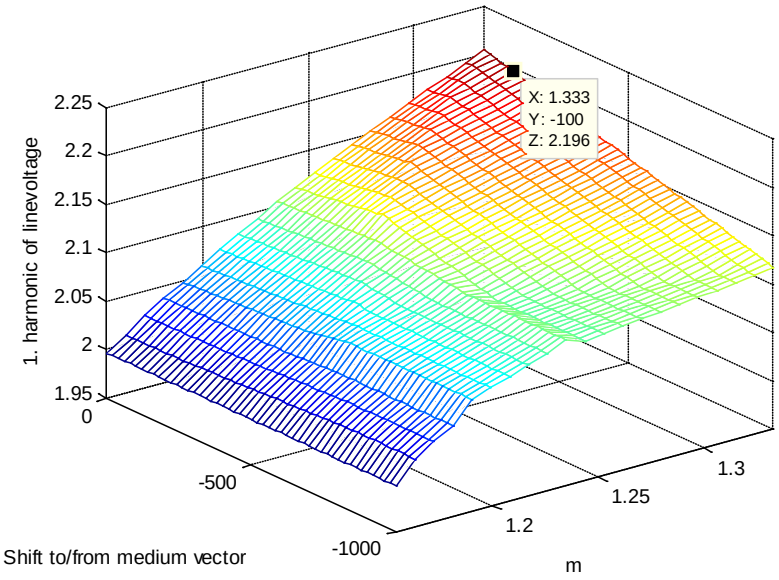

Figure 5.4-8: 1st harmonic line-to-line voltage at different shifts and modulation indexes

This simulation is done with asymmetrical modulation at a switching frequency of 1050 Hz. In the beginning of the overmodulation area there is no big difference in the in the output voltage when changing the shift limit and this is related to the few samples when the reference vector is locked to an angle. At a high modulation index the limit of the shift should not exceed 100 too much, but even at 200 the output line-to-line voltage has a value of 2.187 which is 99.2% of the wanted output value. One interesting result is that the reference vector can be shifted as much as 500 and still have a better 1st harmonic output compared to for instance a switching frequency equal 1000 Hz. These simulations confirm that this method can be used without changing the 1st harmonic remarkably.

5.5 Balancing in Overmodulation with Double-Signal

Since Double-Signal has a different modulation technique than Space Vector it was tested to see how DS was able to remove an initial voltage offset with a modulation index close to six-step. The response time was very slow and hence it was decided to implement the same balancing algorithm as for Space Vector. The response with this method is shown in the figure below.

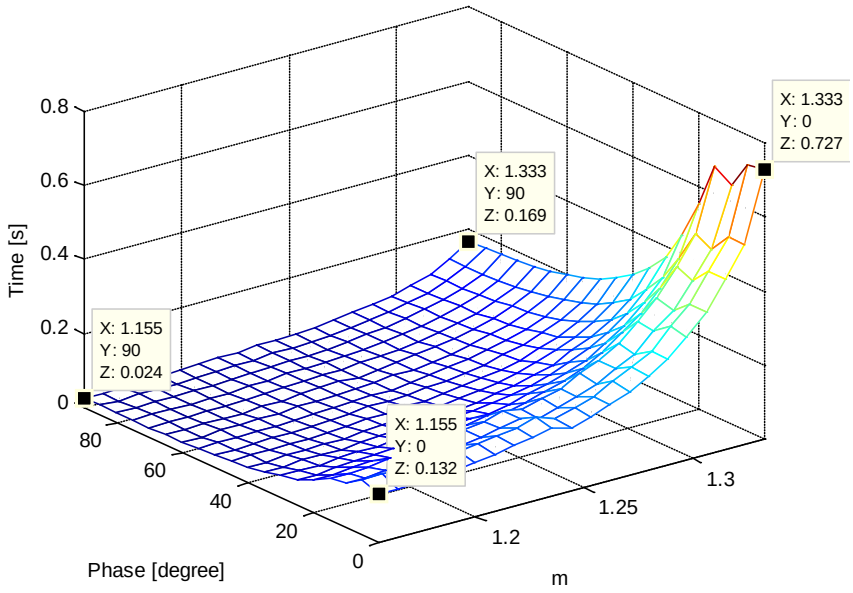

Figure 5.5-1: Time to remove an unbalance of 4000 V (c=1.8mF, Î=1000A) in overmodulation for Double-Signal

As seen the response is different compared to Space Vector at a low modulation index. This is because their balancing techniques are different when the reference hits inside the hexagon. At higher modulation the overmodulation balancing technique becomes more dominant and at six-step the response is the same as for Space Vector.

6 Laboratory Work and Comparison with Simulations

One of the tasks in the problem description was to implement some of the control methods analyzed in [13] and in this master thesis to an already built three level converter at NTNU. In February it was decided that the methods should be implemented by using a FPGA with help from Kjell Ljøkelsøy at SINTEF Energy Research Ph.D. student Sverre Gjerde at NTNU. The programs used in the implementation were Xilinx and Active DSP. The results where first captured on the oscilloscope and then the data was imported to the laptop with "Open Choice Desktop" and saved as a CSV-file which again was imported to MATLAB.

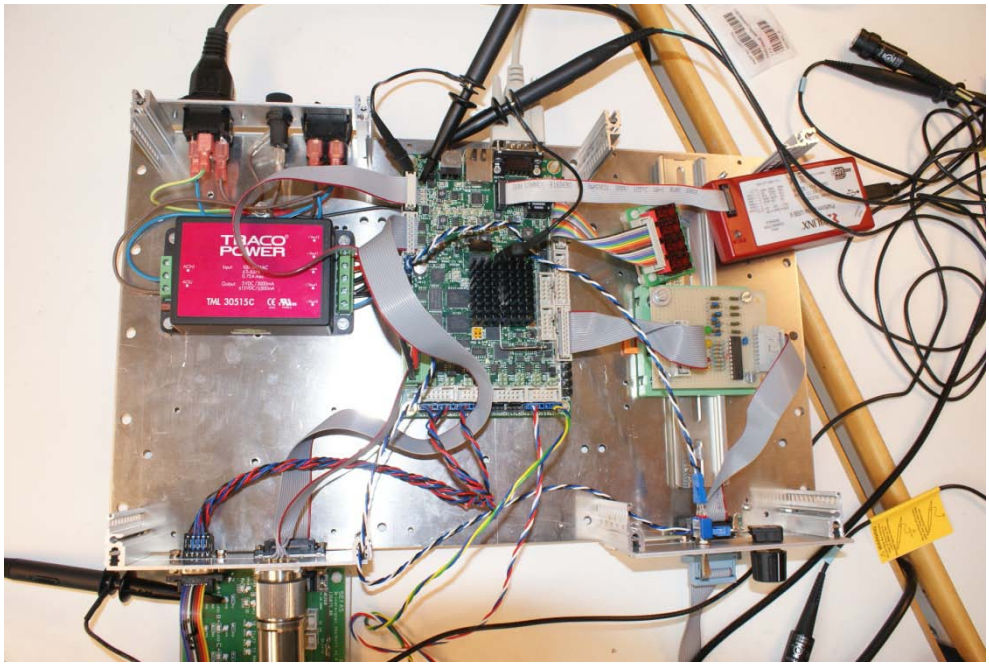

Figure 5.5-1: FPGA card in the laboratory

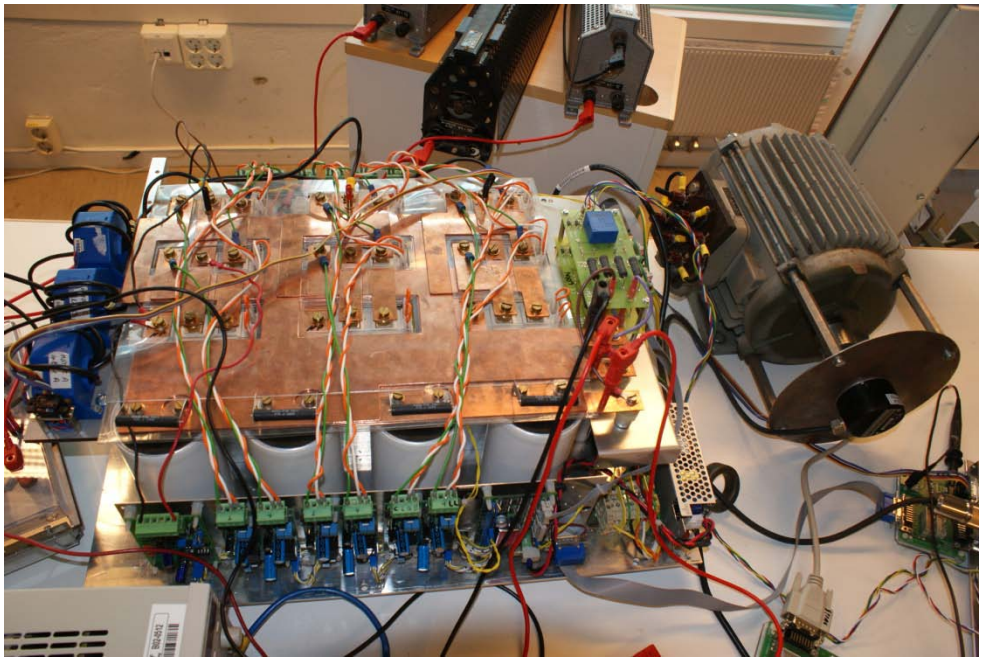

Figure 5.5-2: The three-level converter in the laboratory

6.1 Implementation in the laboratory

An existing lab set up with an inverter and a FPGA board developed by SINTEF was used. The FPGA board consists of a Virtex 5 FPGA unit and a PowerPC 400 processor. A C++ module for double signal modulation was rewritten in Xilinx software development kit to have the option of space vector modulation. The execution of the space vector code had to be changed compared to how it was implemented in the models in SIMULINK and PSCAD. The input parameters to the module were phase voltage references instead of phase voltage amplitude and space vector angle. All the variables needed to be integer to reduce power intensive operations. Because of the loss of decimals all variables were scaled up by 1000. It was decided to rewrite the entire algorithm to make it faster. A method with binary search of sectors was implemented and no trigonometric operations were used.

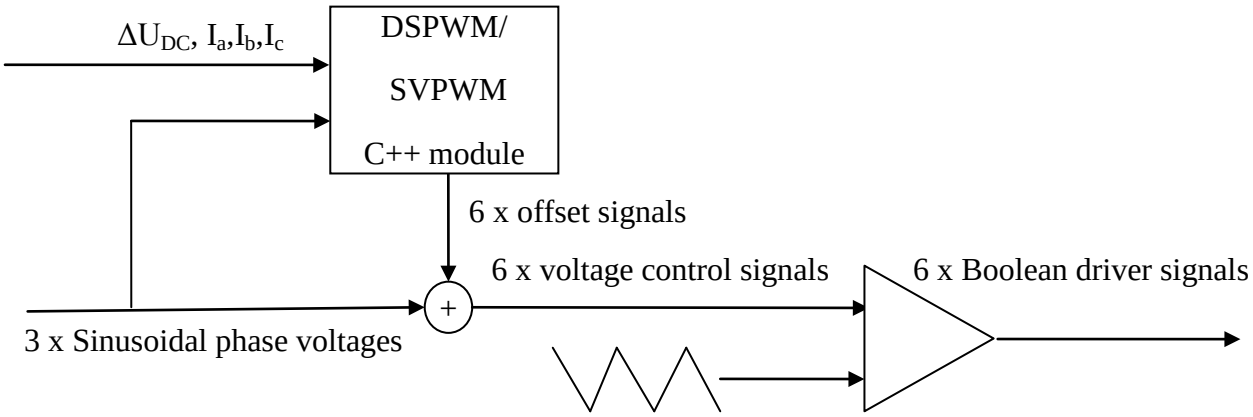

Figure 6.1-1: Implementation in FPGA

In Figure 6.1-1 part of the system is illustrated. The C++ module used got measurements of DC bus voltage unbalance and phase currents read from the register together with sinusoidal phase voltage references that was calculated in the FPGA. The module calculates six offsets. One for switch 1 and one for the switch 2 on each of the bridge legs. They are added to their respective phase voltage reference signals to calculate 6 control voltages. This is compared with a triangular wave. All the operations illustrated in the figure are done in FPGA-modules except the C++ module that runs in the processor of the board.

By binary search it is meant that the sector diagram would be divided into two, then these two sections are divided into two and all of these divided again until all the sectors could be found. No “else if”-statement should be used. This means that independent of what sector that is searched for the number of tests is equal. However there are 24 sector and at some instant the sector diagram has to be divided into 3. The division is the following: 3*2*2*2 = 24, in other words one “else if”-statement had to be used. To achieve the division line voltage references was used to determine the borders of the sectors. The space vector reference can be decomposed with line voltage values along the axis shown in Figure 6.1-1. If U_{ab} is greater than 0 and U_{bc} is lower than 0 the reference is somewhere in the area 3 in Figure 6.1-2. Else if

U_{ab} + U_{bc} is greater than 0 the area is 1 and if none of these are true the area is 2. The coordinate system is somewhat similar to that done in [2].

The area 3 can be divided into two by testing if U_{ab} is greater than 1000 as seen in Figure 6.1-3. These can then be divided by testing if U_{bc} is less than -1000 as seen in Figure 6.1-4. And so on.

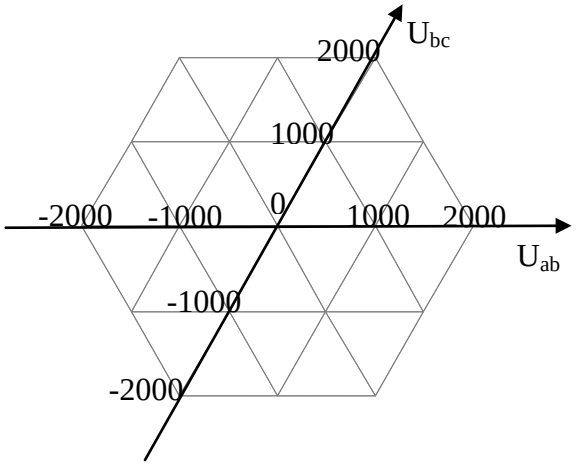

Figure 6.1-2: Hexagon coordinate system

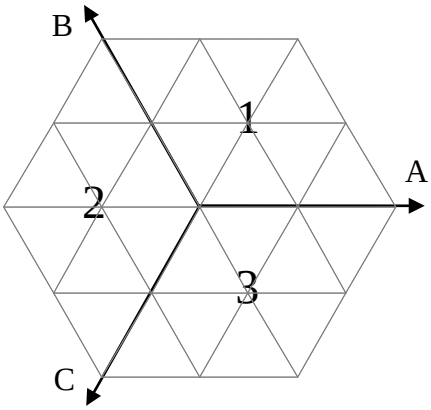

Figure 6.1-3: Large division of hexagon

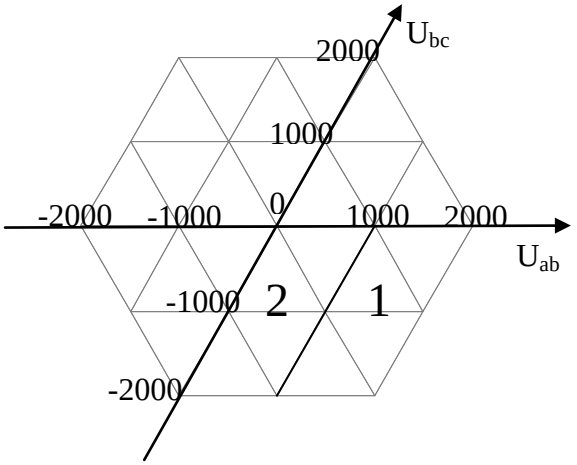

Figure 6.1-4: Subdivision of hexagon

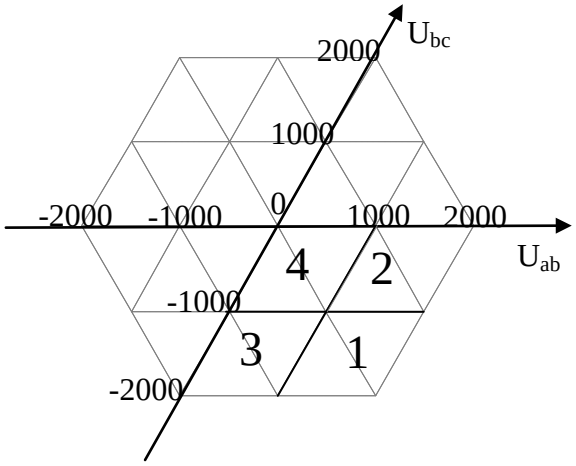

Figure 6.1-5: Sub subdivision of hexagon

Once the sector is found the space vector on times are calculated from the line voltages by the use of formulas found in [12]. And the control signals to each of these on times are generated. The formula for these calculations can be found in [1]. These are however time to turn on each of the switches. To achieve a control signal between zero and 1000 this formula can be used:

$$V_{contr} = 1000 - \frac{1000 \cdot t_{on}}{T_{tri}} \tag{6.1}$$

Finally the offsets are calculated by subtracting the control voltage from the phase voltage references.

In overmodulation a preprocessor algorithm is applied. The line-to-line voltages are altered to have a reference pointing to the hexagon border. Then they are processed as normal. The same preprocessor algorithm is used for Double-Signal in overmodulation. However the line-to-line voltages are calculated back to phase voltages before the modulation algorithm is run as normal.

6.2 Laboratory Results of Space Vector and Double-Signal PWM

The aim of the laboratory work was to verify the methods simulated in this master thesis and in [13]. The load used in the simulations was a pure resistive three phase load where each phase resistance had a value of 9.3 ohm. The two DC-sources connected had a value of 20 V each with a total DC-link voltage of 40 V. The current flowing in the circuit will be quite low with these values, and this was necessary due to low current capability of the DC-sources.

It was decided to simulate Space Vector and Double-Signal without DC-bus balancing at the beginning to verify that the simulation methods gave the wanted 1st harmonic output. Tests have also been made to compare the results of symmetric and asymmetric modulation at a low switching frequency where a difference should occur. Some errors occurred on the control signal when the fundamental frequency was set too high. Thus the fundamental frequency had to be set lower than the 50 Hz as used in the simulations.

6.2.1 Laboratory Results of Space Vector

The output voltages from the converter are shown with a couple of examples below when using space vector.

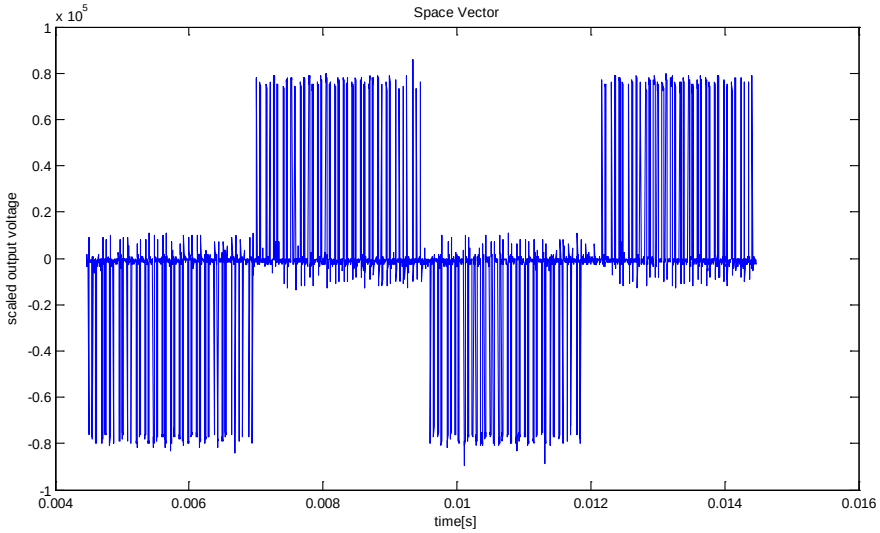

Figure 6.2-1: Line-to-line output voltage with Space Vector at a modulation of 0.2

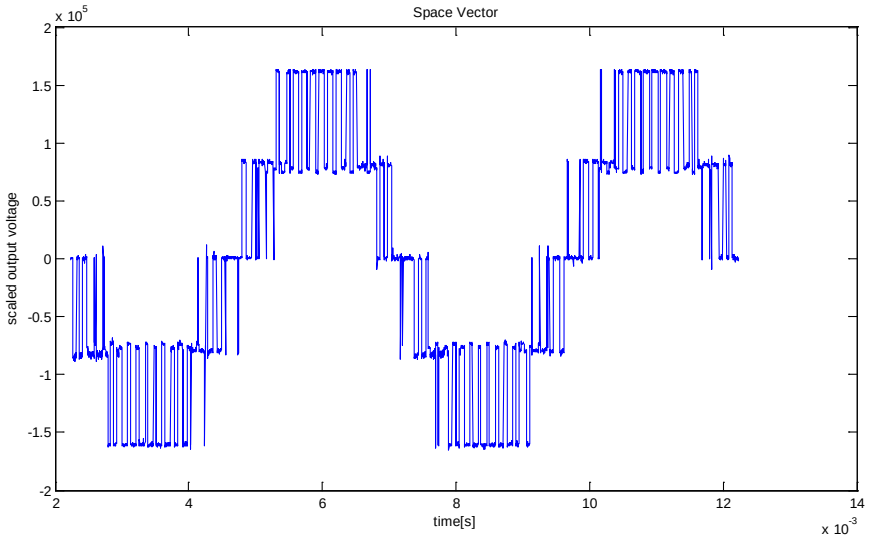

Figure 6.2-2: Line-to-line output voltage with Space Vector at a modulation of 1.0

The first example has a modulation index of 0.2, and the converter is acting as it should. Compared to ideal simulations the output voltage is clearly more disturbed in this case, which is natural since the diodes and switches are not acting ideally in real life. The second example is when the modulation index is 1.0, and now the line-to-line voltage is switching between five levels as it should do. It was tested to have a higher fundamental frequency in this system, but then the control signal got to disturbed and some unwanted switching transitions occurred, thus it was decided to not increase the switching frequency.

In the simulations there are used ideal switches and diodes, which will never be the case in real life implementations. There will be overshoots in the voltages when a power diode is turned on according to [8] and there will be on-state losses in the semiconductors. In this laboratory setup the semiconductors are designed in such a way that there are possibilities of connecting DC-sources with a voltage 10 times higher than the ones used in this experiment. Hence there will be considerable influence from the switches and diodes in the output voltage, and this can be seen above. There is not a very clear maximum and minimum value and this is probably due to the influence from the switches and diodes. Nevertheless there seems to be a stabile average value and this is a satisfactory result. Table 6.2-1 contents the most important laboratory data from Space Vector with steps of 0.1 in the modulation index.

Table 6.2-1: Space Vector line-to-line output voltage values

Modulation factor	Line-to-line voltage	THD_i	THD_v
0.1(0.173)	0.160	1.98%	156.12%
0.2(0.346)	0.33	1.59%	90.68%
0.3(0.520)	0.495	1.25%	99.75%
0.4(0.693)	0.662	0.87%	53.29%
0.5(0.866)	0.829	0.95%	53.98%
0.6(1.04)	1.01	0.98%	28.67%
0.7(1.21)	1.18	0.97%	34.16%
0.8(1.39)	1.35	1.01%	34.04%
0.9(1.56)	1.53	1.21%	36.73%
1.0(1.73)	1.72	1.07%	30.55%
1.155(2.0)	1.99	0.92%	18.31%

As it can be seen from the table the 1st harmonic output voltage corresponds well to the modulation index. The values are in all cases a bit below what it should be, and some of the errors could be related to the dead time that exists and the non-ideal behavior of the switches and diodes. The THD_i give very good results, though it should be mentioned that there might be some inductance in the circuit which already have reduced the THD_v compared to the results in [13] and that the THD_i is very sensitive to the time interval of the harmonic analysis. Since m_f is not an integer there might be some periods which have better samplings compared with others. In general it seems like the results are within the limits where they should be.

Figure 6.2-3 and Figure 6.2-4 are showing the harmonic spectra of the line-to-line output voltage. From these two figures it can be seen that the switching transitions are asynchronous because there is no regular pattern around the multiples of m_f.

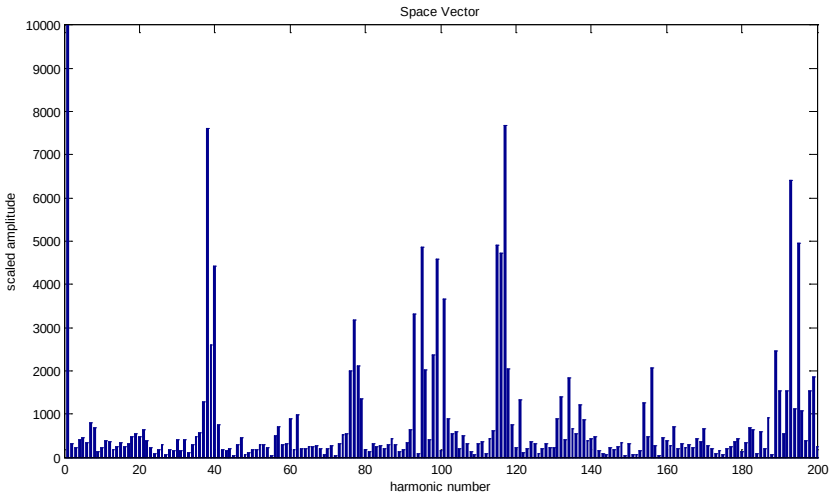

Figure 6.2-3: Harmonic spectra of the line-to-line voltage of Space Vector with a modulation index of 0.2

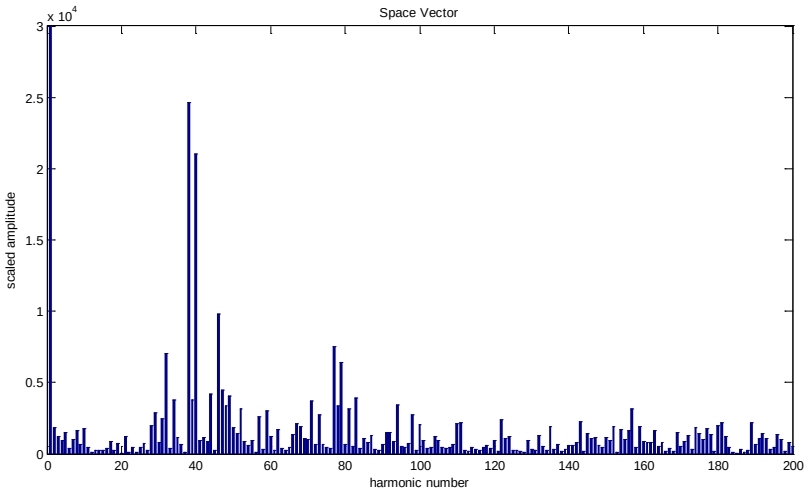

Figure 6.2-4: Harmonic spectra of the line-to-line voltage of Space Vector with a modulation index of 1.0

6.2.2 Laboratory Results of Double-Signal

The same simulations were made for Double-Signal as for Space Vector and the same examples are given.

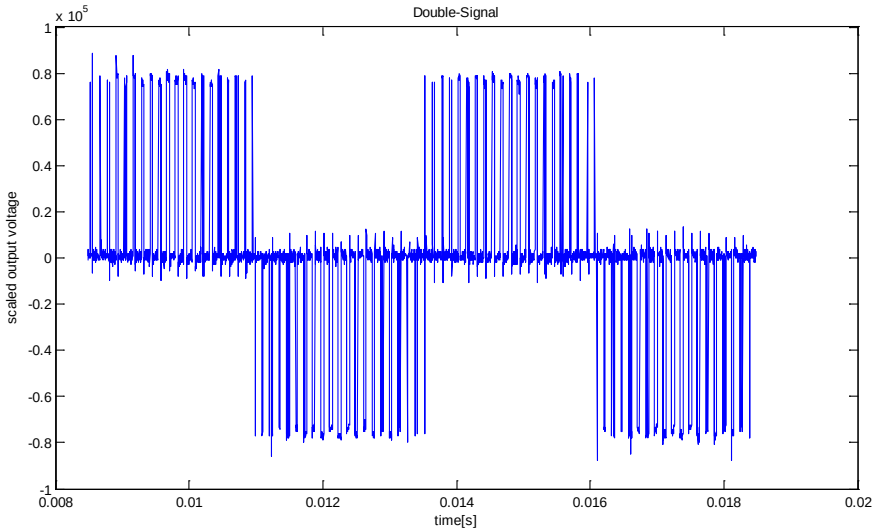

Figure 6.2-5: Line-to-line output voltage with Double-Signal at a modulation of 0.2

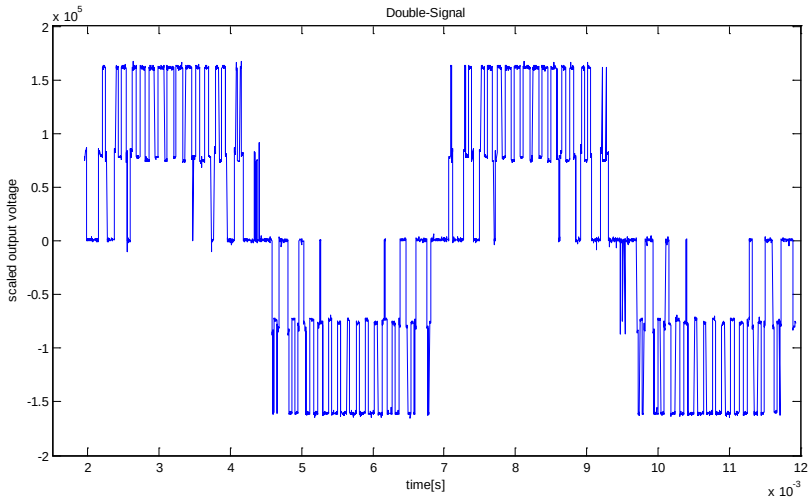

Figure 6.2-6: Line-to-line output voltage with Double-Signal at a modulation of 1.0

The first example is showing the line-to-line voltage for Double-Signal with a modulation of 0.2 and the figure shows that there are less switching transitions for this case compared with Space Vector, which is expected from the simulations. As for SV the diodes and switches are not ideal and hence some errors will occur. The second example is showing the output voltage with a modulation of 1.0 and the switching pattern is corresponding well with the simulations.

Table 6.2-2 is showing the simulation results of Double-Signal.

Table 6.2-2: Double-Signal line-to-line output voltage values

Modulation factor	Line-to-line voltage	THD_i	THD_v
0.1(0.173)	0.158	4.19%	232.7%
0.2(0.346)	0.327	3.24%	143.0%
0.3(0.520)	0.497	2.48%	103.4%
0.4(0.693)	0.659	1.16%	50.90%
0.5(0.866)	0.837	1.03%	50.24%
0.6(1.04)	1.01	0.77%	35.52%
0.7(1.21)	1.18	1.07%	32.55%
0.8(1.39)	1.36	1.26%	38.24%
0.9(1.56)	1.53	1.19%	39.68%
1.0(1.73)	1.72	1.10%	36.44%
1.155(2.0)	1.98	1.85%	39.91%

The 1^{st} harmonic outputs are close to the wanted values, and the errors have the same explanations as for Space Vector. The most interesting results in this table are that the THD_i is low for 0.8, 0.9 and 1.0 compared to the simulations. As discussed in 6.2.1 this could be a result of choosing a time interval which made the THD_i low, but these time intervals were the best with regard to the switching transitions. The resolution in the values from the laboratory work is much lower compared to the ones from the simulations, hence there could be a possible error created because of this. Due to time limitations these results have not been studied further in this master thesis, but so should be done in further work. Nevertheless it is a good result since the THD_i is lower than expected.

Figure 6.2-7 and Figure 6.2-8 are showing the harmonic spectra for Double-Signal at a modulation index of 0.2 and 1.0 respectively. In general the maximum values are higher for Double-Signal, but there are more distinct areas where there distortion occurs. Especially for a modulation of 0.2 the total harmonic distortion is much higher for Double-Signal compared to Space Vector and this can easily be seen from the much higher maximum values for DS. When the modulation index is 1.0 the maximum values are more in the same range as for Space Vector and the total harmonic distortions are also close in value.

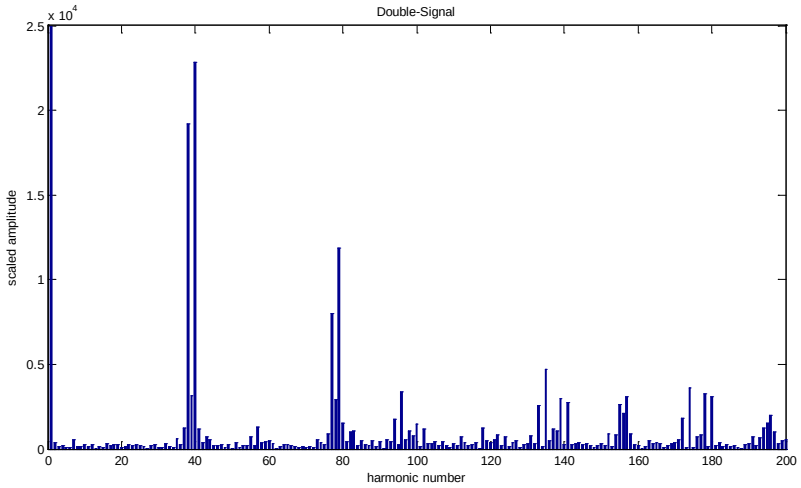

Figure 6.2-7: Harmonic spectra of the line-to-line voltage of Double-Signal with a modulation index of 0.2

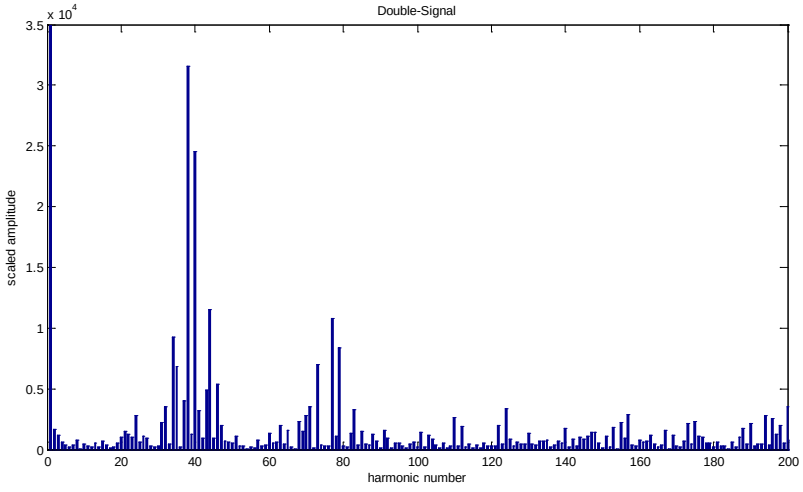

Figure 6.2-8: Harmonic spectra of the line-to-line voltage of Double-Signal with a modulation index of 1.0

The results seem to be very positive when it comes to the 1st harmonic output voltage and THD_i for both of the modulation methods. There are some uncertainty regarding THD_i, and this should be studied. One of the explanations could be that asynchronous modulation was used and with an mf_f below 21 there could be some errors involved.

6.3 Laboratory Results of Symmetrical and Asymmetrical Modulation of Space Vector

As it has been discussed previous in this report the simulations are showing that asymmetrical modulation will give a better result than symmetrical modulation. In the laboratory this was tested by using Space Vector modulation. The fundamental frequency was 8 Hz and the switching frequency was approximately 50 Hz.

Table 6.3-1 is showing the laboratory results of the symmetrical simulations of Space vector at different modulation indexes.

Table 6.3-1: Line-to-line output voltage for symmetrical SV modulation

Modulation factor	Line-to-line voltage	THD_i	THD_v
0.1(0.173)	0.16	8.99%	216.7%
0.2(0.346)	0.314	6.89%	106.6%
0.3(0.520)	0.47	5.59%	76.39%
0.4(0.693)	0.623	6.57%	85.75%
0.5(0.866)	0.804	4.71%	50.61%
0.6(1.04)	0.936	7.53%	62.11%
0.7(1.21)	1.14	3.90%	34.46%
0.8(1.39)	1.29	3.91%	31.42%
0.9(1.56)	1.44	6.22%	45.78%
1.0(1.73)	1.59	5.95%	45.28%
1.155(2.0)	1.85	5.59%	39.41

The results are clearly much worse compared to the results with symmetrical simulations when the switching frequency was around 1000 Hz. The 1st harmonic output is lower than the wanted output, but never below 90 %. At a modulation index of 0.6 the THD_i is much higher compared to a modulation of 0.5 and 0.7. This could be a result of bad synchronizing.

Table 6.3-2 is showing the corresponding laboratory results for asymmetrical modulation.

Table 6.3-2: Line-to-line output voltage for asymmetrical SV modulation

Modulation factor	Line-to-line voltage	THD_i	THD_v
0.1(0.173)	0.163	5.16%	185.1%
0.2(0.346)	0.317	6.70%	116.1%
0.3(0.520)	0.493	3.41%	84.50%
0.4(0.693)	0.643	5.70%	84.69%
0.5(0.866)	0.822	2.85%	42.73%
0.6(1.04)	0.991	2.35%	36.38%
0.7(1.21)	1.16	1.68%	31.49%
0.8(1.39)	1.33	2.26%	30.30%
0.9(1.56)	1.52	1.74%	25.77%
1.0(1.73)	1.61	5.91%	44.81%
1.155(2.0)	1.92	4.85%	28.94%

The results are clearly better compared to symmetrical modulation. The 1st harmonic output voltage is better in all of the cases and the same is the situation for the THD_i. Hence it can be

concluded that asymmetrical modulation gives better results at a low switching frequency compared to symmetrical, which was expected.

6.4 Laboratory Results of Overmodulation

It has been shown previous in this report that the 1st harmonic line-to-line output voltage is very sensitive to the switching frequency. Since the switching frequency is not synchronized to the fundamental voltage the measured values in the laboratory must be expected to vary. The method of locking the reference vector to a certain angle was implemented and tested in the laboratory. The line-to-line output voltage at a modulation index of 1.334 is shown in the figure below.

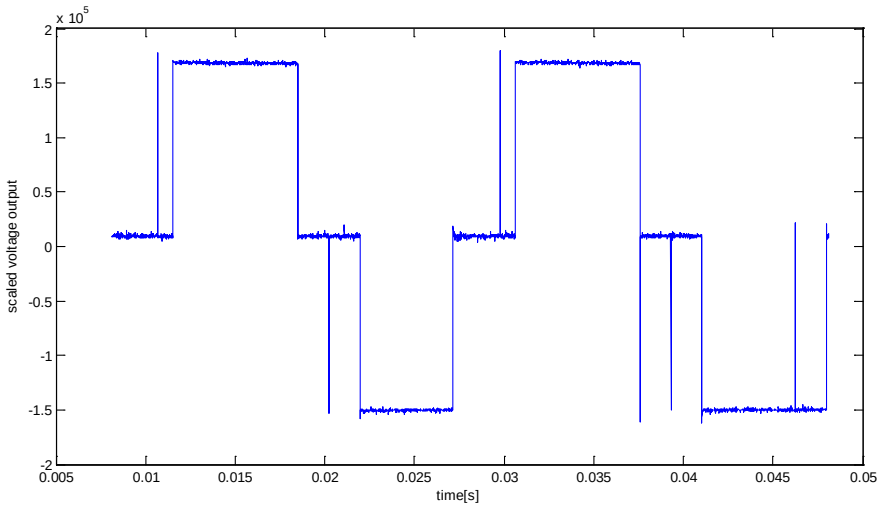

Figure 6.4-1: Line-to-line voltage with a m_a equal 1.334

At this modulation index the output voltage should be in six-step operation, while the figure shows that the converter is almost working in six-step. The reason for the error could be that there is some disturbance on the reference phase voltages, and they don't sum up to zero probably because of rounding errors. When the converter is operating in six-step the control signals are either in positive or negative saturation, and then they are very sensitive to small errors. Nevertheless the signal is close to six-step and therefore it is expected that the method would work given correct phase voltage references.

Table 6.4-1: Line-to-line output voltage in overmodulation

Modulation index	1st harmonic line-to-line voltage
1.20(2.078)	2.046
1.25(2.165)	2.063
1.30(2.252)	2.204
1.334(2.311)	2.136

The values in the table are confirming the simulations results earlier in this report which showed that the output voltage in overmodulation is very sensitive to the switching frequency.

The laboratory data shows that m_a equal to 1.3 has a higher 1st harmonic output than 1.334, which it should not have. The signal has clearly more switching transitions and it is shown below.

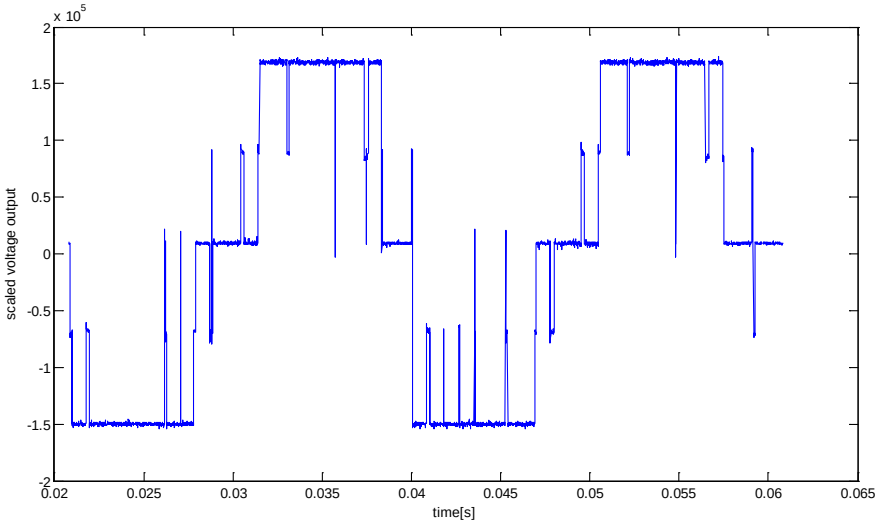

Figure 6.4-2: Line-to-line voltage with a m_a equal 1.30

Figure 6.4-1 is showing a signal much closer to a six-step operation than Figure 6.4-2, which show that the modulation method is working how it should do and the higher 1st harmonic output for m_a equal 1.3 is due to the sampling instant.

These results are confirming the importance of having synchronized sampling and to have three phase symmetry in order to get good results when operating in overmodulation.

6.5 Laboratory Results of DC-bus balancing

The simulations have shown that there is a need for DC-bus balancing at normal operation to avoid fluctuation in the capacitor voltages. It was therefore decided to test this in the laboratory.

The results were that the converter seemed to handle the balancing by itself, and there was not spotted any oscillations at all. The reason for this is most likely due to the very low current that is flowing in the system. Since the voltage oscillations are that low there might be a possibility for the capacitors to balance through the resistance across the DC-bus, which is present due to safety after shut down of the converter.

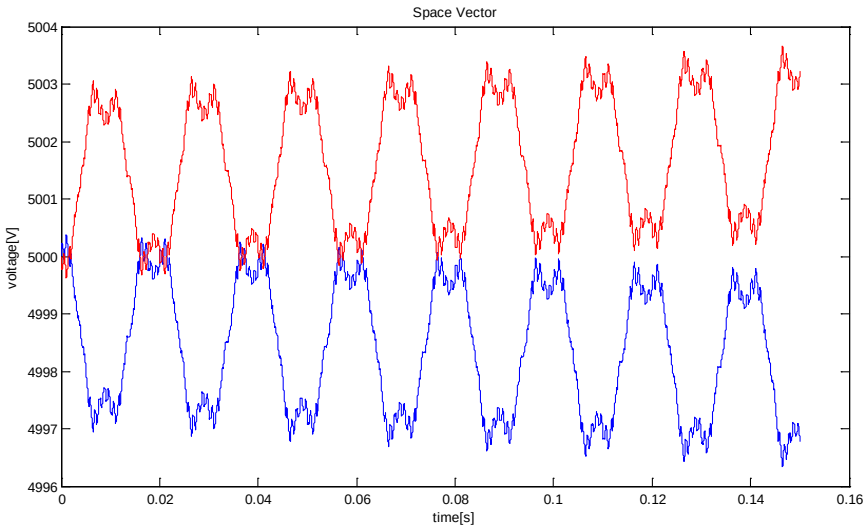

Figure 6.5-1: Simulations of the capacitor voltages equal the values in the laboratory

The figure above is showing the simulated capacitor voltages with values equal to the values in the laboratory and they are showing that the oscillations are low compared to the DC-link voltage. Since the voltage is being balanced with the equipment connected to the converter in this case, there should be done experiments with DC-sources which have a higher voltage and current rating. It is not an optimal situation to run the converter at a much lower voltage than it is designed for at least in terms of testing.

7 Discussion

The development of the current equations shows that there is no difference in the currents flowing when using Space Vector or Double-Signal. This means that there will be no different stresses on the capacitors and the conductors in the converter depending on which modulation method that is used. Hence this should not influence the choice of which modulation method that is preferred.

Simulations show that asymmetrical modulation can give very good results even with a low m_f if the samplings are done at correct angles. This is especially true for Space Vector. The THD_i is very sensitive to where the first sampling is done and it should be aimed for sampling at this point. Asymmetrical modulation with a low switching frequency can give the same THD_i as symmetrical modulation with a higher switching frequency. Thus by using asymmetrical modulation instead of symmetrical modulation with a low m_f the switching frequency can be reduced and then the switching losses will be reduced.

With the methods presented in this report the DC-bus balance can be controlled in the entire modulation range. The method proposed in this thesis for balancing in overmodulation has as condition that there should be a sampling at the three angles where ΔU_{DC} should be zero at ideal conditions. If there is no sampling at these points the method doesn't work as it should and thus it is not very flexible when it comes to different switching frequencies. However it has been shown that the switching frequency should be a multiple of three in order to get correct 1^{st} harmonic output voltage in overmodulation, and with these frequencies the algorithm will work as it should.

Double-Signal and Space Vector have shown to have different properties in different operation. Space Vector seems to have a much better THD_i at any given switching frequency and degree of modulation. However tests are not conducted at very high switching frequencies relative to the fundamental. When it comes to balancing of the DC-bus voltage, their abilities of balancing are related to the phase delay of the output currents. Double-Signal has much faster balancing when the load is reactive, while Space Vector is much better when the load is active. Space Vector has shown to produce third harmonic voltage oscillations over the capacitors, especially when the load is reactive. However they do not seem to produce any negative distortion of the output. The number of switch transitions varies between the two methods [13]. Especially at a low modulation degree Space Vector modulation seems to have more switching and this could imply that the switching losses are higher. However the Space Vector modulation technique presented uses all redundant switch states and some of them could be removed. This will influence the THD_i and its ability to balance. As proposed in [13] it could be an idea to have several modulation techniques and change between them depending on the state of the DC-bus, the behavior of the load and the modulation index.

The laboratory results correlate well with the simulated results in general. Since the switching frequency was not synchronized with the fundamental frequency in the laboratory there should be some errors compared to the simulated results. The results in overmodulation confirm the importance of three phase symmetry in the higher range of the modulation area.

Without this the output voltage will be far from what it is expected to be and the output voltage will be oscillating and this is not acceptable in a real life implementation.

8 Conclusion

In this master thesis it has been found that both Space Vector and Double-Signal have the possibility to balance the DC-bus at normal operation conditions, with different capacitor values and with unsymmetrical load. From the simulations it has not been found that it is necessary to have a PI controller in order to remove a steady state offset. Disturbance might occur in real life implementation, and then there could be a need for a PI controller. This has to be tested in each case.

Asymmetrical modulation can reduce the THD_i compared to classical symmetrical modulation, especially when m_f is low. Which value the THD_i will get is highly dependent on the angle where the reference vector is sampled the first time. Simulations show that for some cases the THD_i can be reduced with 50 % from the worst case to the best case at a certain modulation index.

In overmodulation extra precaution is needed concerning switching frequency and balancing algorithm. Simulations have shown that it is critical to have three phase sampling symmetry in in order to achieve the wanted output voltage in overmodulation. This has also been confirmed by laboratory work. By changing where the reference vector has been locked in overmodulation the possibility of balancing is increased and at the same time there is a very little change in the 1^{st} harmonic line-to-line output voltage.

It has been shown that Space Vector and Double-Signal have different qualities and which one that is the most suitable is depending on the operation. Both methods were tested in the laboratory with two separated DC-sources and both Space Vector and Double-Signal are working as they should.

9 Scope of further work

- Investigate how the balancing algorithm in overmodulation could influence sub harmonics
- Compare switching losses of Space Vector and Double-Signal
- Analyze modified Space Vector algorithm when less vectors are used compared to this thesis
- Investigate natural balancing
- Study DC-bus balancing in the laboratory with DC-sources which have higher current capability than the ones used in this master thesis
- Further studies of the THD_i values of the modulation methods in the laboratory

10 References

[1] Gullvik, W.: Modelling, Analysis and Control of Active Front End (AFE) Converter, PhD-dissertation NTNU, 2007:218.

[2] Lund, Richard.: Multilevel Power Electronic Converters for Electrical Motor Drives, Doctoral Theses at NTNU, 2005:62

[3] McGrath, Holmes, Lipo: Optimized Space Vector Switching Sequences for Multilevel Inverters, APEC 2001, vol. 2, pages 1123-1129, 2001

[4] Seo, Choi, Hyun: A New Simplified Space-Vector PWM Method for Three-Level Inverters, IEEE Trans. Power Elect., Vol 16, no. 4, pages 545-550, July 2001

[5] Pou, Zaragoza, Rodrìguez, Ceballos, Sala, Burgos, Boroyevich: Fast-Processing Modulation Strategy for the Neutral-Point-Clamped Converter With Total Elimination of Low-Frequency Voltage Oscillations in the Neutral Point, IEEE Trans. Ind. Elect., vol54, no. 4, pages 2288-2294, Aug 2007

[6] Zaragoza, Pou, Ceballos, Robles, Jaen, Corbalàn: Voltage-Balance Compensator for a Carrier-Based Modulation in the Neutral-Point-Clamped Converter, IEEE Trans. Ind. Elect., vol 56, no. 2, pages 305-314, Feb 2009

[7] Li, Bhattacharya, Huang: Performance Comparison of a New Current Regulator for 3-Level NPC Inverter for Sinusoidal and Non-Sinusoidal Current Tracking Applications, IECON 2008, 34th Annual Conference of IEEE Ind. Elect., pages 879-884, Nov 2008

[8] Mohan, Undeland, Robbins: Power Electronics. Converters, Applications and Design, John Wiley & Sons, INC, 2003

[9] Geir Higraff. Masteroppgave: Modellering og simulering av komponenter til elektriske motordrifter I PSCAD, Juni 2004

[10] Yamanaka, Hava, Kirino, Tanaka, Koga, Kume: A Novel Neutral Point Potential Stabilization Technique Using the Information of Output Current Polarities and Voltage Vector, IEEE Trans. Ind. Appl., Vol 38, No.6, Nov/Dec 2002

[11] Bolognani, Zigliotto: Novel Digital Continuous Control of SVM Inverters In the Overmodulation Range, IEEE Trans. Powere Elect., Vol 33, no. 2, March/April 1997

[12] de Pablo, S.; Rey, A.B.; Herrero, L.C.; Martinez, F.; A graphical method for SVM duty cycles computation. Application on two-level and multi-level inverters, Pow. Elec. And App., 2009, 13th European Conf., Sept 2009

[13] Sveinung Floten, Tor Stian Haug. Specialization project. Modulation methods for three-level inverters. December 2009

[14] Bendre, Ashish: Modeling of topologies, modulation and control of stacked DC bus multi level converters. Doctor of Philosophy, University of Wisconsin-Madison.

[15] Tomta, Gjermund. Hovedoppgave: Tre-nivå omformer. NTNU Desember 1999.

[16] Abdul Rahiman Beig, G. Narayanan and V. T. Ranganathan: Modified SVPWM Algorithm for Three Level VSI With Synchronized and Symmetrical Waveforms, IEEE Transaction on Industrial Electronics, Vol. 54, NO. 1, February 2007

[17] Joachim Holtz, Nikolaos Oikonomou: Neutral Point Potential Balancing Algorithm at Low Modulation Index for Three-Level Inverter Medium-Voltage Drives. IEEE trans. On Industry Appl. Vol. 43, NO. 3, May/June 2007

[18] Du Toit, Mouton, H., “Natural balancing of three-level neutral-point-clamped PWM inverters”, IEEE Transaction on Industrial electronics, V49, I5, pp 1017-1025, 2002

[19] Liu, C.; Wu, B.; Xu, D.; Zargari, N.; Rizzo, S.; “Progressive Natural Balance of Neutral-Point Voltage of Three-level NPC Inverter With a Modified SWM Scheme”, Applied power electronics conference and exposition 2006, APEC ’06. Twenty-first Annual IEEE, 2006

[20] Jens G. Balchen, Trond Andresen, Bjarne A. Foss: ”Reguleringsteknikk”, 5. Utgave, Institutt for kybernetikk, NTNU. Januar 2005

[21] Tom F. Nestli, ”Electric Drives Chapter 8 – Feedback Controllers for Motor Drives”, TET4120 Electric Drives, NTNU 2008

[22] Akira Nabae, Isao Takahashi, Hirofumi Akagi: “A new Neutral-Point-Clamped PWM Inverter”, IEEE Transaction on Industry Applications, Vol. 1A-17, NO. 5, September/October 1981

Appendix A: Laboratory Results Space Vector

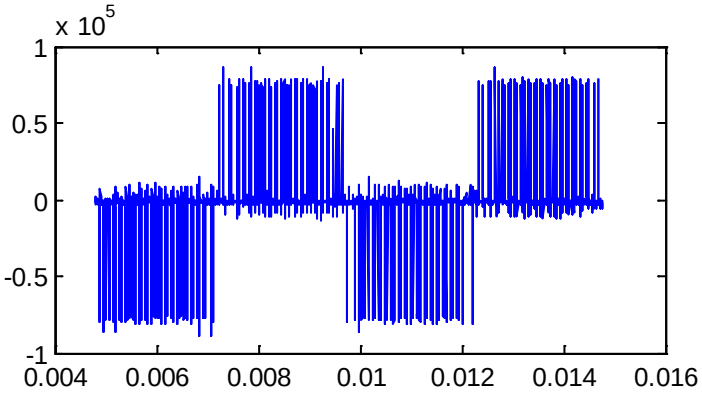

Figure A.1-1: Space Vector m_a equal 0.1

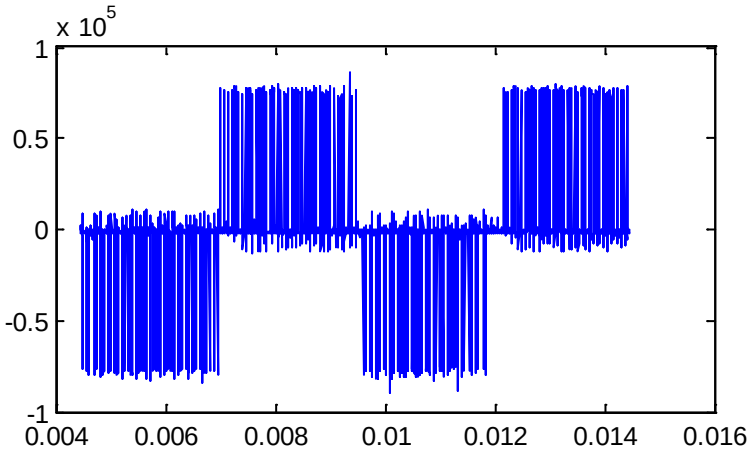

Figure A.1-2: Space Vector m_a equal 0.2

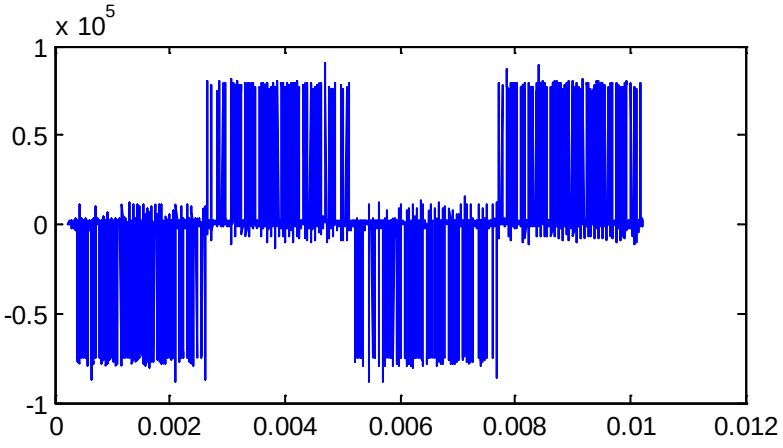

Figure A.1-3: Space Vector m_a equal 0.3

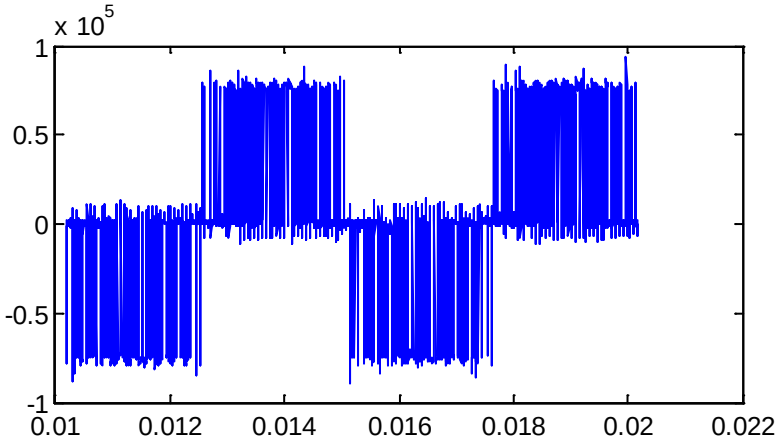

Figure A.1-4: Space Vector m_a equal 0.4

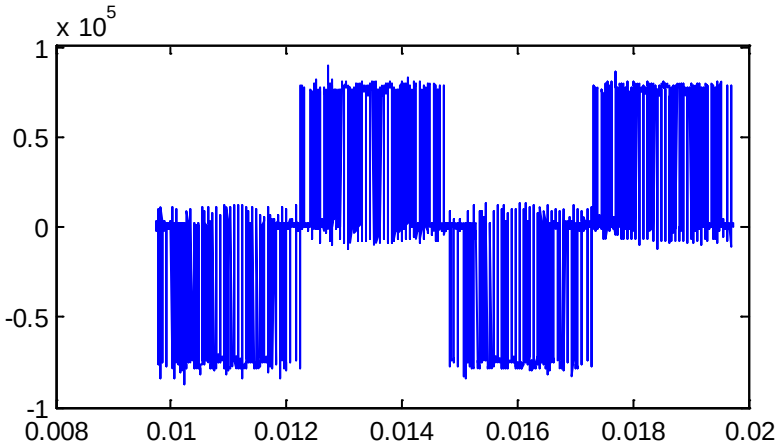

Figure A.1-5: Space Vector m_a equal 0.5

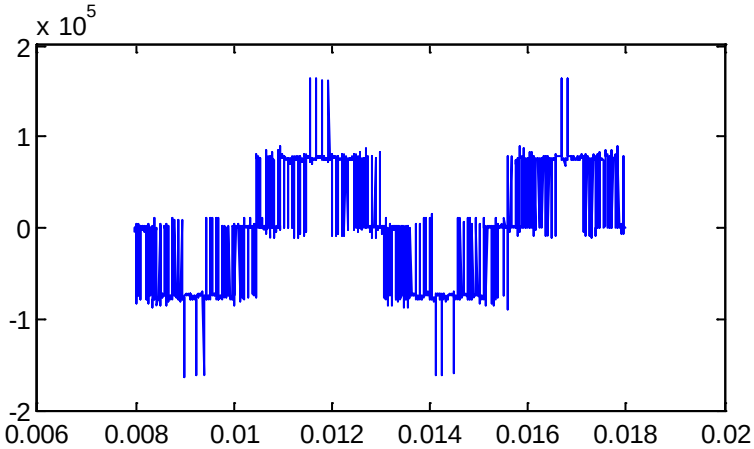

Figure A.1-5: Space Vector m_a equal 0.6

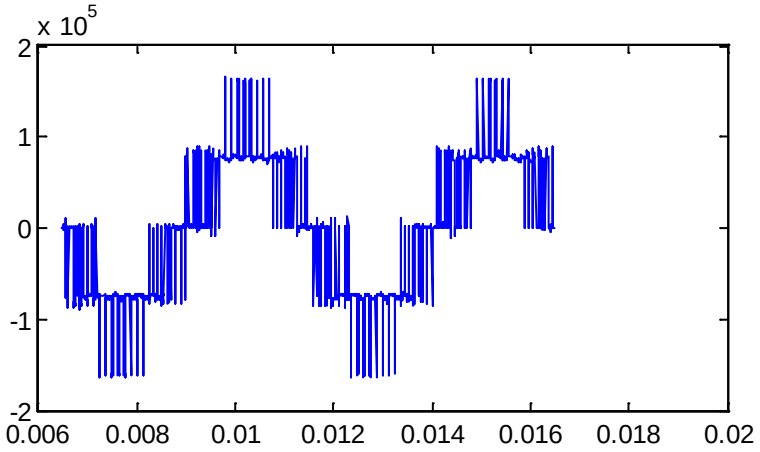

Figure A.1-7: Space Vector m_a equal 0.7

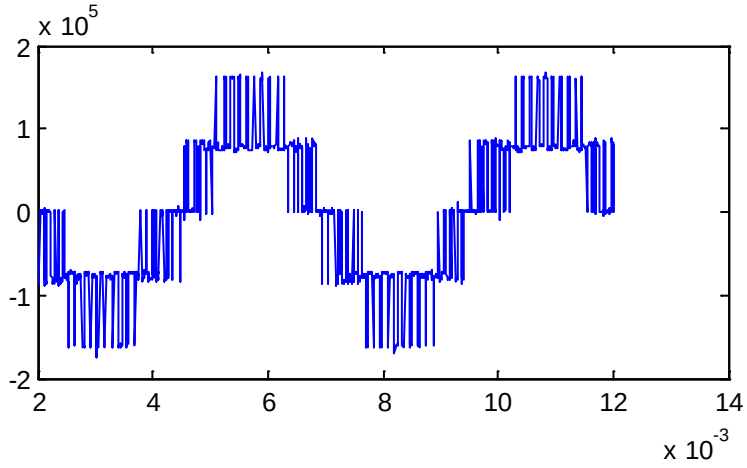

Figure A.1-8: Space Vector m_a equal 0.8

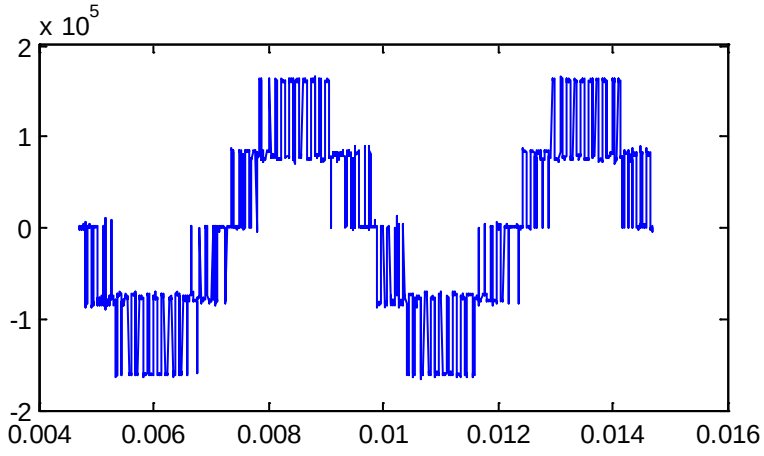

Figure A.1-9: Space Vector m_a equal 0.9

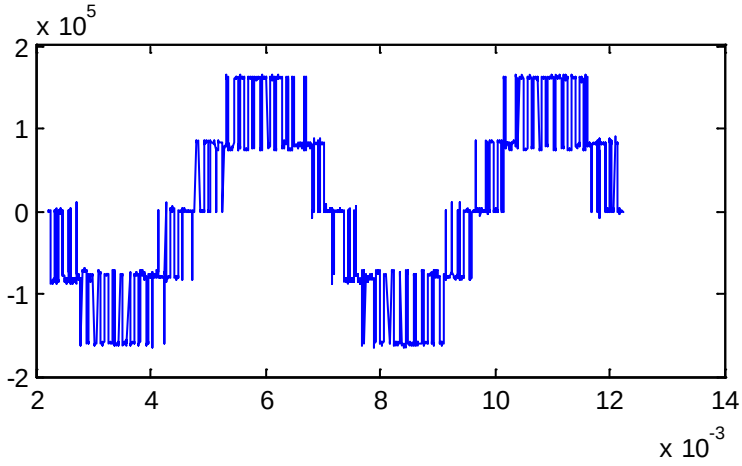

Figure A.1-10: Space Vector m_a equal 0.9

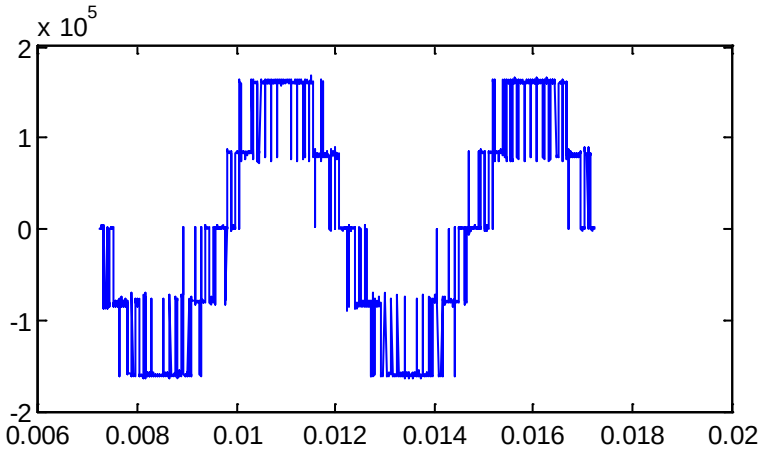

Figure A.1-11: Space Vector m_a equal 1.1547

Appendix B: Laboratory Results Double-Signal

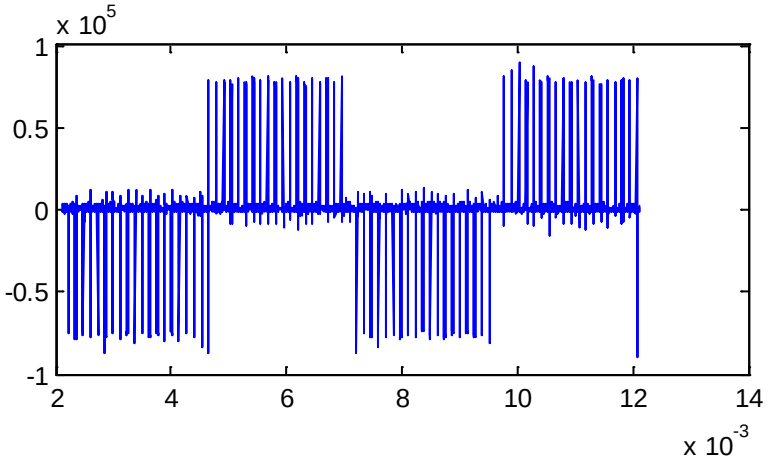

Figure B.1-1: Space Vector m_a equal 0.1

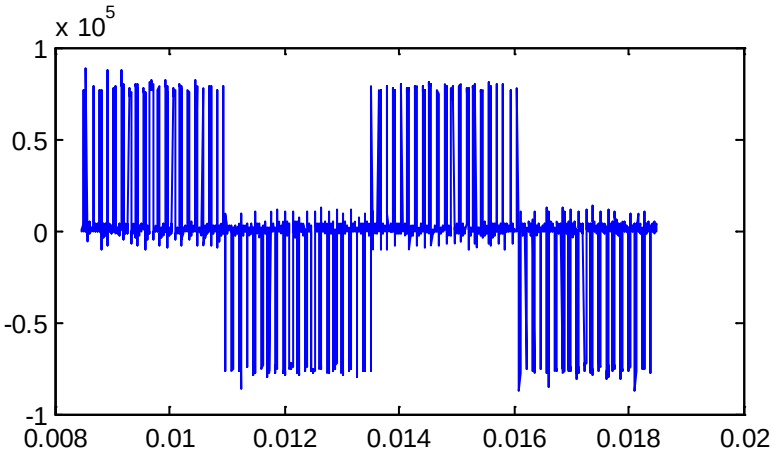

Figure B.1-2: Space Vector m_a equal 0.2

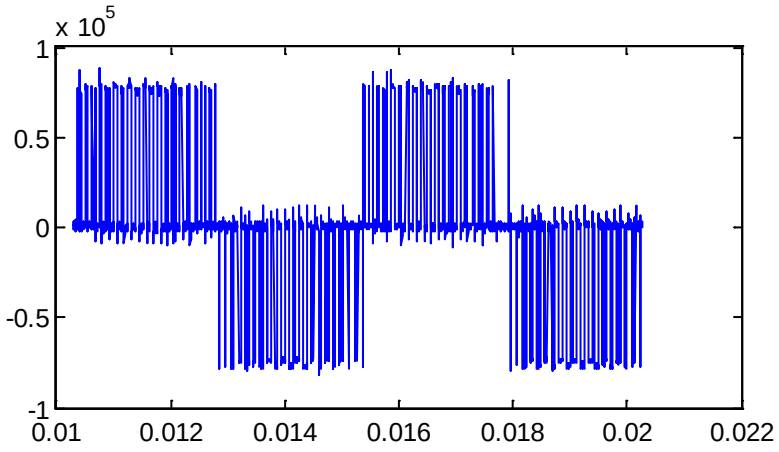

Figure B.1-3: Space Vector m_a equal 0.3

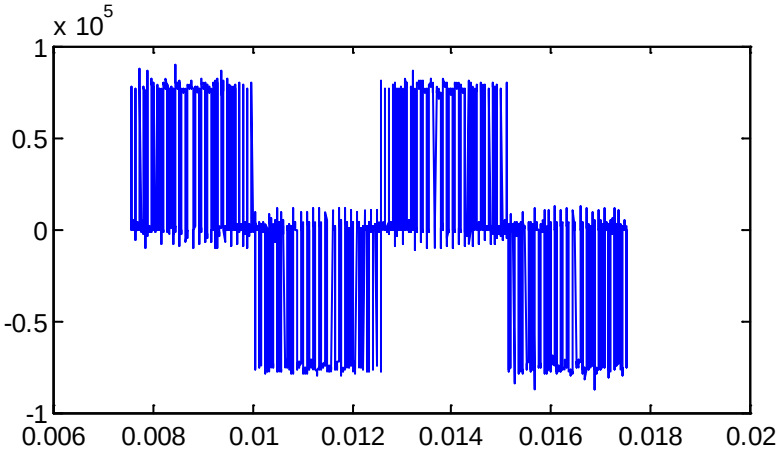

Figure B.1-4: Space Vector m_a equal 0.4

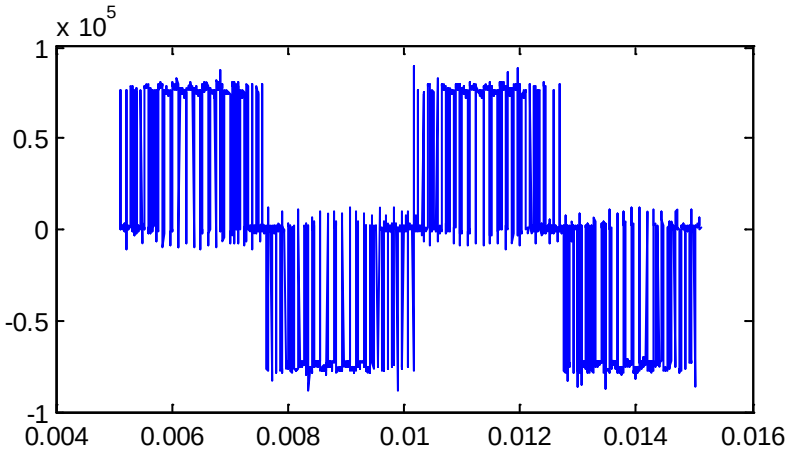

Figure B.1-5: Space Vector m_a equal 0.5

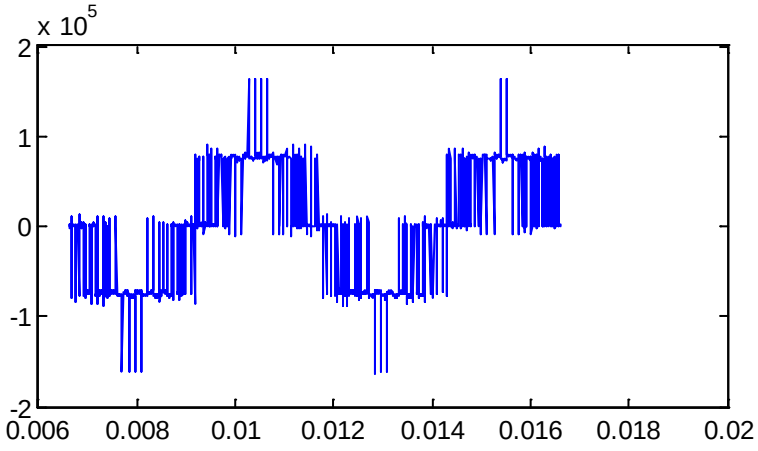

Figure B.1-6: Space Vector m_a equal 0.6

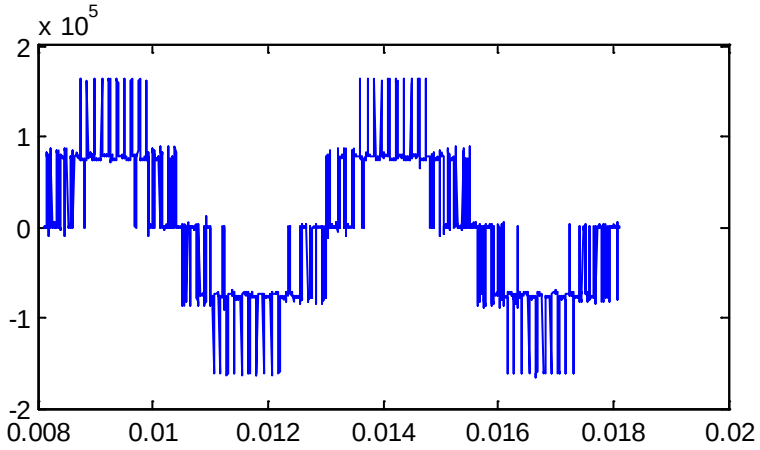

Figure B.1-7: Space Vector m_a equal 0.7

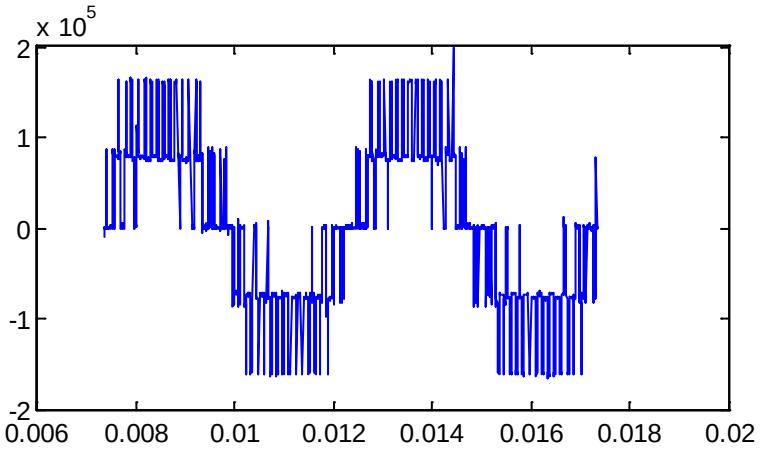

Figure B.1-8: Space Vector m_a equal 0.8

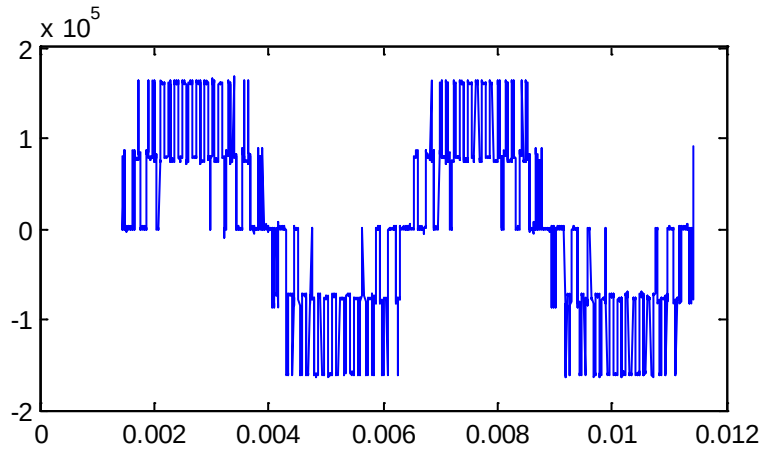

Figure B.1-9: Space Vector m_a equal 0.9

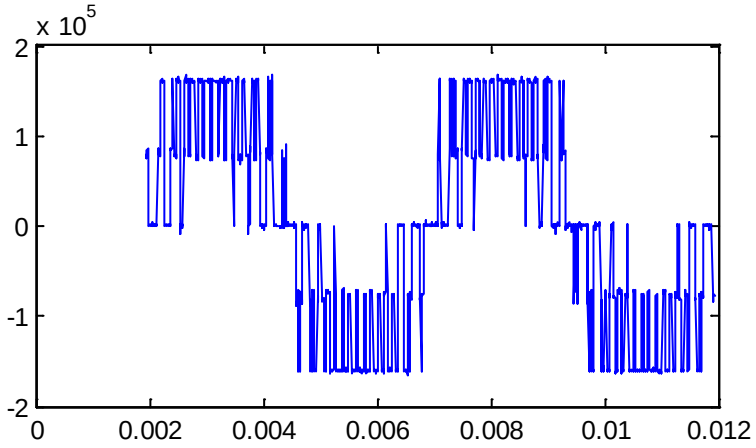

Figure B.1-10: Space Vector m_a equal 1

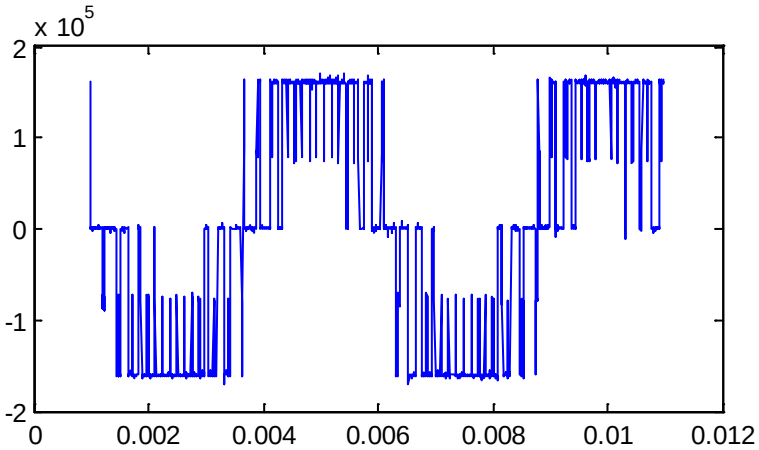

Figure B.1-11: Space Vector m_a equal 1.1547

Appendix C: Laboratory Results of Symmetrical Modulation

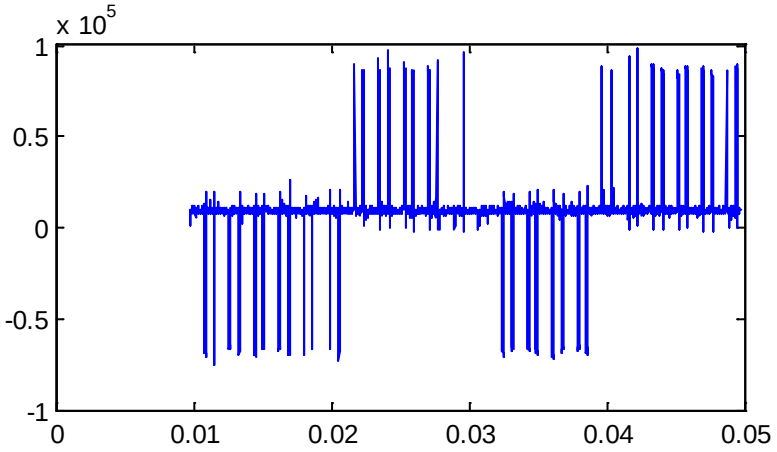

Figure C.1-1: Symmetrical modulation with m_a equal to 0.1

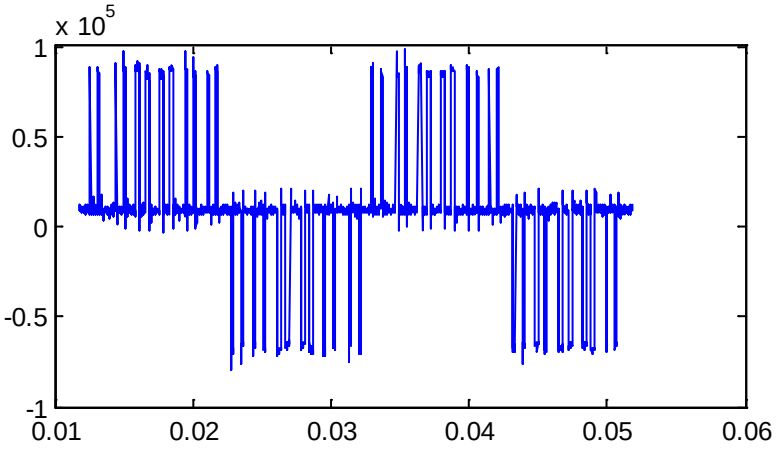

Figure C.1-2: Symmetrical modulation with m_a equal to 0.2

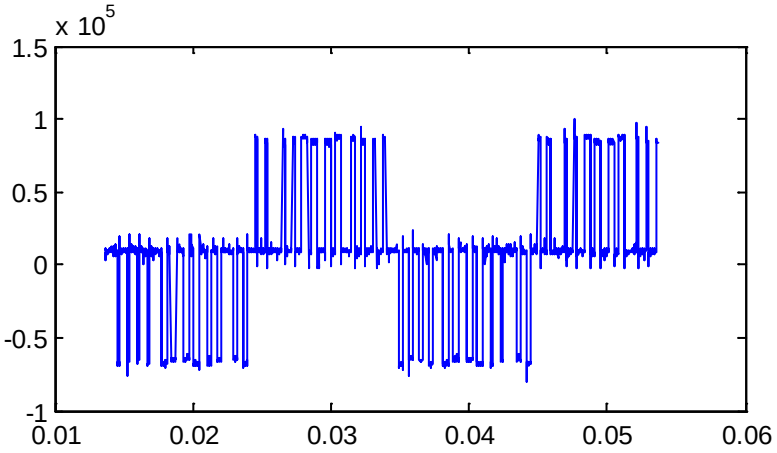

Figure C.1-3: Symmetrical modulation with m_a equal to 0.3

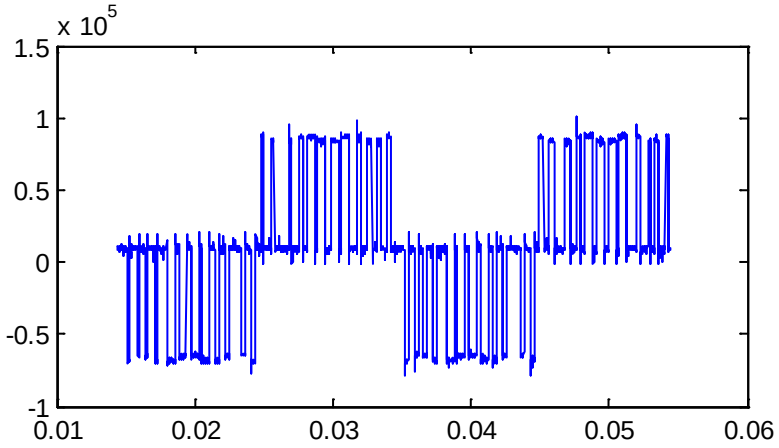

Figure C.1-4: Symmetrical modulation with m_a equal to 0.4

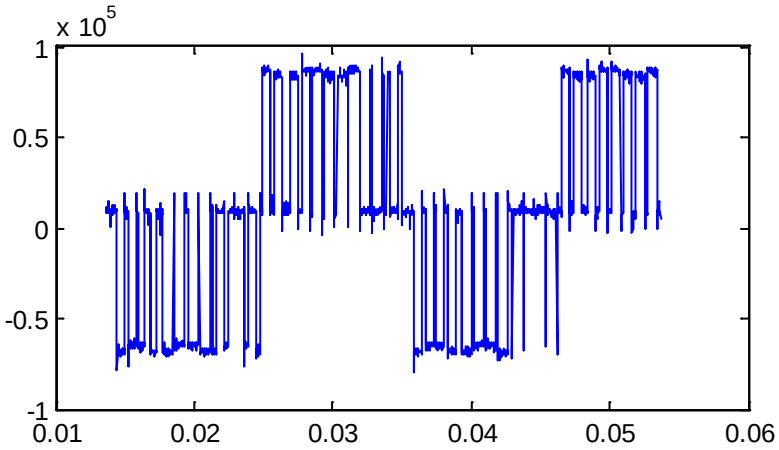

Figure C.1-5: Symmetrical modulation with m_a equal to 0.5

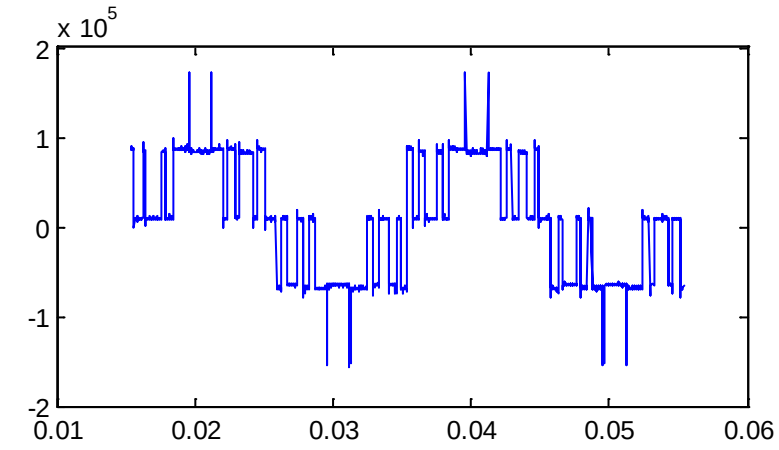

Figure C.1-6: Symmetrical modulation with m_a equal to 0.6

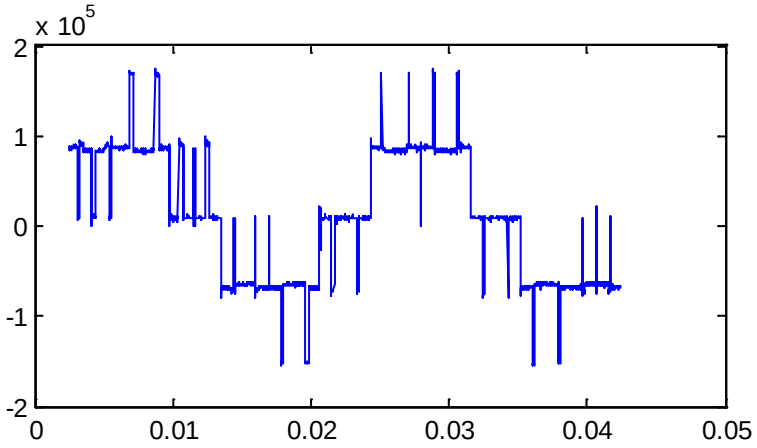

Figure C.1-7: Symmetrical modulation with m_a equal to 0.7

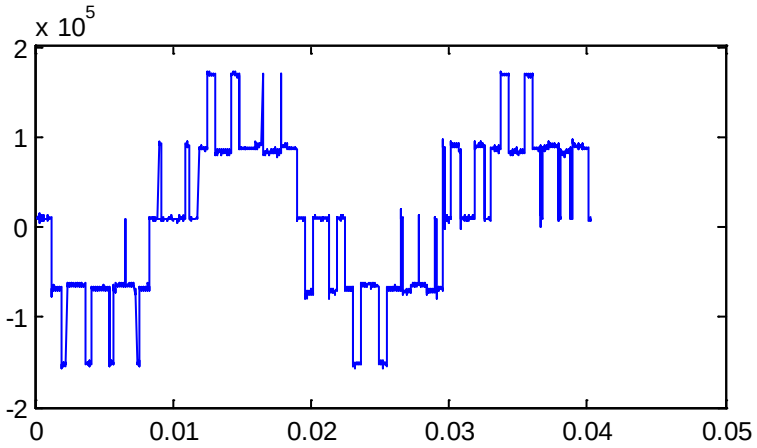

Figure C.1-8: Symmetrical modulation with m_a equal to 0.8

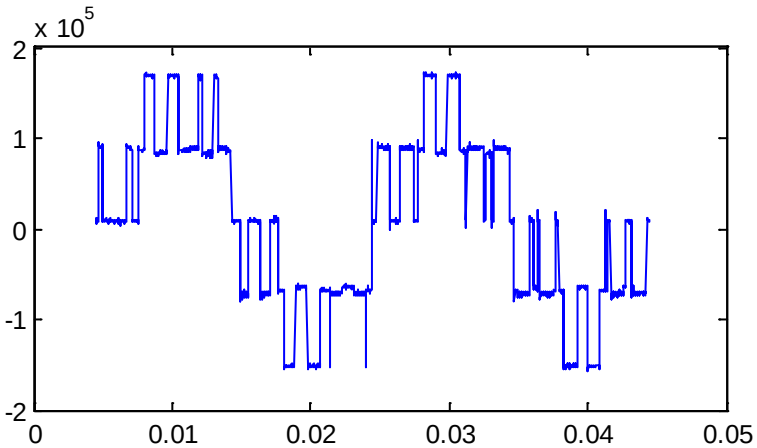

Figure C.1-9: Symmetrical modulation with m_a equal to 0.9

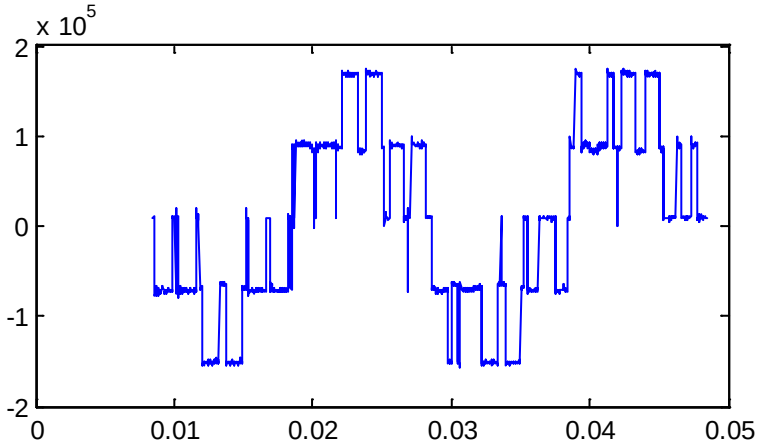

Figure C.1-10: Symmetrical modulation with m_a equal to 1.0

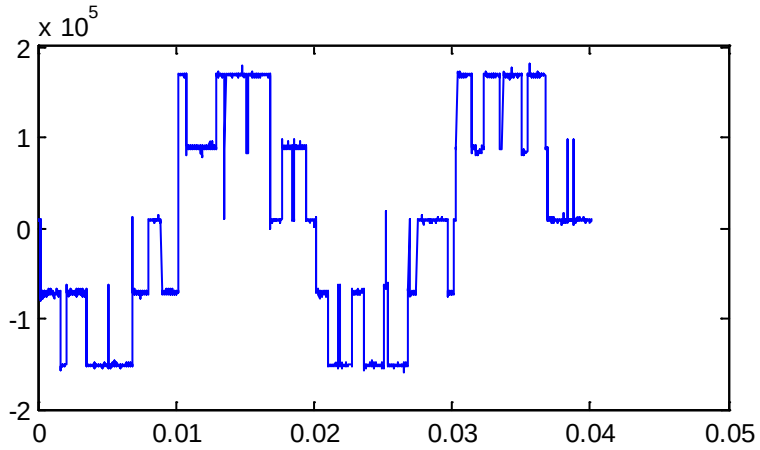

Figure C.1-11: Symmetrical modulation with m_a equal to 1.1547

Appendix D: Laboratory Results of Asymmetrical Modulation

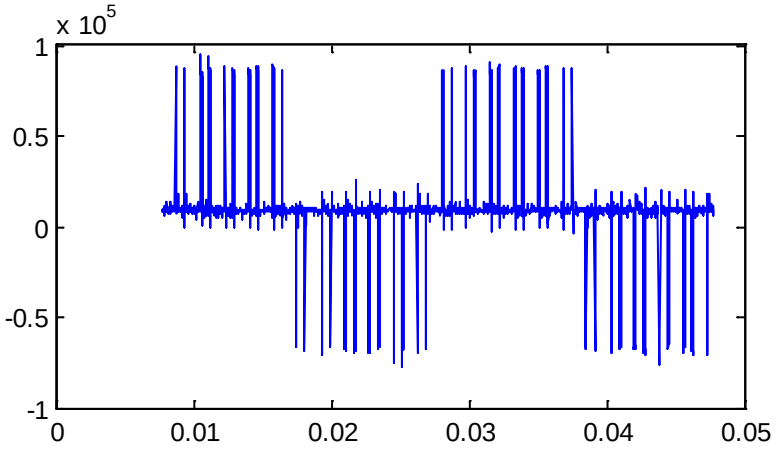

Figure D.1-1: Asymmetrical modulation with m_a equal to 0.1

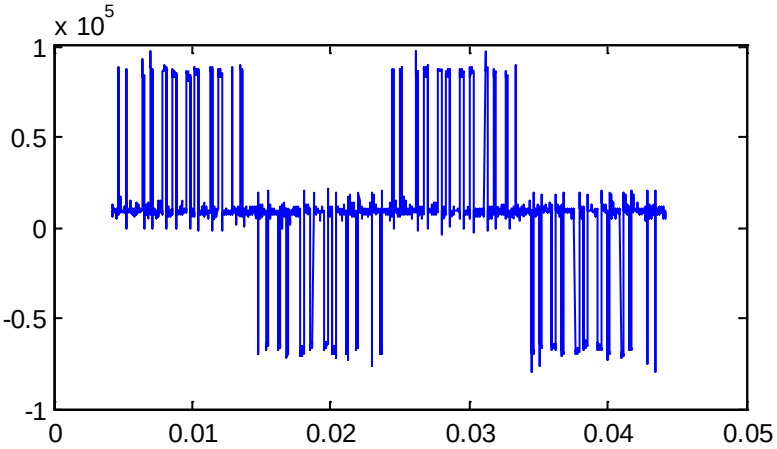

Figure D.1-2: Asymmetrical modulation with m_a equal to 0.2

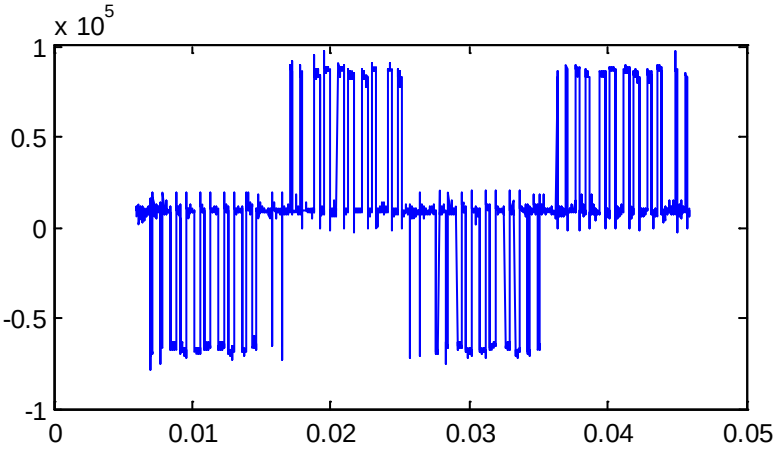

Figure D.1-3: Asymmetrical modulation with m_a equal to 0.3

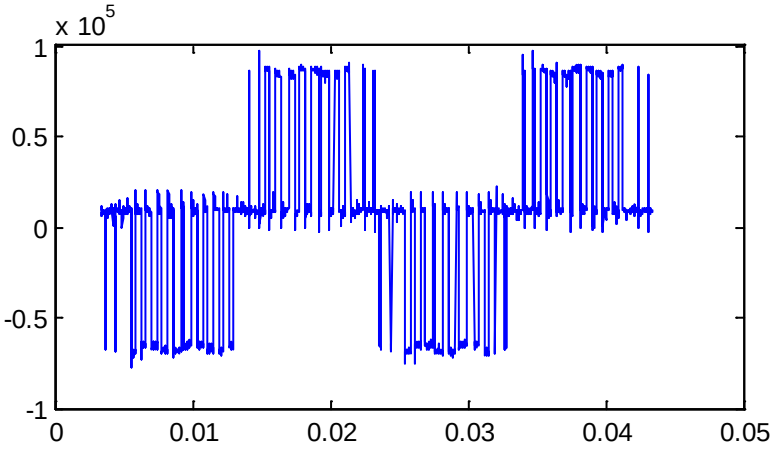

Figure D.1-4: Asymmetrical modulation with m_a equal to 0.4

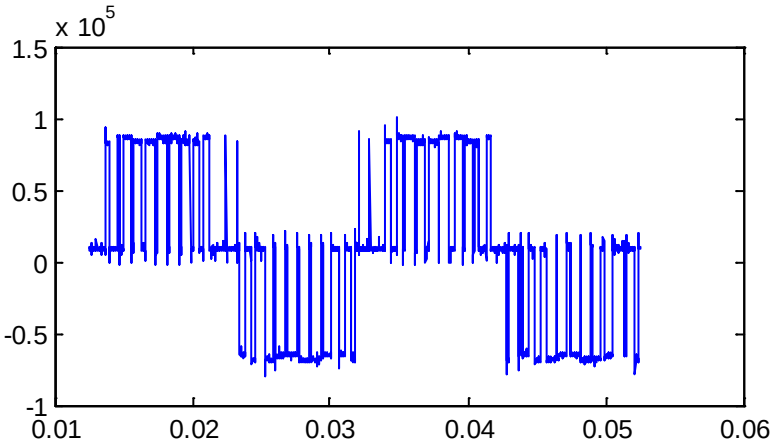

Figure D.1-5: Asymmetrical modulation with m_a equal to 0.5

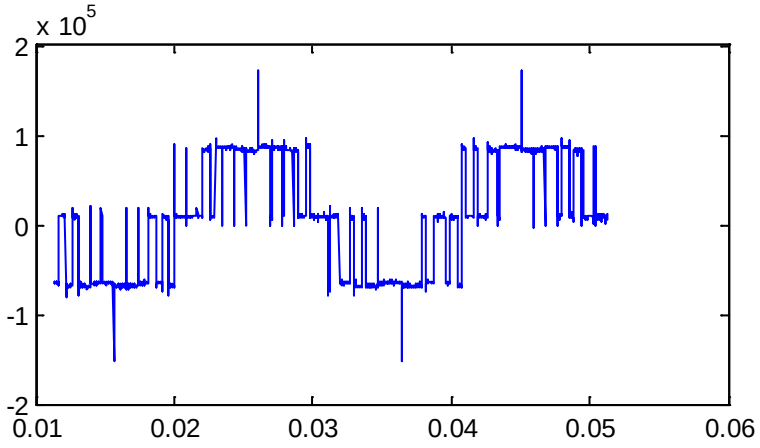

Figure D.1-6: Asymmetrical modulation with m_a equal to 0.6

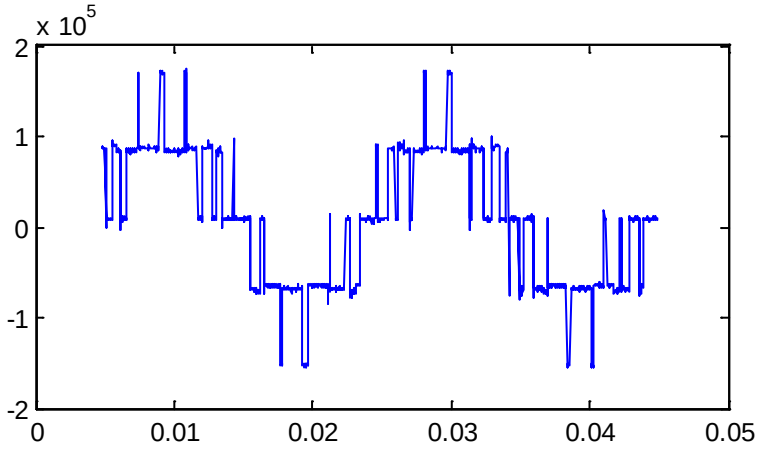

Figure D.1-7: Asymmetrical modulation with m_a equal to 0.7

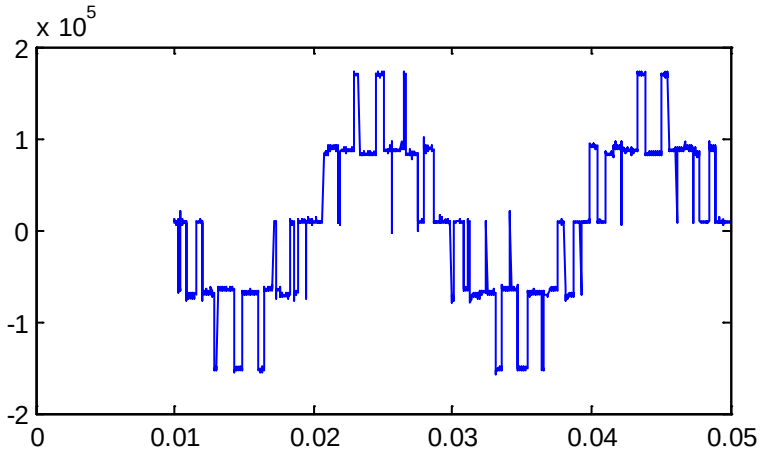

Figure D.1-8: Asymmetrical modulation with m_a equal to 0.8

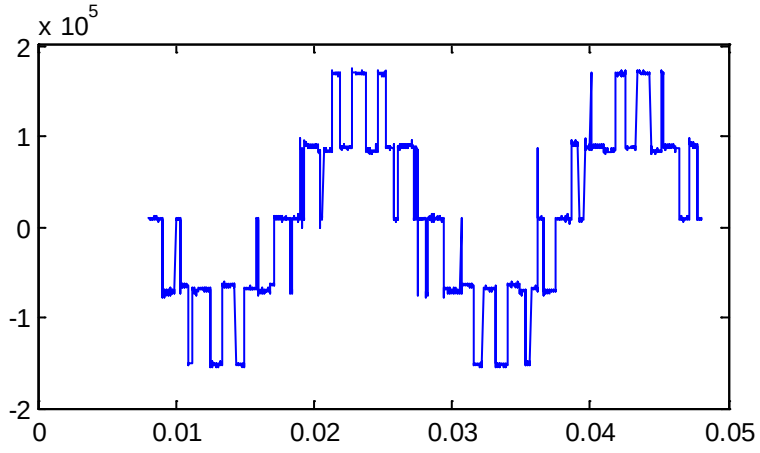

Figure D.1-9: Asymmetrical modulation with m_a equal to 0.9

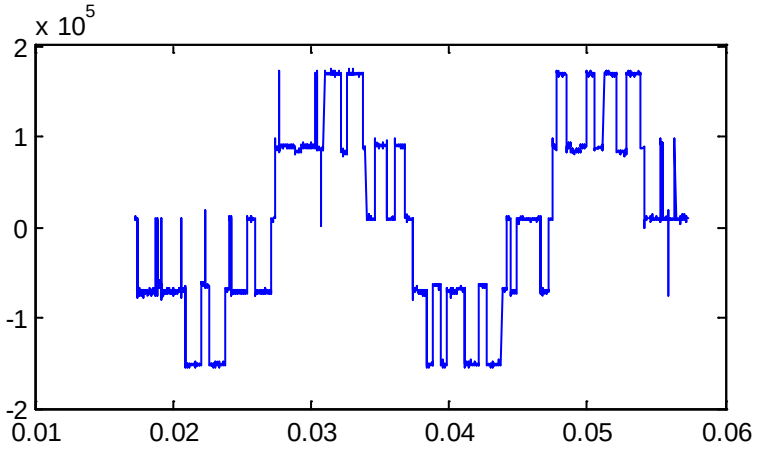

Figure D.1-10: Asymmetrical modulation with m_a equal to 1.0

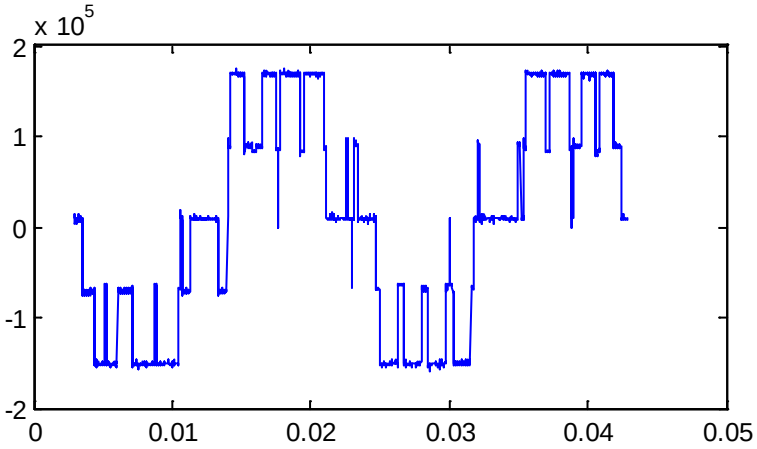

Figure D.1-11: Asymmetrical modulation with m_a equal to 1.1547

Appendix E: List Lab Equipment

TTi PL 303-P Power Supply 30V 3A

- Serial number 306422
- Serial number 306423

SI-9000 Differential probe

- Elkraft: I06-0181

XILINX Plattform Cable U88II

- Model DLC 10
- Serial XU – 30116

Tektronix TDS 3014B Four Channel Color Digital Phosphor Oscilloscope

- TDS3014B B030644

Three-level converter at NTNU